

# Pacific Northwest National Laboratory

Operated by Battelle for the  
U.S. Department of Energy

November 27, 2001

Dr. Kimberly Gruss  
U.S. Nuclear Regulatory Commission  
One White Flint North  
11555 Rockville, Pike  
Rockville, Maryland 20852-2738

Dear Kim:

Please find enclosed our revised draft of the report entitled "Update of CSFM Methodology for Determining Temperature Limits for Spent Fuel Dry Storage in Inert Gas." This draft report has been technically peer reviewed by PNNL staff and reviewed by PNNL management.

The revised draft includes changes to the report that respond to approximately 80% of the 108 specific and 11 general NRC comments received by PNNL on the report. The 20% of the NRC comments that were not specifically addressed in this revised draft were those that criticized the general CSFM approach to modeling creep and creep rupture. The CSFM modeling approach in this report used standard creep and creep rupture models published in the open literature and used in textbooks on this subject. In addition, the statement of work (SOW) for this effort indicated that the original CSFM approach (Rev. 0) would be the starting point for changes to obtain an updated methodology for predicting temperature limits for spent fuel dry cask storage. These comments were discussed with you on September 19, 2001 and it was agreed that it would not be productive to address those comments that were critical of the general CSFM approach.

The major changes to the revised draft enclosed, as agreed to on our September 19, 2001 discussions, were; 1) elimination of Chapter 3 (detailed discussion of CSFM Rev. 0), 2) elimination of the appendix that discussed cavity formation as a mechanism for failure, 3) inclusion as an appendix a description of how the DATING code calculates spent fuel temperature limits with a decreasing temperature and stress in the spent fuel, and 4) use of equation editor for report equations.

You also verbally requested that the CSFM Rev.1 creep model be compared in plots to all of the strain versus time data collected in this report. This consists of approximately 45 plots that would require significant effort to include in the report. Consequently, these plots were transmitted to you by mail on September 20, 2001.

902 Battelle Boulevard • P.O. Box 999 • Richland, WA 99352

Telephone (509) 372-4605 □ Email [carl.beyer@pnl.gov](mailto:carl.beyer@pnl.gov) □ Fax (509) 372-6485

Dr. Kimberly Gruss  
November 27, 2001  
Page 2

The transmittal of this revised draft completes this effort unless NRC identifies further work and funding.

Sincerely,

*Robert Gruel for*

C.E. Beyer

CC: Bob Gruel, PNNL - w/o enclosures  
Wayne Hodges, NRC - w/o enclosures

**DRAFT**

**UPDATE OF CSFM METHODOLOGY FOR DETERMINING TEMPERATURE  
LIMITS FOR SPENT FUEL DRY STORAGE IN INERT GAS**

E. R. Gilbert  
E. P. Simonen  
C. E. Beyer  
P. G. Medvedev

July 2001

Prepared for  
Spent Fuel Project Office  
Office of Nuclear Reactor Regulation  
U.S. Nuclear Regulatory Commission  
under Contract DE-AC06-76RLO 1830  
JCN J5167

Pacific Northwest Laboratory  
Richland, WA 99352

## ABSTRACT

The CSFM methodology has been revised (Rev.1) based on new creep and creep rupture data from unirradiated and irradiated specimens of Zircaloy cladding from SNF. The creep and creep rupture database collected for this effort is nearly all new and different from the database collected for CSFM Rev. 0. CSFM Rev. 1 retains the same six creep mechanisms for steady-state creep, and only the grain boundary sliding (GBS) and low temperature climb (LTC) mechanisms are significant within the range for dry cask storage which is the same as for CSFM Rev. 0. However, the creep models have been modified from Rev. 0 to include the addition of a primary creep model, changes to the unirradiated creep coefficients for GBS, LTC and Coble creep mechanisms, and incorporation of a creep reduction factor due to irradiation damage for some creep mechanisms. The CSFM Rev. 1 uses only one creep rupture model (Monkman-Grant) within the temperature and stress range for dry cask storage while the Rev. 0 methodology assumed that two rupture models, diffusion controlled cavitation growth (DCCG) and Monkman-Grant, were active within this range. The Rev. 1 Monkman-Grant coefficient has been modified from that used in the Rev. 0 rupture correlations.

## EXECUTIVE SUMMARY

The CSFM methodology has been revised (Rev.1) based on new and different creep and creep rupture data from unirradiated and irradiated specimens of Zircaloy cladding from SNF. The creep and creep rupture database collected for this effort is nearly all new from the database collected for CSFM Rev. 0.

From the review of the data and use of the revised CSFM methodology proposed in this report, the following findings, conclusions and recommendations are made:

### Findings and conclusions

- The CSFM methodology Rev. 1 results in similar predicted temperature limits (within 5°C) to the Rev. 0 methodology for low and high burnup fuel with 5 years cooling time. However, for 10 year cooled low and high burnup fuel, the CSFM Rev. 1 methodology predicts lower temperature limits than the Rev. 0 methodology by 10°C to 20°C for stresses between 110 to 140 MPa. The DATING code is used to predict the temperature limits for both CSFM Rev. 0 and CSFM Rev. 1 methodology. (Section 5.1)
- Thermal annealing tests for SNF cladding indicate that cask drying at temperatures below 400°C should have little impact on creep and temperature limits for times less than a month. Exposure of the SNF cladding to pre-storage temperatures above 400°C may anneal the irradiated microstructure and increase the creep rate, thereby reducing the calculated cask storage temperature limit. Thermal annealing at temperatures above 400°C may also result in hydride reorientation that could reduce ductility and reduce storage temperature limits. (Section 4.3.4).
- Comparison of CSFM Rev. 1 DATING results (using the conservative Monkman-Grant coefficient) to other recent methodologies that predict dry cask storage

temperature limits demonstrate that the CSFM Rev. 1 methodology is not as conservative as some and more conservative than others. (Section 5.1)

- Two steady-state creep models were developed (1A and 1B) and concluded that 1B was slightly better. The two models predict nearly the same temperature limits within the range of conditions for dry cask storage. (Section 4.4)
- Comparison of new creep data for irradiated cladding to data from unirradiated cladding suggests that the steady-state creep rate for some creep mechanisms is significantly decreased as a result of irradiation. (Sections 3.2 and 4.3.1)
- Examination of the unirradiated creep data shows a large variability (factor of 10 to 1000) in the data at a given temperature and stress. This variability appears to decrease for the irradiated creep data but the variability is still relatively large (factor of 5 to 20). The variability in the creep data appears to be due to fabrication parameters (Sections 3 and 4).
- Analyses of the creep rupture data for both unirradiated and irradiated cladding suggest that there is no difference in rupture life between unirradiated and irradiated cladding. Some of the rupture data suggest that there may be a dependence between rupture strain or time-to-rupture and hydride content but this can not be quantified because of the lack of rupture data from high burnup rods with high hydrogen levels. (Sections 4.2, 4.3.2 and 4.3.3)
- Analyses of the creep rupture data for both unirradiated and irradiated cladding indicate that rupture life is consistent with the Monkman-Grant correlation. This conclusion is considered preliminary because there is only one unirradiated and no irradiated rupture data within the design-basis stress range for dry storage. (Section 4.2).

- The creep rupture data also suggest that the Monkman-Grant coefficient (strain-to-failure) decreases with decreasing temperature. The decrease in the coefficient with temperature may be due to different failure mechanisms such as triple point and transgranular cracking that may become more active at the lower temperatures and a decrease in strain-to-failure. (Section 4.2.2)
- The proposed Monkman-Grant correlation is only valid for high burnup fuel with hydrogen levels less than 660 ppm and no oxide spallation. (Section 4.3.3)

As noted, the Monkman-Grant correlation for Rev. 1 shows that the creep strain-to-failure is not a single value. Rather, it is dependent on the initial storage temperature of the cladding, e.g., the strain-to-failure varies from 3.6% (best estimate value at 400°C) to below 1% depending on temperature and the desired level of conservatism. In comparison, ISG-11 (NRC 2000) prescribes a 1% creep strain limit and a criteria using cladding oxide thickness as the basis for determining fuel failure. The ISG-11 1% strain limit is based on a limited set of tensile and burst to rupture data and the current understanding of the properties of high burnup fuel at the time ISG-11 was issued.

The ISG-11 (NRC-2000) 1% uniform strain criterion may be overly conservative for temperatures above 350 °C but may be a reasonable conservative value for temperatures below 350 °C. The Monkman-Grant correlation was preferred for CSFM Rev. 1 rather than the simple strain limits of 2% and 1%, because it fits the rupture data well and can be related to theoretical rupture models.

## **Recommendations**

- Creep data are needed from high burnup SNF rods with high corrosion within the temperature and stress range for dry cask storage of 310°C to 380°C and 110 to 150 MPa, respectively. These data are needed because very little creep data exist in this temperature and stress range and no data exist in this range for high burnup fuel with high cladding oxidation and oxide spallation.

- Creep rupture data from high burnup fuel rods with high corrosion (including rods with oxide spallation) are needed within the temperature and stress range for dry cask storage of 310°C to 380°C and 110 to 150 MPa, respectively. It may not be possible to obtain rupture data within a reasonable amount of time at the stresses typical for dry cask storage; therefore, it is recommended that stress levels be increased to the necessary level for rupture rather than increasing temperature level.
- Creep rupture data are needed from high burnup rods after some time in interim dry cask (post) storage to confirm there is sufficient deformation life required for permanent storage following dry cask storage.
- Fracture toughness data are also needed from high burnup rods with high oxidation and spallation near room temperature. These data are needed from both pre- and post-storage high burnup rods to confirm that the rods can be retrieved after interim dry cask storage for placement in a permanent storage facility

It is noted that the information in this draft report is preliminary and should not be used for licensing decisions until it has been peer reviewed by a panel of experts on creep behavior of zirconium alloys and high burnup fuel behavior

# CONTENTS

ABSTRACT .....	i
EXECUTIVE SUMMARY .....	ii
ACRONYMS AND ABBREVIATIONS .....	xiii
1. INTRODUCTION.....	1.1
2. BACKGROUND.....	2.1
2.1. Regulatory Basis and Need for Temperature Limits.....	2.1
2.2. Expected Design-Basis Conditions .....	2.2
2.3. History of Temperature Limit Methodologies .....	2.5
2.4. Background of CSFM Rev. 0.....	2.10
3. DEVELOPMENT AND DESCRIPTION OF CREEP AND RUPTURE DATABASE .....	3.1
3.1. Creep of Unirradiated Cladding .....	3.4
3.2. Creep of Irradiated Cladding.....	3.12
3.3. Description of Stress Rupture Database.....	3.19
3.4. Summary of Findings .....	3.22
4. REVISIONS TO CSFM METHODOLOGY BASED ON CURRENT DATA .....	4.1
4.1. Description of Derivation of Revised CSFM Creep Coefficients.....	4.2
4.1.1. Primary Stage Creep.....	4.4
4.1.2. Steady-State Creep of Unirradiated Cladding .....	4.6
4.2. Derivation of Creep Rupture Coefficients .....	4.21
4.2.1. Creep Rupture Data Between 350°C and 420°C.....	4.22
4.2.2. Temperature Dependence of Creep Rupture Between 280°C and 420°C and Development of Bounding Monkman-Grant Coefficient.....	4.24
4.2.3. Comparison of Creep Rupture Data to Various DCCG Rupture Models .....	4.29
4.3. Effects of Irradiation, Hydrogen, and Annealing on Creep and Rupture Strains of Zircaloy .....	4.32
4.3.1. Effects of Irradiation on Creep.....	4.32
4.3.2. Effects of Irradiation on Creep to Rupture.....	4.36
4.3.3. Effects of High Burnup and Hydrided Microstructures on Creep and Rupture .....	4.36

4.3.4. Effects of Annealing and Hydride Reorientation on Creep and Rupture (Temperatures Above Dry Cask Storage Conditions).....	4.39
4.4. Validation of CSFM Rev. 1 Methodology with Creep Data.....	4.42
4.4.1. Validation of CSFM Rev. 1A with Unirradiated and Irradiated Zircaloy Creep Data. ....	4.42
4.4.2. Validation of CSFM Rev. 1B with Unirradiated and Irradiated Zircaloy Creep Data.....	4.43
4.5. Deformation Mechanism Maps.....	4.52
4.6. Life Fraction Rule .....	4.52
5. CSFM REV. 1 CALCULATED TEMPERATURE LIMITS .....	5.1
5.1. Comparison of CSFM Rev. 1 and Rev. 0 Calculated Temperature Limits.....	5.1
5.2. Sensitivity and Uncertainty Analyses on Temperature Limits.....	5.4
5.3. Comparison of CSFM Rev.1 Temperature Limits to Those Calculated with Other Methodologies.....	5.6
5.4. Comparison of CSFM Rev. 1 Temperature Limits using Monkman-Grant Correlation Versus Use of a Strain Limit for Rupture. ....	5.11
6. FINDINGS, CONCLUSIONS AND RECOMMENDATIONS .....	6.1
6.1. Findings.....	6.1
6.2. Conclusions .....	6.3
6.3. Recommendations .....	6.5
7. REFERENCES.....	7.1
APPENDIX A - SUPPLEMENT .....	A.1

## FIGURES

2.1	Cladding Temperature and Stress Decay for High Burnup (PWR 60 GWd/MTU) and Starting Stress of 120 MPa. ....	2.4
2.2	Temperature and Stress Decay of Low Burnup (PWR 30 GWd/MTU) Fuel Using Helium Cooling Curve from Levy et al. (1987), and Starting Stress of 120 MPa.....	2.4
3.1	Evidence of Consistency in the Creep Behavior of Unirradiated Cladding between Frenkel and Wiesz (1973) and Spilker et al. (1997). ....	3.6
3.2	Temperature and Stress Range of Unirradiated Creep Data and Design Basis Range (Narrow Box) for Dry Cask Storage. ....	3.7
3.3	Temperature and Stress Range of Post-Irradiated Creep Data and Design Basis Range (Narrow Box) for Dry Cask Storage.....	3.13
3.4	Steady-State Strain Rate of the Framatome Cladding. ....	3.16
3.5	Effect of Irradiation on the Creep Properties of Zircaloy.....	3.16
3.6	Temperature and Stress Range of Stress Rupture Data and Design Basis Range (Narrow Box) for Dry Cask Storage. ....	3.20
3.7	Effect of Strain Rate on Uniform Elongation for Irradiated and Unirradiated Zircaloy.....	3.20
3.8	Initiation of Crack in Hydride Rim and Termination in Ductile Ligament of Zircaloy-4 (Fuketa et al. 1996). ....	3.22
4.1	Deformation by the GBS-GBD Mechanism and Climb/Glide Mechanism.....	4.9
4.2	Comparison of Equation 4.6 for Deformation by GBS-GBD with Creep Results from Unirradiated Sandvik Cladding by Limback and Andersson (1996).....	4.9
4.3	Activation Energy of 166 KJ/mole for Creep of Irradiated Framatome Cladding is Consistent with Activation Energy of 167 KJ/mole Reported by Viergge and Herzig (1990) for GBD. ....	4.12
4.4	Deformation by the Coble Mechanism.....	4.12
4.5	Comparison of the Stress Dependence for the Unirradiated GBS-GBD and Coble Creep Equations with Experimental Data at 350°C. ....	4.14
4.6	The Coble and GBS-GBD Creep Models Bound Irradiated KWO Siemens Cladding Creep Data by Kaspar et al. (1985a and 1985b). ....	4.14
4.7	The Coble and GBS-GBD Creep Models Bound Unirradiated Cladding Creep Data by Cappelaere and Bouffioux (2000). ....	4.15

4.8	Coble and GBS-GBD Creep Models Compared with Irradiated Creep Data for Framatome SNF Cladding by Limon et al. (2000).	4.15
4.9	Comparison of LTC Mechanism Model with Unirradiated and Irradiated Zr-2/-4 Cladding Creep Data at 350°C.	4.17
4.10	Comparison of the Climb/Glide Mechanism Model with Zircaloy Cladding Creep Data at 350°C.	4.19
4.11	Effect of Hydrogen on Steady-State Creep Rate for Unirradiated Zr-4.	4.20
4.12	Comparison of Creep Rupture Data with CSFM Rev. 0, T = 350 - 420°C.	4.23
4.13	Regression Analysis of the Experimental Data to Determine the Temperature Exponent in Equation (4.11).	4.25
4.14	Stress Rupture Data Correlated on a Monkman-Grant Plot of Rupture Time vs. Strain Rate, Irradiated Samples are Shown as Filled Points.	4.26
4.15	Ratio of Measured versus Calculated Rupture Time Using the Mean Monkman-Grant Relationship (Equation 4.12).	4.27
4.16	Measured vs. Calculated Rupture Time Using the Mean Monkman-Grant Relationship (Equation 4.12).	4.28
4.17	Ratio of Measured vs. Calculated Rupture Time Using the Conservative Monkman-Grant Relationship (Equation 4.13).	4.28
4.18	Measured versus Calculated Rupture Time Using the Conservative Monkman-Grant Relationship (Equation 4.13).	4.29
4.19	Comparison of Predicted Temperature Limits by CSFM Rev. 0 and Schwartz and Witte DCCG Model.	4.30
4.20	Comparison of LLNL DCCG Fracture Mechanisms with Creep Rupture Data for Zircaloy Cladding.	4.31
4.21	Creep Reduction Factor for Framatome Cladding Data in the Regimes for the High-Stress LTC or Climb/Glide Creep Mechanisms, and the Low-Stress GBS-GBD Creep Mechanism.	4.33
4.22	Graphic Representation of Equation 4.16 as a Function of Hoop Stress.	4.35
4.23	Graphic Representation of Equation 4.17 as a Function of Hoop Stress.	4.35
4.24	Effect of Corrosion on Creep Rupture from Results by Goll et al. (2001).	4.38
4.25	Predicted Versus Measured Creep Rate Using CSFM Rev. 1A for All Data.	4.45

4.26 Comparison of CSFM Model 1A with Unirradiated and Irradiated Zr-2/-4 Cladding Creep Data at 300°C. ....	4.45
4.27 Comparison of CSFM Model 1A With Unirradiated and Irradiated Zr-2/-4 Cladding Creep Data at 325°C. ....	4.46
4.28 Comparison of CSFM Model 1A with Unirradiated and Irradiated Zr-2/-4 Cladding Creep Data at 350°C. ....	4.46
4.29 Comparison of CSFM Model 1A with Unirradiated and Irradiated Zr-2/-4 Cladding Creep Data at 380°C. ....	4.47
4.30 Comparison of CSFM Model 1A with Unirradiated and Irradiated Zr-2/-4 Cladding Creep Data at 400°C. ....	4.47
4.31 Comparison of CSFM Model 1A with Unirradiated and Irradiated Zr-2/-4 Cladding Creep Data at 420°C. ....	4.48
4.32 Predicted Versus Measured Creep Rate Using CSFM Rev. 1B for All Data. ....	4.48
4.33 Comparison of CSFM Model 1B with Unirradiated and Irradiated Zr-2/-4 Cladding Creep Data at 300°C. ....	4.49
4.34 Comparison of CSFM Model 1B with Unirradiated and Irradiated Zr-2/-4 Cladding Creep Data at 325°C. ....	4.49
4.35 Comparison of CSFM Model 1B with Unirradiated and Irradiated Zr-2/-4 Cladding Creep Data at 350°C. ....	4.50
4.36 Comparison of CSFM Model 1B with Unirradiated and Irradiated Zr-2/-4 Cladding Creep Data at 380°C. ....	4.50
4.37 Comparison of CSFM Model 1B with Unirradiated and Irradiated Zr-2/-4 Cladding Creep Data at 400°C. ....	4.51
4.38 Comparison of CSFM Model 1B with Unirradiated and Irradiated Zr-2/-4 Cladding Creep Data at 420°C. ....	4.51
4.39 Deformation Mechanism Map for the CSFM Rev. 1A Model for Zircaloy Cladding. ....	4.54
4.40 Deformation Mechanism Map for the CSFM Rev. 1B Model for Zircaloy Cladding. ....	4.55
5.1 Comparison of CSFM Rev. 1 and Rev. 0 Calculated Temperature Limits as a Function of Stress for Low Burnup Fuel (30 GWd/MTU) with 5 and 10 year Cooling (Using the Helium Cooling Curve from CSFM Rev. 0). ....	5.3
5.2 Comparison of CSFM Rev. 1 and Rev. 0 Calculated Temperature Limits as a Function of Stress for High Burnup Fuel (60 GWd/MTU) with 5 and 10 year Cooling. ....	5.3

5.3	Sensitivity of Varying Rev. 1 Creep Rates and Rupture Time (Monkman-Grant Coefficient) by a Factor of 2 on Calculated Temperature Limits for High Burnup (60 GWd/MTU) Fuel Cooled for 10 Years.....	5.5
5.4	Sensitivity of Varying Rev. 1 Creep Rates and Rupture Strain (Monkman-Grant Coefficient) by a Factor of 2 on Calculated Temperature Limits for Low Burnup (30 GWd/MTU) Fuel Cooled for 10 years.....	5.5
5.5	Comparison of Calculated Temperature Limits from CSFM Rev. 1 (conservative Monkman-Grant) and Spilker et. al 1996 Model (1% Strain Limit) for High Burnup Fuel (60 GWd/MTU and 10 Year Cooled). ....	5.7
5.6	Comparison of Calculated Temperature Limits from Conservative CSFM Rev. 1 (Bounding Monkman-Grant) and Spilker et. al 1996 Model (1% Strain Limit) for Low Burnup Fuel (30 GWd/MTU and 10 Year Cooled). ....	5.7
5.7	Comparison of Calculated Temperature Limits from CSFM Rev. 1 (Conservative Monkman-Grant) and Siegmann 2000 Model Using Best Estimate Creep and Failure Strain for High Burnup Fuel (60 GWd/MTU and 10 Year Cooled). ....	5.9
5.8	Comparison of Calculated Temperature Limits from CSFM Rev. 1 (Conservative Monkman-Grant) and Siegmann 2000 Model Using Best Estimate Creep and Failure Strain for Low Burnup Fuel (30 GWd/MTU and 10 Year Cooled). ....	5.9
5.9	Comparison of Calculated Temperature Limits from CSFM Rev. 1 (Conservative Monkman-Grant) and Siegmann 2000 Model Using Best Estimate Creep and Conservative Failure Strain (0.499% at 2% Probability) for High Burnup Fuel (60 GWd/MTU and 10 Year Cooled). ....	5.10
5.10	Comparison of Calculated Temperature Limits from CSFM Rev. 1 (Conservative Monkman-Grant) and Siegmann 2000 Model Using Best Estimate Creep and Conservative Failure Strain (0.499% at 2% Probability) for Low Burnup Fuel (30 GWd/MTU and 10 Year Cooled). ....	5.10
5.11	Comparison of CSFM Rev. 1 Calculated Temperature Limits Versus Stress Using a Monkman-Grant Correlation and a Starin Limit Criterion for High Burnup Fuel with 10-Year Cooling.....	5.12

## TABLES

2.1	Previously Recommended Temperature Limits for Dry Storage of Pressurized Water Reactor Spent Nuclear Fuel Based on Past Modeling. ....	2.9
3.1	Summary of Conditions for Creep Tests with Unirradiated Zircaloy .....	3.11
3.2	Summary of Publications with Post-Irradiation Creep Data.....	3.18

## ACRONYMS AND ABBREVIATIONS

ANL	Argonne National Laboratory
BWR	boiling water reactor
CFR	code of federal regulations
CRF	creep reduction factor
CSFM	commercial spent fuel management
CWSR	cold worked stress relieved
DATING	determining allowable temperatures in inert and nitrogen gases
DCCG	diffusion-controlled cavity growth
DOE	Department of Energy
GBD	grain boundary diffusion
GBS	grain boundary sliding
HTC	high-temperature climb
ISG	interim staff guidance
LLNL	Lawrence Livermore National laboratory
LTC	low-temperature climb
MTU	metric ton of uranium
NRC	Nuclear Regulatory Commission
PNNL	Pacific Northwest National Laboratory
PWR	pressurized water reactor
SAR	safety analysis report
SNF	spent nuclear fuel
SRA	stress-relieved annealed

## 1. INTRODUCTION

For more than 25 years dry storage casks have been tested and used to store commercial spent nuclear fuel (SNF) as a passive alternative to high-maintenance pool storage. Moving commercial SNF from reactor spent fuel pools into interim (20- to 40-year) dry cask storage is attractive to nuclear power utilities because, as their spent fuel pools begin to fill up, it enables them to maintain full core off-loading capability in the event of a plant shutdown or need for core maintenance/repair.

Federal regulations (10 CFR Part 72) and the U. S. Nuclear Regulatory Commission (NRC) Interim Staff Guidance (ISG) Document 11 (NRC 2000) for high burnup SNF are in place to protect SNF from gross degradation during its storage. Engineering and analytical methodologies have been developed to prevent overheating and subsequent degradation of the SNF by corrosion and mechanical degradation in dry storage. The purpose of this report is to provide a methodology for cask designers and the regulators to calculate the temperature limits for SNF, with an adequate margin to assure safety and prevent gross degradation of the fuel rods, while in storage. In addition, the information contained in this report will be used by the NRC staff to re-examine the acceptance criteria provided in ISG-11.

The U.S. Department of Energy (DOE) Commercial Spent Fuel Management (CSFM) project sponsored an effort to develop an analytical model for determining allowable temperature limits for SNF during dry cask storage. The analytical model was based on theoretical creep deformation and fracture mechanisms and was supported by creep and creep rupture data from zirconium and zirconium alloys (Chin and Gilbert 1989).

Because of the paucity of creep and creep rupture data from Zircaloy (Zr-2 and Zr-4) used to clad nuclear fuel, the original effort under the CSFM project involved constructing deformation and fracture maps from the data for other alloy systems to predict the behavior of SNF under dry cask storage conditions. At the time the CSFM methodology was developed, the appropriate creep and creep rupture data were not

available to rigorously validate the mechanisms or the map boundaries between mechanisms. The limited data from zirconium and zirconium alloys were used to show behavioral consistency with the maps, where possible. These maps were required to complement existing short-term (< 1 year) creep and creep rupture data on irradiated and unirradiated Zircaloy that were considered inadequate for rigorous extrapolation of cladding stress rupture behavior to the much longer-term (20- to 40-year) dry storage conditions. The CSFM methodology predicted that, for peak fuel rods with burnup levels of up to ~45 GWd/MTU and cooled in spent fuel pools for 5 years prior to dry storage, a nominal temperature limit of ~380°C was required to prevent a failure of any type of the SNF cladding during interim dry storage. The original CSFM methodology thus enabled the calculation of the maximum allowable initial cladding temperature for the dry cask SNF storage. The original CSFM methodology is denoted as CSFM Rev. 0 throughout the remainder of this report.

The NRC is currently evaluating the technical basis of requirements for the storage of high burnup (greater than 45 GWd/MTU) SNF. The NRC, DOE, and U.S. nuclear industry will be conducting research over the next several years to obtain data on the characteristics, mechanical properties, and long-term creep behavior of high burnup SNF cladding. These data will be used to support the licensing basis for storage of high burnup SNF.

As part of this effort, the NRC has funded the Pacific Northwest National Laboratory (PNNL) to develop an interim approach for calculating maximum allowable temperature limits for high burnup spent fuel under dry cask storage conditions. Using newly available data on creep and creep rupture for unirradiated and irradiated Zircaloy cladding, PNNL has worked toward three objectives:

- to modify the CSFM models/mechanisms (i.e., equations) based on new data that are prototypical of SNF cladding;

- to assess damage caused by irradiation and hydriding that occur during in-reactor service, particularly at high burnup, and their effects on the deformation and fracture mechanisms; and
- to update the CSFM Rev. 0 methodology for calculating allowable temperature limits

This report documents PNNL's work to date on the use of new data and theoretical modeling to revise the CSFM methodology. Nearly all of the irradiated creep and creep rupture data collected for this report are new from those used for CSFM Rev. 0. The revised CSFM methodology is denoted as CSFM Rev. 1. Provided in Section 2 are important background information, the regulatory basis and industry need for calculating SNF cladding temperature limits, as well as the ranges of conditions (e.g., pressure and temperature) expected for dry cask storage. Also included in Section 2 is a description of other past methodologies used for calculating cladding temperature limits, including the CSFM Rev. 0 methodology. The creep and creep rupture data selected as the basis for development of CSFM Rev. 1 are summarized in Section 3. Modifications to CSFM leading to CSFM Rev. 1 are presented in Section 4. An example of CSFM Rev. 1 calculated temperature limits are presented in Section 5. Findings, conclusions and recommendations are presented in Section 6. The references cited in the text of this report are provided in Section 7. Appendix A contains a description of the computer code DATING (Determining Allowable Temperatures in Inert and Nitrogen Gases) Rev. 1 that employs CSFM Rev. 1 methodology to calculate maximum allowable temperature limits.

## **2. BACKGROUND**

This section provides important background information on the regulatory basis and needs for SNF dry cask storage temperature limits; expected design basis conditions; and a history of past methodologies for determining temperature limits including a discussion of the original CSFM Rev. 0 methodology.

### **2.1. Regulatory Basis and Need for Temperature Limits**

The current U.S. regulations for the storage of spent nuclear fuel (10 CFR Part 72) have three general objectives. The first objective, stemming from regulatory requirements, is to confine the fuel safely; safe confinement is accomplished by providing substantial and redundant confinement boundaries between the spent fuel and the environment. The second, based on the first requirement, is to prevent unacceptable degradation of the fuel cladding during the storage period. The third objective is that the storage system be designed to prevent criticality and to allow ready retrieval of the spent fuel from the storage system. This third objective is based on NRC's interest to achieve efficiency and compatibility between storage and transportation requirements for dual-purpose casks (NRC, 2000). Thus, the U.S. regulations for storage of spent fuel require that the spent fuel cladding be protected during storage against degradation that leads to gross rupture. Alternatively, the fuel must be confined such that degradation of the fuel during storage will not pose operational safety problems with respect to its removal from storage.

The U.S. regulations for transportation (10 CFR Part 71) do not have specific requirements to preserve cladding integrity during transportation. The current transportation regulations emphasize the ability of the cask to provide the necessary level of containment of the spent fuel to protect public health and safety. This general philosophy requires that the geometric configuration of the spent fuel in a transportation cask be preserved under the conditions specified for normal and hypothetical accident conditions as analyzed and specified in a licensee's Safety Analysis Report (SAR). Thus, using the conditions and tests prescribed by the regulations for normal conditions of transportation, a licensee must ensure that the spent fuel will remain subcritical.

Additionally, the licensee must demonstrate that there will be no loss or dispersal of spent fuel, no significant increase in radiation levels at external surfaces, and no substantial reduction in the effectiveness of the spent fuel package to provide radiation protection. Similarly, under the regulation's prescribed hypothetical accident test conditions, a licensee must ensure that any damage to the spent fuel would not result in criticality or compromise the shielding and containment effectiveness of the package.

One way to ensure that these regulations are met is to demonstrate that the cladding will not degrade at temperatures less than or equal to a predetermined temperature limit and provide assurance that this temperature limit is not exceeded during dry storage. This limit is generally calculated from the information on the degradation phenomena, environmental conditions, and mechanical loads on the cladding. More specifically, cladding integrity of spent fuel is ensured by maintaining calculated cladding temperatures below prescribed limits associated with expected degradation (e.g., pinholes and cracks) for normal conditions of storage. As such, creep rupture has been determined to be the dominant failure mechanism of spent fuel cladding (Blackburn et al. 1978; Peehs and Fleisch 1986; NRC 1997). To calculate the maximum allowable cladding temperature limits, NRC licensees customarily have used the CSFM methodology as described by Levy et al. (1987) and Cunningham et al. (1987). For normal conditions of storage, Zircaloy fuel cladding temperature limits calculated using this methodology typically are below 380°C for fuel assemblies cooled for 5 years. Similarly, cladding temperature limits are typically 340°C for fuel assemblies cooled for 10 years. The temperature limits will be more restrictive with increased fuel cooling time, largely because of the slower fuel heat decay as a function of time. Temperature limits also decrease due to the increased rod pressures and stress in high burnup fuel.

## **2.2. Expected Design-Basis Conditions**

The design-basis conditions for dry storage are initial storage temperature, temperature decay rate, and cladding stress due to the internal pressure of the fuel rod. The peak rod (conservative) cladding hoop stress generally used for today's high burnup fuel (peak

rod-average burnup of 60 GWd/MTU) are between 120 to 145 MPa, depending on the fuel rod design. These stresses correspond to maximum cladding temperature limits between 310°C and 370°C allowable for storage, depending on the cooling time before dry storage, i.e., temperature decay rate. Because the high burnup SNF cladding is a subject to increased oxidation and hydriding, a correction for clad thinning due to oxidation and hydride rim formation must be included in the stress calculation. This issue is further discussed in the following sections.

The cladding temperature and hoop stress both decay with time as illustrated in Figures 2.1 and 2.2 for high and low burnup fuel, respectively, with 10 years' cooling prior to dry cask storage and the same initial hoop stress of 120 MPa. Generally, low burnup fuel (< 45 GWd/MTU) will have a lower cladding hoop stress than the 120 MPa assumed in Figure 2.2, due to lower internal rod pressure and less clad thinning due to corrosion and hydride rim. However, this is not always the case particularly for a high duty plant with average discharge burnups above 30 GWd/MTU or high corrosion. A high duty plant is one that has high linear power rates and/or high primary coolant outlet temperatures. The highest duty plants are those with both high power and high outlet temperature.

The initial temperatures in Figures 2.1 and 2.2 are calculated with CSFM Rev. 1, but the rate of the temperature and stress decay with time in storage depends only on the burnup and the elapsed time since fuel discharge from the reactor. As noted above, the rate of temperature and stress decay are important in determining the dry cask storage temperature. For example, fuel that cools quickly will have a higher temperature limit than slow-cooling fuel. The temperature limit for both high and low burnup fuel increases approximately by 40 °C when the cooling time is only 5 years as compared to the 10-year cooled fuel in Figure 2.1 and 2.2. However, slow-cooling fuel has had a longer cooling time and a lower heat load such that more of this fuel can be placed in a single cask. Therefore, there is an optimum balance between cooling time and temperature limits to maximize the amount of fuel that can be placed in a single cask.

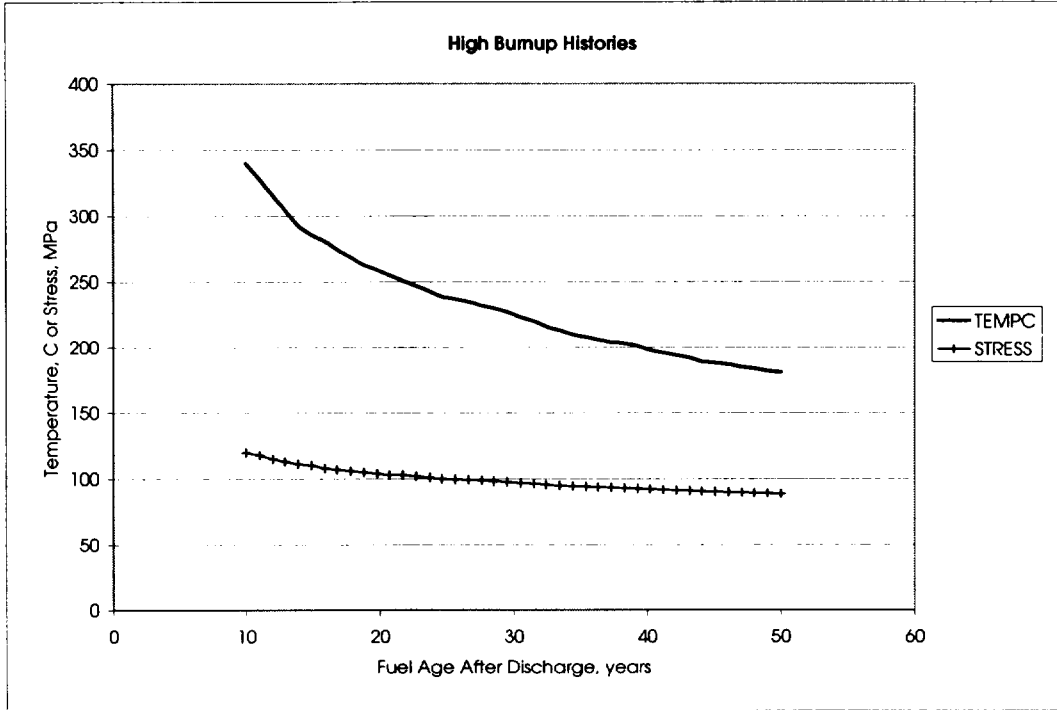


**Figure 2.1 Cladding Temperature and Stress Decay for High Burnup (PWR 60 GWd/MTU) and Starting Stress of 120 MPa.**

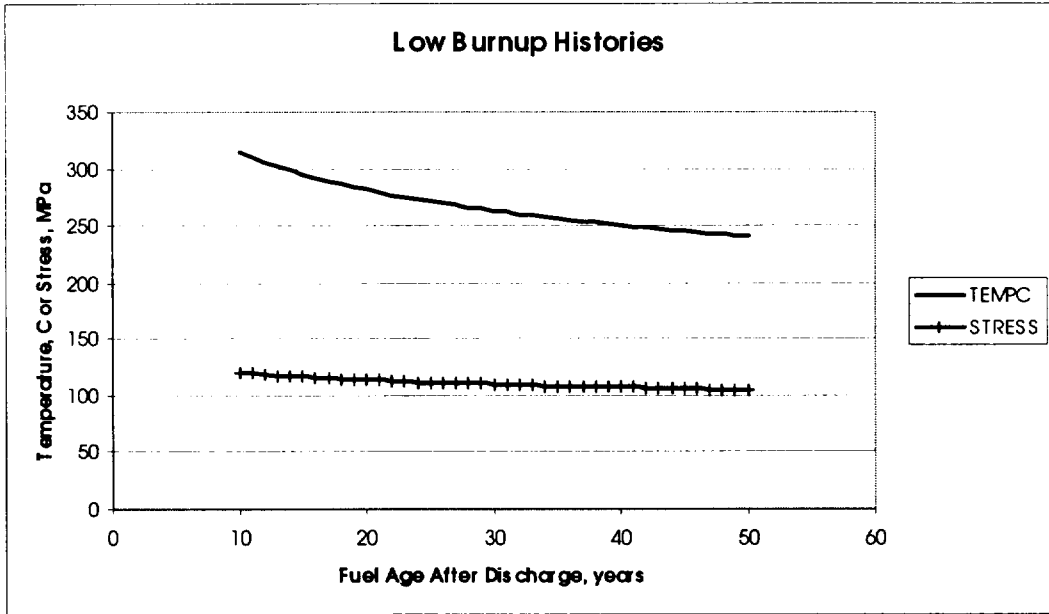


**Figure 2.2 Temperature and Stress Decay of Low Burnup (PWR 30 GWd/MTU) Fuel Using Helium Cooling Curve from Levy et al. (1987), and Starting Stress of 120 MPa.**

Many utilities are mixing both low and high burnup fuel with different cooling times in the same dry storage casks to maximize the amount of high burnup fuel that can be stored in a single cask. This makes the calculation of temperature versus time for the rods in the cask much more complex because different fuel has different heat loads as a function of time. This also makes the determination of a single temperature limit for the fuel more complex.

### **2.3. History of Temperature Limit Methodologies**

Initial predictions of temperature limits for pressurized-water reactor (PWR) Zircaloy cladding were based on empirical extrapolations of existing short-term (< 1 year) unirradiated creep rupture data (Blackburn et al. 1978). Blackburn et al. (1978) recommended a temperature limit of 380°C at a maximum initial stress of 140 MPa (Table 2.1). This approach used the Larson-Miller parameter developed from a limited amount of stress and rupture time data for unirradiated Zircaloy at high stresses.

Peehs and Fleisch (1986) derived a temperature limit of 450°C at a maximum initial stress of 70 MPa (Table 2.1) by extrapolation of an empirical creep strain versus time correlation developed from unirradiated Siemens Zircaloy cladding and subsequently normalized to irradiated Siemens FRG-2 Zircaloy-4 (tested at 395°C and a hoop stress of 70 MPa). A uniform strain limit of 1% was assumed by Peehs and Fleisch for this calculation.

More recently Spilker et al. (1997) have shown that the unirradiated FRG-2 material was the most creep-resistant of seven unirradiated cladding types tested by Siemens and was 20 times more creep-resistant, i.e., lower creep rates, than Siemens Type 1 fuel cladding. As will be shown in Section 4 of this report, the FRG-2 cladding creep appears to be atypical of the creep behavior (slower creep) of most Zircaloy cladding types tested by other fuel manufacturers. It should be noted that there is still a large scatter in creep behavior (up to a factor of 100) for different cladding types that appears to be due to fabrication and microstructural differences. Peehs and Fleisch (1986) did not attempt to account for the less creep-resistant fuel cladding types in their model development and,

therefore, their methodology lacked applicability to cladding types other than the FRG-2 cladding for determining dry cask storage limits. Therefore, the Peehs and Fleisch approach tends to predict higher cladding temperature limits than most other approaches. In addition the temperature limits calculated by these authors were for a relatively low cladding stress of 70 MPa even for low burnup fuel. This is one of the reasons for the large difference (in addition to the non-conservative creep model) in calculated maximum initial storage temperatures between Peehs and Fleisch and those calculated earlier by Blackburn et al. (1978).

Because most material deformation and failure mechanisms change with temperature and stress it was recognized that an empirical approach had major problems particularly since they were either not based on applicable data (Peehs and Fleisch 1986) or the data were not in the range for dry cask storage (Blackburn et al. 1978). For this reason the DOE sponsored the development of the CSFM methodology, based on theoretical material deformation and fracture mechanisms over a wide stress and temperature range, for use in determining temperature limits for interim dry storage of SNF prior to permanent storage at Yucca Mountain.

The CSFM Rev. 0 (Chin et al. 1986; Tarn et. al 1986; Chin and Gilbert 1989) predicts time-to-rupture based on theoretical deformation and fracture models that were initially based on other (non-zirconium) alloys and were then normalized to the creep and fracture data of unirradiated zirconium alloys. To provide conservatism to accommodate less creep-resistant cladding alloys, the Rev. 0 creep models were developed to bound most of the unirradiated creep data available at that time. The Rev. 0 methodology relied on maps of deformation (creep) and fracture (creep to rupture) to determine the dominant creep and fracture mechanisms in the temperature and stress range of interest. The dominant creep mechanisms were found to be high-temperature climb (HTC), low-temperature climb (LTC), and grain boundary sliding (GBS) for dry cask storage conditions. The fracture mechanisms were found to be cavitation power law, as described by a Monkman-Grant relationship (Monkman and Grant 1956), and diffusion-controlled cavity growth (DCCG) fracture mechanisms under dry cask storage

conditions. The DATING Rev.0 code (Simonen and Gilbert 1988) was developed to apply CSFM Rev.0 methodology to the varying temperature and stress conditions of dry cask storage. The Rev. 0 methodology predicted lower temperature limits than those predicted by Blackburn et al. (1978) by about 20°C and over 60°C lower than those predicted by Peehs and Fleisch (1986) for the same initial cladding stress.

Lawrence Livermore National Laboratory (LLNL) (Schwartz and Witte 1987) reviewed the CSFM Rev. 0 methodology and concluded that only the DCCG fracture model was applicable to dry cask storage conditions. Schwartz and Witte proposed changes to the DCCG model coefficients from those used by CSFM Rev. 0. Schwartz and Witte used the Raj and Ashby (1975) DCCG failure equation constants for Zircaloy SNF cladding with a modification to the cavity area fraction for failure to be achieved. Failure was conservatively defined when cavity growth achieves 15% of the area fraction to allow safe handling at the end of the interim dry storage period. A comparison of temperature limits calculated by CSFM Rev. 0 and the Schwartz and Witte model shows that the latter predicted slightly lower SNF temperature limits (~5°C) for low burnup fuel at a stress of 100 MPa (see Table 2.1) where the DCCG model is predicted to be active by Rev. 0.

Pescatore and Cowgill (1994) also performed a review of the CSFM Rev. 0 methodology for the Electric Power Research Institute and concluded that it predicted temperature limits lower than those published by Peehs and Fleisch (1986). Pescatore and Cowgill also concluded that temperature limits derived by the CSFM methodology were too conservative. The lower temperature limits of the CSFM model were attributed to the effects of the theoretical model for DCCG, which was not verified by testing. However, it should be noted that use of the DCCG model in CSFM Rev. 0 increases the calculated temperature limit in the temperature and stress range for which this model is applicable, i.e., removal of the DCCG fracture mechanism and use of only the Rev. 0 cavitation power law fracture mechanism decreases the calculated temperature limits.

Spilker et al. (1997) proposed a methodology for predicting temperature limits based on an empirical creep model of creep strain versus time that bounded the data for Siemens

Types 1 through 8 (unirradiated) cladding. The methodology assumed a conservative 1% strain limit. This methodology generally predicts lower temperature limits than those predicted by the CSFM Rev. 0 methodology by 10°C to 20°C depending on stress level, burnup, and cooling time.

Hayes et al. (1999a and 1999b) provided a critical review of the parameters and application of the DCCG model by Schwartz and Witte (1987) and also those DCCG parameters used by CSFM Rev. 0. Hayes et al. also recommended that the DCCG failure mechanism be used for dry cask storage conditions and further recommended more conservative parameters than those previously proposed by Schwartz and Witte or CSFM Rev.0. The parameters recommended by Hayes et al. resulted in significantly lower temperature limits than those calculated using the Schwartz and Witte coefficients or using the CSFM Rev. 0 methodology. A comparison of the Schwartz and Witte and Hayes et al. recommended DCCG rupture models to actual time-to-rupture data is provided in Section 4.2.3 of this report. These comparisons demonstrate that the DCCG failure model does not follow the trends in the rupture data collected in this report.

It should also be noted that the CSFM Rev. 0 fracture map predicts that the DCCG failure mechanism is only active at stresses between approximately 0 to 110 MPa rather than at all stress levels as assumed by Schwartz and Witte (1987) and Hayes et al (1999). Above 110 MPa, the Rev. 0 fracture map predicted that failure was controlled by the cavitation power law creep failure mechanism and, therefore, use of the DCCG mechanism would not be applicable for SNF with design-basis stresses that exceeded approximately 110 MPa. Design stress levels generally increase with increasing burnup such that peak (power) high burnup rods will have stresses between 120 to 145 MPa and higher (depending on amount of corrosion and hydride rim thickness).

A comparison of the cladding design stresses and the corresponding temperature limits as predicted by some of the methodologies discussed above is provided in Table 2.1. The temperature limits in this table were taken from those provided in the references and, therefore, do not have a common value of stress. However, from examination, the Peehs

and Fleisch (1986) methodology is the least conservative, i.e., predicts higher temperature limits, Blackburn et al. (1978) is next, while CSFM Rev.0 and Schwartz and Witte (1987) predict similar temperature limits. Spilker et al. (1997) predict the lowest temperature limits in Table 2.1. Temperature limits are not provided in this table using the recommended DCCG coefficients from Hayes et al. (1999) but due to the large degree of conservatism in this model it is anticipated that predicted temperature limits would be below 300°C for this model and, therefore, is the most conservative of the models discussed.

At the present time, new methodologies are being developed by cask designers to determine temperature limits for the fuel in these casks. Most of these methodologies are based on modifications to the methodologies described above.

<b>Table 2.1 Previously Recommended Temperature Limits for Dry Storage of Pressurized Water Reactor Spent Nuclear Fuel Based on Past Modeling.</b>			
<b>Design Stress, MPa</b>	<b>Temperature Limit, °C</b>	<b>Burnup, GWd/MTU</b>	<b>Investigation</b>
~140	380	~33	Blackburn et al. (1978)
70	400 to 450	40	Peehs and Fleisch (1986)
100	380	45	Chin and Gilbert (1989)
100	~ 375	45	Schwartz and Witte (1987)
80	348 to 357	55	Spilker et al. (1997)

## **2.4. Background of CSFM Rev. 0**

The CSFM Rev. 0 (Chin et al. 1986; Tarn et al. 1986, Chin and Gilbert 1989) was intended to be a reasonably conservative approach for determining temperature limits for dry cask storage in the US. The CSFM Rev. 0 methodology replaced the Blackburn et al. (1978) model and provided an alternative to the Peehs and Fleisch (1986) model. The CSFM Rev. 0 methodology consists of six deformation and six fracture mechanisms that are active in different temperature and stress ranges. Deformation and fracture maps (two dimensional in terms of temperature and stress) were generated for Zircaloy cladding to define the stress and temperature ranges where the different mechanisms were active. The constitutive equations used to construct these maps were based on experimental data where data were available; if data were not available within a given temperature and stress range, then theoretical modeling was used to define the boundaries. The construction of the maps from the constitutive equations is described in Chin et al. (1986).

Of the six deformation mechanisms, only high-temperature climb, low-temperature climb, and grain boundary sliding (either by grain boundary diffusion or lattice diffusion) were believed to be important for the stress and temperature conditions encountered by the cladding for dry cask storage. Therefore, only these three deformation mechanisms had an impact on temperature limits for dry storage.

Of the six fracture mechanisms only the cavitation power law and DCCG fracture mechanisms were believed to be important for the stress and temperature conditions encountered for dry cask storage.

For a changing temperature and stress with time, as for dry storage, the CSFM Rev. 0 methodology assumed a life fraction rule. The life fraction rule assumes that damage from all mechanisms is independent and additive. The life fraction rule can be expressed as

$$1 = \sum_{i=1}^n \frac{\Delta t_i}{\tau_i} = \frac{\Delta t_1}{\tau_1} + \frac{\Delta t_2}{\tau_2} + \frac{\Delta t_3}{\tau_3} + \dots + \frac{\Delta t_n}{\tau_n} \quad (2.1)$$

where

- $\Delta t_i$  = time spent at the  $i^{\text{th}}$  temperature,
- $\tau_i$  = period required to fracture a specimen under the  $i^{\text{th}}$  temperature (isothermal) and stress (isostress) conditions.

When the cumulative fraction, the summation of the life fractions ( $\Delta t_i/\tau_i$ ), reaches one failure is assumed. The time period required for fracture,  $\tau_i$ , is calculated from the strain to failure ( $\epsilon_F$ ) divided by the steady-state creep rate. The CSFM Rev. 0 methodology determined failure strain ( $\epsilon_F$ ) based on the temperature, stress and the creep-to-rupture mechanism for this temperature and stress. The CSFM Rev. 0 methodology determined the steady-state creep rate based on the temperature, stress and the creep mechanism for this temperature and stress.

A more detailed description of the deformation and fracture mechanisms, as well as the constitutive equations for these mechanisms and the data on which they are based, are provided in more detail in Chin et al. (1986), Tarn et al. (1986), and Chin and Gilbert (1989). A description of the DATING code that was created to predict temperature limits for dry cask storage using the CSFM Rev. 0 methodology is described in Simonen and Gilbert (1988).

### **3. DEVELOPMENT AND DESCRIPTION OF CREEP AND RUPTURE DATABASE**

This section discusses the creep and creep rupture test results used to develop the CSFM Rev.1 methodology.

Most of the creep data were obtained from references that report creep tests with pressurized-tube specimens. Most of the tube specimens were stressed by pressurization with helium, argon, or oil. The pressurizing medium affects the creep-to-rupture results. Helium is released first from the specimen through micron-sized microcracks that form during tertiary creep. Increasingly larger microcracks are required to release argon and oil. Therefore, the time-to-rupture and the strain at rupture are the highest for oil and the lowest for helium. It would be ideal to use only the results of those pressurized tests that used argon or helium as a pressurization fluid, but doing so would limit the creep-to-rupture data to a database too small for modeling rupture.

The simultaneous changes in volume, diameter, and wall thickness for pressurized-tube tests with a constant mass of ideal pressurizing gas (i.e., closed ends) compensate to maintain constant true stress as the test article strain increases. During constant pressure tests (constant engineering stress), the true stress increases with strain. For the uniform hoop strains of interest during dry storage (< 4%), the differences between engineering and true stress are less than 10%. The differences between engineering and true stress are negligible within the scatter of the creep data (a factor of 3 or greater) for strains up to 4% or 5%. The scatter in uniform creep strain to failure is significant and varies from 1% to 7% while the total strain to failure generally varies to an even greater extent from 1% to 12% or more.

The creep rupture database developed in this work was found to best fit a Monkman-Grant relationship (Monkman and Grant 1956) with a modification to the Monkman-Grant coefficient from that used in CSFM Rev. 0, as discussed in the following section. The Monkman-Grant relationship determines time-to-rupture and is only dependent on

steady-state creep rate; therefore, steady-state creep rate needs to be determined from creep strain versus time data.

The creep database developed in this study was used for derivation and validation of the steady-state creep rate relationships presented in the following section that are a function of stress, temperature, and neutron fluence. The experimental creep strain and strain rate data were tabulated along with the three independent parameters of stress, temperature, and neutron fluence. A limited amount of data also included corrosion (oxide layer thickness) and hydride levels and these data were also tabulated when available.

The values of steady-state creep rate were often not readily available from presented creep strain data because some of the slow creep tests were terminated within the primary creep stage before achieving steady-state (possibly Einziger and Kohli 1984); some tests only provided end of test uniform strain data that included both primary and steady-state creep (example Goll et al 2001); and other tests only included total strain to failure (primary + steady-state + tertiary) (example Mayuzumi and Murai 1993 and Chung et al. 1987). Some of the data from the references did allow determination of steady-state creep rate because either creep strain versus time data or secondary creep rates were provided (example Spilker et al. 1997 and Limon et al. 2000).

Because the quality of developed relationships increases with the amount of experimental data considered for their derivation and validation, an attempt was made to include as many data points as possible without compromising the conservatism of the methodology. Therefore, the creep strain data were examined to determine whether the use of uniform strain or total strain to failure divided by the terminal time of the test would be a reasonably conservative estimate of steady-state creep rate. Examination of complete strain-time curves to rupture for unirradiated and irradiated cladding indicates that the average strain rate determined from total strain (primary + steady-state + tertiary) is usually less than 3 times greater than the minimum or true steady-state strain rate (Bouffieux and Rupa 2000; Limon et al. 2000; Mayuzumi and Murai 1993). Strain rates deduced from uniform strain (primary + steady-state) will be up to 2 times greater than

the true steady-state rate. For this reason, use of uniform rather than total strain is a better estimate of the steady-state strain rate. It should be noted that a factor of 2 to 3 conservatism in steady-state creep rate is not excessively conservative because, as will be shown in this section, there is up to a factor of 5 variation in creep rate from similar Zircaloy cladding types and a factor of 10 to 20 among different irradiated Zircaloy cladding types (different fabrication parameters) similar to those differences in the SNF inventory. Therefore, the use of uniform or total strains to determine steady-state creep rate is not believed to be overly conservative considering the variability in creep rate data.

For those references that reported an end-of-test strain (either uniform or total) and time (Chung et al. 1987, Goll et al. 2001; and others) the steady state strain rate was computed as the ratio of the final strain to time or rupture strain to rupture time resulting in a conservative estimate of steady-state creep. If both total and uniform strains are cited in the reference the latter was used to determine the steady-state creep rate.

Those references that provided strain-time curves (Billaux et al. 2000; Bouffioux and Rupa 2000; Limon et al. 2000; and others), true steady-state strain rate was estimated as a slope of the portion of the creep curve that corresponded to the secondary stage creep.

Dry cask storage conditions provide a narrow stress and temperature range, where limited amounts of experimental creep and creep rupture data were available. In addition, different cladding fabrication techniques employed by different fuel vendors result in different creep behavior. Therefore, the approach taken in this study was to develop the relationship that would bound the experimental data not only in the range characteristic for dry cask storage, but also outside this range. This included data from the tests performed on unirradiated cladding, low-burnup SNF cladding, and tests performed at high stresses. Including the experimental data outside the immediate range of interest allowed a more extensive validation of the CSFM Rev. 1 models. The inclusion of creep from unirradiated and low burnup cladding allows the CSFM Rev. 1 methodology to be applied to low, medium and limited high burnup spent fuel (i.e., without oxide

spallation); and to also apply to spent fuel subjected to temperatures that allow cladding annealing. The CSFM Rev.1 methodology assumes that spent fuel cladding that becomes fully annealed will have creep rates the same as unirradiated cladding and uses the unirradiated creep rate equations presented in Section 4.1.

The creep data for unirradiated cladding are discussed in Section 3.1 and summarized in Table 3.1. Creep data for the irradiated cladding specimens are discussed in Section 3.2 and summarized in Table 3.2. In Section 3.3, the creep rupture data are discussed. Findings based on examination of the data are summarized in Section 3.4.

### **3.1. Creep of Unirradiated Cladding**

The creep strain database consists of nearly 300 data points (184 from unirradiated and 100 from irradiated Zircaloy cladding), and the tabulation includes temperature, stress, fluence and secondary strain rate. Only Zircaloy creep data at temperatures less than or equal to 420°C were selected for this database in order to stay near the temperature range for dry cask storage. However, the stress range of the creep data was not limited to dry cask storage conditions other than limiting creep rates to below  $10^{-5} \text{ sec}^{-1}$ . Less than 5% of the current unirradiated creep database was taken from the CSFM Rev. 0 developed database such that over 95% of this data is new for CSFM Rev. 1 development. A large amount of the CSFM Rev. 0 database was either at temperatures above 420°C or was from zirconium or zirconium alloys atypical of those used by fuel vendors. Therefore, most of these earlier data were not included in the current database. The current unirradiated creep database is from Zircaloy cladding similar to that used by fuel vendors for fuel rod fabrication.

Published creep results for unirradiated Zircaloy-2 and Zircaloy-4 show a large variability in behavior. Without a comprehensive knowledge of the reasons for the variability, an accurate description of all results cannot be provided by a single relationship. Creep of unirradiated Zircaloy at high stresses has been found to depend on the fabrication history that varies between different fuel vendors. Frenkel and Wiesz

(1973) showed that the creep rate during testing at 350°C and 400°C could be reduced significantly by the thermo-mechanical treatment. The creep rate decreased by up to a factor of 20 with increasing annealing temperatures. These creep tests were performed in the viscous glide domains, where larger grains retard creep. A reduction in creep with increasing annealing temperature and grain size is consistent with the theoretical (CSFM) model predictions for these mechanisms.

Another example of the variability in the creep behavior for unirradiated Zircaloy-4 with fabrication processing is provided by Spilker et al. (1997). They presented creep data for eight fabrication types of Siemens Zircaloy-4 cladding. The creep strains were progressively less for cladding Types 1 through 8. Creep testing on unirradiated and irradiated Type 8 (FRG-2 cladding) demonstrated that this was the most creep-resistant of the eight cladding types. Similar to the results of Frenkel and Weisz (1973), creep was reduced between Type 1 and Type 8 by a factor of 20. Spilker et al. provided no information on differences in the characteristics of the eight cladding types. The variability of the creep behavior is most likely due to variations in the fabrication methods affecting the microstructure and creep. Consistency in the creep behavior of the least creep-resistant Zircaloy-4 cladding Type L1 (Frenkel and Wiesz 1973) and the least resistant Type 1 (Spilker et al. 1997) is illustrated in Figure 3.1 by the creep curves for tests at 400°C.

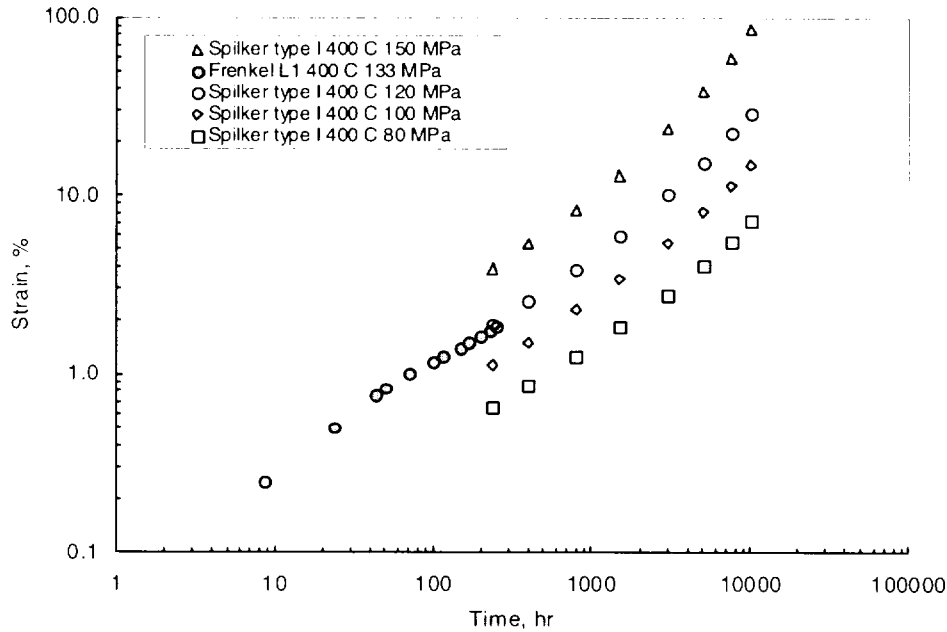


**Figure 3.1 Evidence of Consistency in the Creep Behavior of Unirradiated Cladding between Frenkel and Wiesz (1973) and Spilker et al. (1997).**

The range of test conditions for creep investigations with unirradiated cladding that were reviewed are summarized in Table 3.1. Only creep tests with strain rates less than  $10^{-5} \text{ sec}^{-1}$  were included in this database, because higher creep rates are not of interest for dry cask storage. A plot of the temperature and stress range of the unirradiated creep data shows that it covers a wide range of conditions (Figure 3.2). The figure also shows a large amount of data within the design basis range (shown as a narrow box) for dry cask storage.

Bell (1963) investigated the effect of hydrogen on the creep of Zircaloy-2. The creep tests were conducted on Instron creep machines and carried out to include primary and secondary creep stages. Reported results included steady-state creep rate for all, and strain-time curves for selected test specimens.

Billiaux et al. (2000) reported strain-time curves for both unirradiated and irradiated Siemens cold-worked-stress-relieved (CWSR) Zircaloy-4 cladding. The tests were at

different temperatures and different stress states. Steady-state creep was reached in both tests.

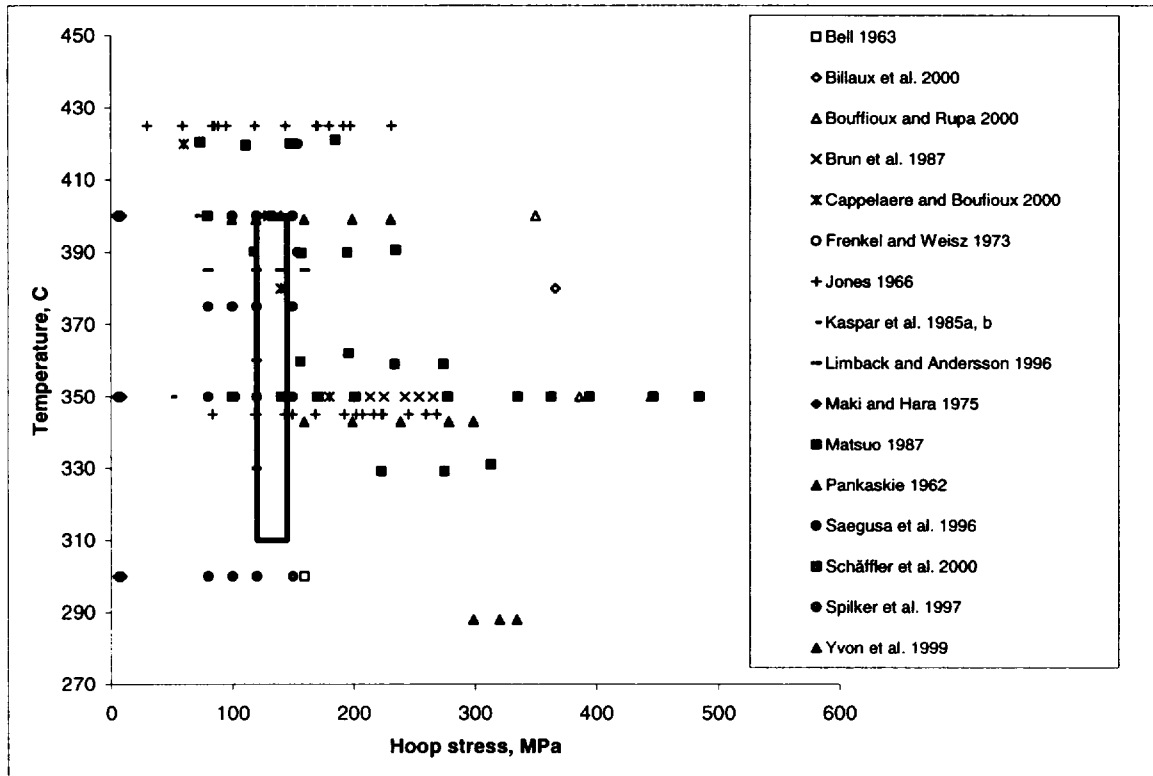


**Figure 3.2 Temperature and Stress Range of Unirradiated Creep Data and Design Basis Range (Narrow Box) for Dry Cask Storage.**

Bouffiuox and Rupa (2000) investigated the effects of uniformly distributed hydrogen on the creep of Framatome unirradiated CWSR Zircaloy-4 cladding. Strain-time plots and steady-state strain rates were included for cladding pressurized with oil, cladding pressurized with argon, and uniaxial cladding specimens. One pressurized cladding test and three uniaxial creep tests were conducted to rupture. All other tests were terminated in the steady-state creep region. Increasing the uniform hydrogen contents in the range of 11 to 1,080 ppm reduced the creep strains and the steady-state strain rates without significantly affecting the fracture strain. These results are qualitatively similar to earlier results on the effect of up to 1,075 ppm uniform hydrogen on the axial creep properties of annealed Zircaloy-2 at 300°C and 400°C (Bell 1963) that demonstrated a reduction in creep rate. The Bouffiuox and Rupa (2000) data suggest that cladding creep is reduced by the introduction of hydrogen. However, it is difficult to separate hydrogen and

irradiation effects because both reduce creep rates for some mechanisms and their combined effect on high burnup cladding does not appear to be additive. Also, SNF cladding has the majority of the hydrogen at the cladding surface (rim) rather than being uniformly distributed. Therefore, these test specimens are atypical of SNF cladding with respect to hydrogen distribution that appears to impact cladding ductility, i.e., failure strains (see Sections 3.3 and 4.3.3).

Brun et al. (1987) evaluated the uniaxial strain rate behavior of recrystallized Zircaloy-4 bar. The creep tests were carried out using dead-load creep machines. Reported data included secondary strain rates and corresponding stresses.

Cappelaere and Bouffioux (2000) made a presentation reporting creep strain versus time from pressurized Zircaloy-4 cladding. Experimental results were presented in the form of strain-time curves featuring primary and secondary creep stages.

Frenkel and Weisz (1973) reported results of the creep testing of Zircaloy 4 cladding tubes by means of gaseous internal pressurization. Strain-time curves featuring primary and secondary creep stages were presented.

Jones (1966) analyzed experimental data obtained by Shober et al. (1957) on the secondary creep rate as a function of stress of annealed and cold-worked Zircaloy-2. The creep rates at the lowest stress values were consistent with the Coble creep mechanism. At higher stresses, the stress exponent increased beyond the linear dependence observed for the Coble mechanism.

Kaspar et al. (1985a, 1985b) reported pressurized cladding creep strain data for unirradiated KWO and FRG-2 cladding. Two duplicate creep tests were conducted with KWO cladding at 50 MPa hoop stress and 350°C, and four duplicate creep tests were conducted with FRG-2 cladding at 70 MPa and 395°C with strain measurements for durations up to 8,000 hours. Strain-time pairs were tabulated covering primary and secondary creep stages.

Limback and Andersson (1996) reported creep strain and steady-state strain rate data for unirradiated Sandvik Zircaloy-2 and -4 cladding. Reported experimental data included plots showing creep strain versus time, as well as a tabulation of primary and secondary creep strains for several stresses and temperatures. The data was analyzed using the modified Matsuo (1987) model that was calibrated and verified.

Maki and Hara (1975) reported the results of very low stress creep tests obtained by externally pressurizing Zircaloy-2 cladding with argon gas. These data, generated at hoop stresses of 5.55 to 8.95 MPa, provide creep rates at the lowest values of hoop stress. Experimental results were presented in the form of strain-time curves featuring primary and secondary creep stages.

Matsuo (1987) reported test results for gas pressurized Zircaloy-4 cladding. Strain-time creep curves, as well as the steady-state creep rate and saturated primary-creep strains, were reported. The stress exponent on the creep rate was 2.1, similar to that for grain boundary sliding by grain boundary diffusion; however, the temperature dependence was consistent with lattice diffusion. The proposed transient creep equation was similar to the Lagneborg (1978) equation and that later described by Limback and Andersson (1996).

Pankaskie (1962) investigated creep properties of Zircaloy-2 for design application. The creep measurements were conducted during tests performed to rupture, and tests that reached secondary, or only primary stages.

Saegusa et al. (1996) reported strain-time curves for unirradiated Zircaloy-4 cladding tested at 154 MPa hoop stress and temperatures of 390°C and 420°C. The tests extended into the range for steady-state creep, and the experimental strain-time curves were included in the report.

Schäffler et al. (2000) reported values of secondary strain rate measured for a wide stress range. The steady-state creep rate data from Schäffler et al. (2000) at 350°C were the

most significant for identifying potential revisions to the CSFM methodology because they were within the design-basis stresses and temperatures expected for dry storage and illustrate the transition in creep by viscous grain boundary sliding by grain boundary diffusion to climb/glide mechanisms. Hoop stress ranged from 100 to 445 MPa for the Framatome Zircaloy-4 cladding (unirradiated) and from 300 to 700 MPa for irradiated cladding to fluences of 0.6, 0.8, 2.4, 4.5, and  $8.5 \times 10^{21}$  n/cm<sup>2</sup>.

Spilker et al. (1997) reported creep test results for duplicate tests of unirradiated Zircaloy-4 Type 1 cladding at 250°C to 400°C at hoop stresses from 80 to 150 MPa. Duplicate tests for five other cladding types were presented for the ranges of 375°C to 387°C and 80 to 150 MPa hoop stress. Large differences in creep strain rates were observed for the different cladding types. As stated earlier, the differences were attributed to unspecified differences in composition and metallurgical state of the cladding resulting from possibly different manufacturing processes. Experimental results included strain time-pairs tabulated for specific testing conditions covering primary and secondary creep stages.

Yvon et al. (1999) reported creep test results for unirradiated Zircaloy-4 at 350°C with internal oil pressurization that resulted in a hoop stress of 445 MPa. The strain-time curve presented in the report featured primary, secondary and tertiary creep stages.

<b>Material</b>	<b>Hydrogen content, ppm</b>	<b>Test Details</b>	<b>Stress, MPa</b>	<b>Temperature, °C</b>	<b>Reference</b>
Zr-2 coolant tubes	14-1075	Instron Creep Machine	80, 159	300, 400	Bell (1963)
Siemens CWSR Zr-4 Cladding	Not specified	Axial Creep	423	380	Billaux et al. (2000)
Framatome CWSR Zr-4 Cladding	6-1040	Pressurized Tube and Uniaxial	140, 200, 350, 386	350, 400	Bouffieux and Rupa (2000)
Zr-4 Bar	7	Axial Creep	184 to 223	350	Brun et al. (1987)
Framatome CWSR Zr-4 Cladding	6-1000	Pressurized Cladding	60 to 180	350 to 420	Cappelaere and Bouffieux 2000
Zr-4 Tubing	Not specified	Pressurized Tube	133	400	Frenkel and Wiesz (1973)
Annealed and Cold Worked Zr-2	Not specified	Axial Creep	14 to 310	345, 425, 500	Jones (1966)
Siemens Zr-4 KWO cladding	Not specified	Pressurized Cladding	50	350	Kaspar et al. (1985a, 1985b)
Siemens Zr-4 FRG-2			70	395	
Sandvik Zr-2/-4 Cladding	Not specified	Pressurized Cladding	80 to 160	330 to 400	Limback and Andersson (1996)
Zr-2 Cladding,	Not specified	External Pressure	5.55 to 8.95	300, 350, 400, 450	Maki and Hara (1975)
Zr-4 Cladding	14-16	Gas Pressurized Cladding	49 to 314	330 to 420	Matsuo (1987)
Zr-2 sheet	Not specified	Axial Creep	100 to 382	288 to 399	Pankaskie (1962)
Zr-4 Cladding	Not specified	Pressurized Cladding	154	390, 420	Saegusa et al. (1996)
Framatome Zr-4 Cladding	Not specified	Pressurized Cladding	100 to 770	350	Schäffler et al. (2000)
Siemens CWSR Zr-4 Cladding	Not specified	Pressurized Cladding	80 to 150	250 to 400	Spilker et al. (1997)
Framatome Zr-4 Cladding	Not specified	Oil Pressurized Cladding	445	350	Yvon et al. (1999)

### 3.2. Creep of Irradiated Cladding

The very small amount of creep data available from irradiated cladding during development of the original CSFM (Rev. 0) methodology showed little difference in creep rates for unirradiated and irradiated cladding. The irradiated cladding tests were limited to the highly creep-resistant Siemens FRG-2 and KWO cladding types (Kaspar et al. 1985a, 1985b). The nominal strains and steady-state strain rates of unirradiated and irradiated FRG-2 cladding agreed within a factor of 2. The strains and strain rates for unirradiated and irradiated Siemens KWO cladding were essentially the same.

The references with creep data from irradiated cladding used to develop the CSFM Rev. 1 methodology are summarized in Table 3.2. Of these references only the Kaspar et al. data were used for developing CSFM Rev. 0. A plot of the temperature and stress range of the post-irradiated creep data from Table 3.2 shows that only ten data points are within the design basis range (narrow box) for dry cask storage (Figure 3.3). These ten data points are from Mayuzumi and Murai (1993), Cappelaere and Bouffioux (2000), Limon et al. (2000), and Einziger and Kohli (1984). It appears that two data points from Cappelaere and Bouffioux are identical to those from Limon et al., and are most likely the same data. Furthermore, Cappelaere and Bouffioux are listed as co-authors in the Limon et al. paper. In addition, the Einziger and Kohli data are of limited value for the model development because of the large scatter in this data (see Section 4.4).

Billaux et al. (2000) reported strain-time curves for irradiated Siemens CWSR Zircaloy-4 cladding tested at 423 MPa and 350°C. Steady-state creep was reached before the test was terminated. No information was provided on test conditions or neutron fluence. Steady-state creep was reached in both tests.

Bredel et al. (2000) reported creep results for argon-pressurized, Framatome SNF cladding. The average hydrogen content was 200 ppm corresponding to a 25- $\mu\text{m}$  corrosion layer. The average burnup was 47 GWd/MTU for specimens prepared from

two similar fuel rods. The tests were terminated after about 40 days. Creep curves presented in the report included primary and secondary stages.

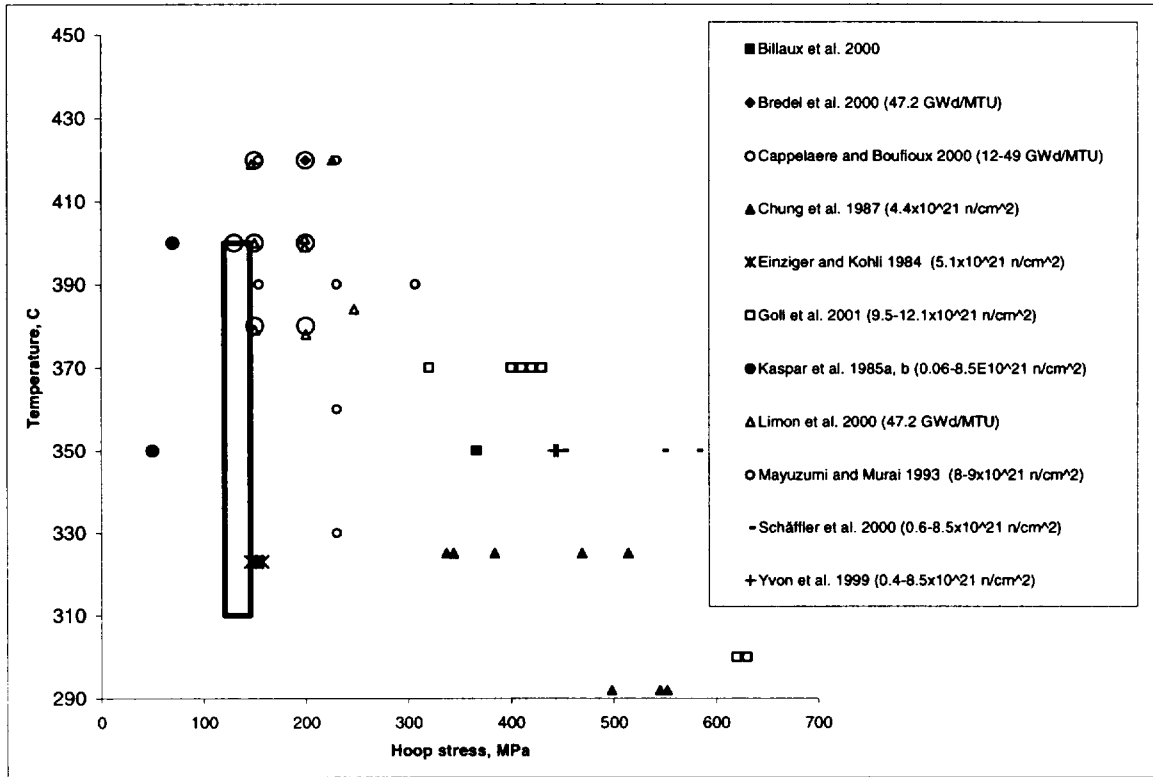


**Figure 3.3 Temperature and Stress Range of Post-Irradiated Creep Data and Design Basis Range (Narrow Box) for Dry Cask Storage.**

Cappelaere and Bouffieux (2000) made a presentation summarizing some of their latest creep strain-time data and a creep model for Framatome Zircaloy-4 SNF cladding. The data and model addressed the stress range of 60 to 200 MPa and the temperature range of 350 to 420°C at neutron fluence values of 0 to  $9 \times 10^{21}$  n/cm<sup>2</sup> (E > 1MeV). The presentation included creep curves featuring primary and secondary stages.

Chung et al. (1987) investigated short-term (108 to 237 hours) stress rupture of Zircaloy-4 SNF cladding from the H.B. Robinson plant. The steady-state creep rates were conservatively estimated from the ratio of the total failure diametral strain (primary + steady-state + tertiary) to the failure time. The tertiary strain for these samples is believed to be relatively small because the total strains were low and micrographs of the failure location confirmed this. Therefore, the steady-state rates are expected to be a

factor of two or less than the actual steady-state strain rates. The Chung et al. results from tests of the Big Rock Point SNF Zircaloy-2 cladding were not used because the failure times and strains may have been reduced by the high fission gas and iodine releases during irradiation.

Einzigler and Kohli (1984) investigated the creep behavior of five full-length tubes of Westinghouse Zircaloy-4 SNF cladding at 323°C and average hoop stresses of ~150 MPa. The average neutron fluence is estimated to be  $\sim 5 \times 10^{21}$  n/cm<sup>2</sup> (E > 1 MeV). The steady-state creep rate was estimated from the ratio of the strain at the end of the test to the test period (31 to 2101 hours). Because the largest measured creep strain was only 0.157%, these strains include a significant amount of primary creep such that the estimated steady-state creep rates may be up to a factor of 2 greater than actual.

Goll et al. (2001) conducted short-time creep and rupture tests with stresses between 320 to 630 MPa on Siemens Zircaloy-4 SNF cladding irradiated to 9.5 and 12.1 × 10<sup>21</sup> n/cm<sup>2</sup> (E > 1 MeV) and rod average burnups of 54 and 64 GWd/MTU, respectively. The tests were conducted by pressurizing the cladding with oil at 300°C and 370°C. Published results included uniform plastic elongation reported for specific stresses. Steady-state strain rates were conservatively estimated from the ratio of the uniform plastic strain to the test period (13 to 189 hours). Specimens that ruptured at 370°C achieved uniform strains from 4.5% to 6%. One specimen ruptured at 300°C with a uniform strain of ≥ 2.5%. The oxide levels varied between 5 μm and 94 μm depending on the axial position of the creep sample taken from the fuel rod.

Kaspar et al. (1985a, 1985b) reported pressurized cladding creep strain data for irradiated KWO and irradiated FRG-2 cladding. Four creep tests with irradiated KWO cladding were conducted at 50 MPa hoop stress and 350°C. Eight creep tests with irradiated FRG-2 cladding were conducted at 70 MPa and 395°C. Strain measurements were reported for test durations up to 8,000 hours. The creep reduction factor for the KWO cladding was ~1. For the FRG-2 cladding, the creep rate reduction factor was ~2. Strain-time pairs were tabulated covering primary and secondary creep stages.

Limon et al. (2000) published creep strain-time curves for Framatome SNF cladding irradiated to  $\sim 8.5 \times 10^{21}$  n/cm<sup>2</sup> ( $E > 1$  MeV) neutron fluence. The tests were conducted for periods of 20 to 60 days within the temperature range of 380°C to 420°C and hoop stresses from 150 to 250 MPa and included primary and secondary creep stages. The specimen tested at 420°C and 226 MPa ruptured in 42 days with a uniform strain of  $\sim 4.5\%$  and a total strain of  $\sim 10\%$ . Thus, the creep curve corresponding to the latter test included primary, secondary and tertiary creep stages.

Mayuzumi and Murai (1993) performed post-irradiated creep tests with Mitsubishi SNF Zircaloy-4 cladding pressurized with argon gas after being irradiated to neutron fluences estimated to be in the range of 8 to  $9 \times 10^{21}$  n/cm<sup>2</sup> ( $E > 1$  MeV). Steady-state creep reduction factors due to irradiation up to  $\sim 50$  were reported. Test temperatures ranged from 330°C to 600°C, and hoop stresses ranged from 77 to 384 MPa. Rupture strains (based on total strain) for tests below 400°C ranged from 3.9% to 7.3%. The rupture strains increased with increasing test temperature. The strain-time plots were presented in the report providing the basis for determination of steady-state rate.

Schäffler et al. (2000) reported values of secondary strain rate measured for a wide stress range. The strain rate data for Framatome cladding (Schäffler et al. 2000) and by Yvon et al. (1999) at neutron fluences in the range of 0 to  $\sim 10 \times 10^{21}$  n/cm<sup>2</sup> ( $E > 1$  MeV) clearly show that neutron fluence significantly decreases the creep strain (Figure 3.4). It is significant to note that while the Framatome cladding was much less creep-resistant than the FRG-2 cladding when unirradiated, the rates tended to be more consistent for the two cladding types after irradiation, as demonstrated by the data from Cappelaere and Bouffioux (2000) and Kaspar et al. (1985a, and 1985b), respectively, in Figure 3.5. Mayuzumi and Murai (1993) showed that the creep rate from Mitsubishi Zr-4 cladding also were reduced similar to those observed by Cappelaere and Bouffioux (2000) after being irradiated to an estimated 8 to  $9 \times 10^{21}$  n/cm<sup>2</sup> ( $E > 1$  MeV) neutron fluence (Figure 3.5).

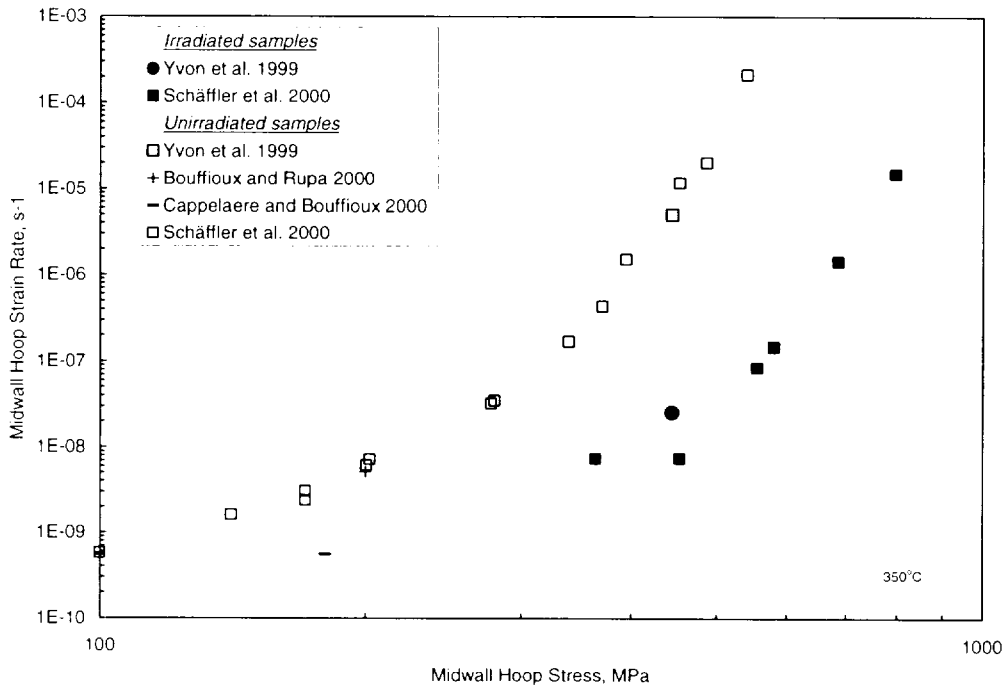


**Figure 3.4 Steady-State Strain Rate of the Framatome Cladding.**

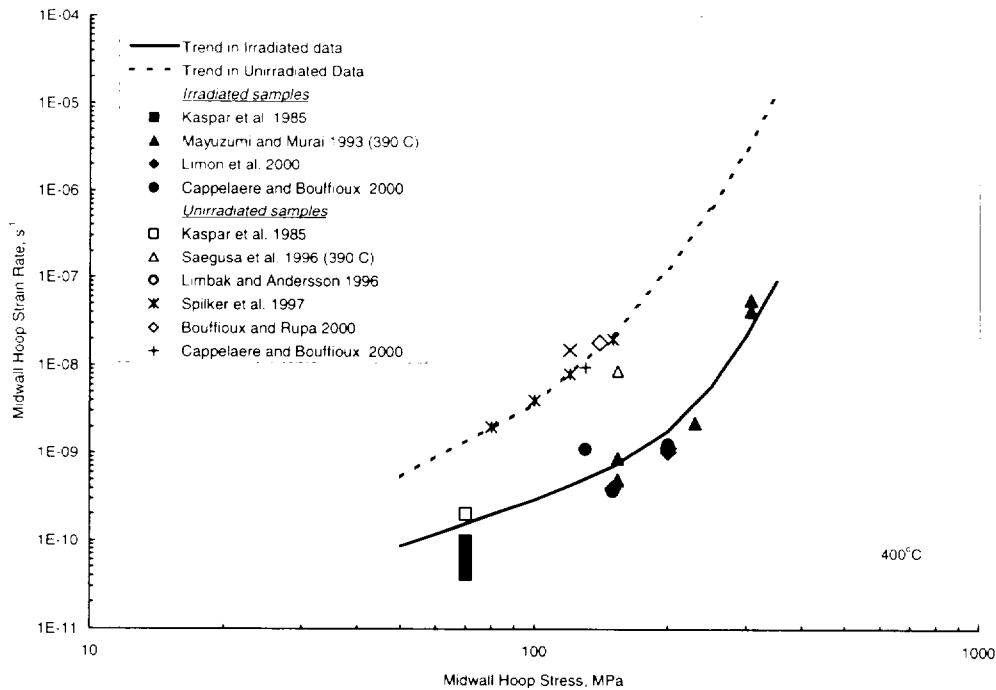


**Figure 3.5 Effect of Irradiation on the Creep Properties of Zircaloy.**

Yvon et al. (1999) reported creep test results for irradiated Zircaloy-4 at 350°C with internal oil pressurization that resulted in a hoop stress of 445 MPa. The creep properties were assessed for the specimens irradiated to the levels from  $0.4 \times 10^{21}$  to  $9.2 \times 10^{21}$  n/cm<sup>2</sup>. The strain-time curves presented in the report featured primary, secondary creep stages, and some evidence of tertiary creep for the lower-fluence specimens.

Table 3.2 Summary of Publications with Post-Irradiation Creep Data

Material			Neutron Fluence, $\times 10^{21}$ n/cm <sup>2</sup> (E > 1MeV)	Pressurization fluid	Stress, MPa	Temperature, °C	Reference
Manufacturer	Hydrogen content, ppm	Outer oxide thickness, $\mu$ m					
Siemens CWSR Zr-4	Not specified	Not specified	Not Specified	Not Specified	423	350	Billaux et al. (2000)
Framatome Zr-4	200	25	8.5	Argon	150, 200	380,400,420	Bredel et al. (2000)
Framatome Zr-4	Not specified	Not specified	0 to 9	Argon	130, 150, 200	380, 400, 420	Cappelaere and Bouffieux 2000
H.B. Robinson Zr-4	Not specified	Not specified	4.4	Expanding mandrel	469 to 552	292, 325	Chung et al. (1987)
Westinghouse Zr-4	30-100	5-17	5.1	He+10%Xe	~150	323	Einzigler and Kohli (1984)
Siemens CWSR Zr-4	Not specified	5-94	9.5 and 12.1	Silicon oil	320 to 630	300 and 370	Goll et al.(2001)
Siemens Zr-4 KWO	Not specified	Not specified	5 to 10	Gas	50	350	Kaspar et al. (1985a, b)
Siemens Zr-4 FRG-2	Not specified	Not specified	0.06 to 0.12		70	395	
Framatome Zr-4	100-400	20-50	8.5	Argon	150 to 250	380 to 420	Limon et al. (2000)
Mitsubishi Zr-4	Not specified	Not specified	8-9	Argon	77 to 384	330 to 600	Mayuzumi and Murai (1993)
Framatome Zr-4	Not specified	Not specified	0.6 to 8.5	Oil	300 to 665	350	Schäffler et al. (2000)
Framatome Zr-4	Not specified	6-32	0.4 to 9.2	Oil	310 to 550	350 to 380	Yvon et al. (1999)

### 3.3. Description of Stress Rupture Database

In the absence of creep rupture data for irradiated Zircaloy-2 and Zircaloy-4, the original CSFM methodology assumed a factor of 10 reduction in the strain to failure for irradiated cladding versus the strain to failure for unirradiated cladding. This reduction was based on results of tensile tests of short duration. It was expected that the failure strains for slow strain rate creep would be reduced by irradiation also, but there were no data to support this assumption.

The current creep rupture database includes 29 data points that include tabulation of time-to-rupture, temperature, stress, and steady-state strain rates. Limited information was available on the levels of hydriding and oxidation of the samples subjected to creep deformation and creep rupture tests. As for the creep database the rupture data was limited test temperatures of 420°C or below but the stress level was not limited other than as stated before to limit the creep rates to below  $10^{-5} \text{ sec}^{-1}$ .

A plot of the temperature and stress range of the creep rupture data shows a smaller database than for creep (Figure 3.6). This also shows only one data point near the design basis range (narrow box) for dry cask storage. Note that the one data point near design basis conditions was from 15% cold worked Zircaloy-2 which is not very prototypic of Zircaloy-4 PWR cladding with 75% cold work and then stress relief annealed. The rupture data for irradiated and unirradiated Zr-4 and Zr-2 cover a range of temperatures from 288°C to 400°C and times-to-rupture from 1 to 10,000 hours.

Uniform strain to rupture does not appear to be dependent on strain rate between rates of  $10^{-8}$  to  $10^{-4} \text{ s}^{-1}$ , as shown in Figure 3.7. Note that there are some slow strain rate ( $< 10^{-5} \text{ s}^{-1}$ ) rupture data with uniform strains at or below 1% while others are as high as 8-10%. As will be shown in Section 4.2.2, some of this variability in uniform rupture strain is due to a temperature effect such that lower test temperatures result in lower rupture strains.

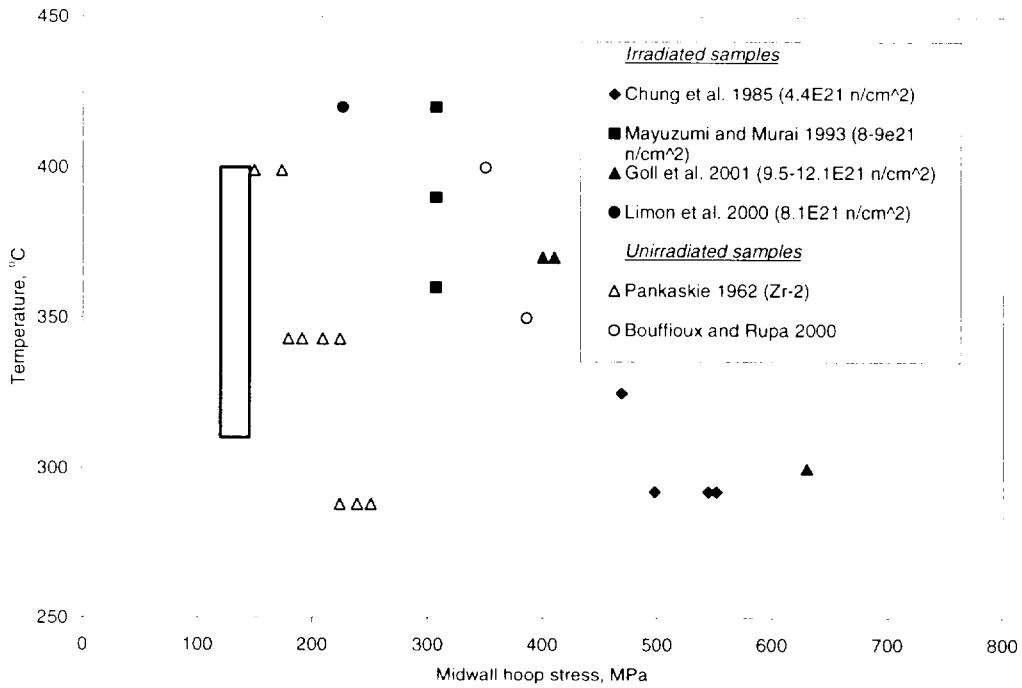


**Figure 3.6** Temperature and Stress Range of Stress Rupture Data and Design Basis Range (Narrow Box) for Dry Cask Storage.

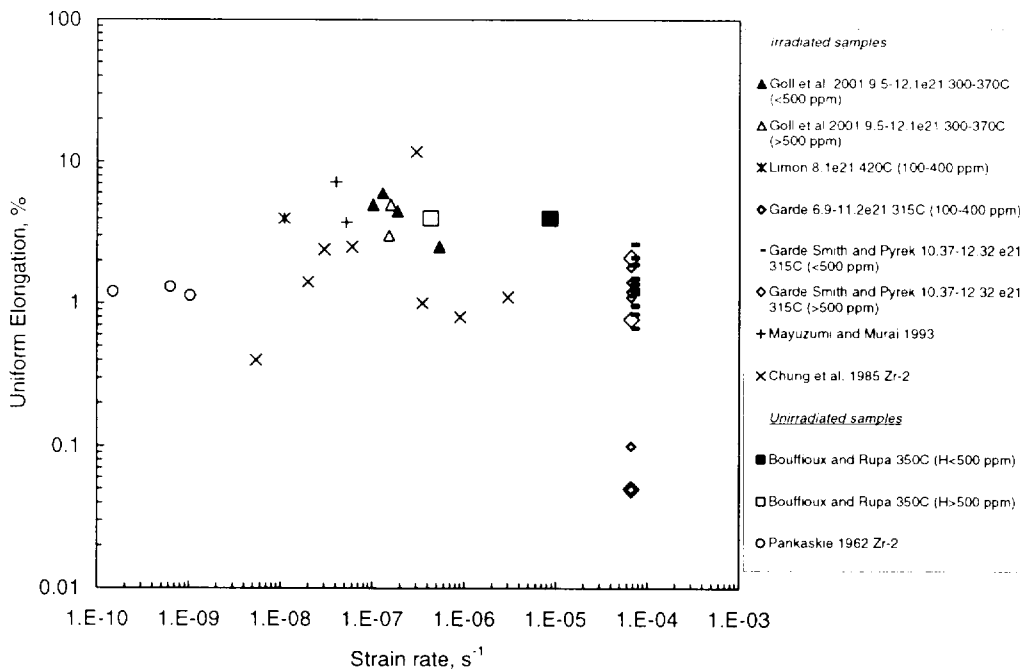


**Figure 3.7** Effect of Strain Rate on Uniform Elongation for Irradiated and Unirradiated Zircaloy.

Those data in Figure 3.7 with uniform strains less than 0.1% and total strain less than 1% (very low ductility) are from cladding reported by Garde et al. (1996) and Garde (1986) with oxide spallation. These data were not used for the creep rupture database because they were for relatively fast tensile tests (strain rates  $\sim 10^{-4}$ ). However, it is insightful to discuss these data because they are the only ones available from SNF cladding with oxide spallation and provide insights into the effect of spallation and high density hydrides on cladding ductility and failure mechanisms.

The Garde et al. (1996) cladding that showed low ductility had spalled oxide and hydride blisters at the spalled location with average hydride levels above 700 ppm. The lower ductility and low stress failure resulted at the spalled oxide location because cracking appears to be enhanced within the hydride blister in the outer rim of the cladding. As illustrated in Figure 3.8, the crack can be arrested by the remaining ligament of uniformly hydrided Zircaloy-4 for conditions of fast strain rates. From this observation, it appears that the nonuniformly hydrided rim cannot be relied upon for load bearing. However, the remaining ductile ligament may resist fracture by arresting propagation of cracks if the remaining ligament is of sufficient thickness, and the stress low enough to resist plastic strain and creep-to-rupture. This observation is partly supported by Garde et al. (1996) who observed a significant drop in ultimate tensile strength and yield strength from high burnup cladding with high oxide thickness and high hydrogen levels due to hydride blisters. When Garde et al. assumed that the cladding thickness was reduced due to the oxide and hydride rim thickness, the ultimate tensile strength and yield strength values were near (they were still lower by  $\sim 10-15\%$ ) those expected for the irradiated Zr-4 without high oxidation and high density hydrides. Therefore, susceptibility of high burnup cladding to rupture depends on oxide and hydride rim thickness, thickness of the cladding, stress, and temperature. Based on this information it is recommended that both the oxide and hydride layers should not be considered as load bearing material and, therefore, oxide and hydride thickness should be deducted from the as-fabricated cladding thickness for determining dry cask temperature limits. From the Garde et al. data it is concluded that irradiated cladding with oxide spallation has very low clad ductility and possible crack formation may lead to creep rupture.

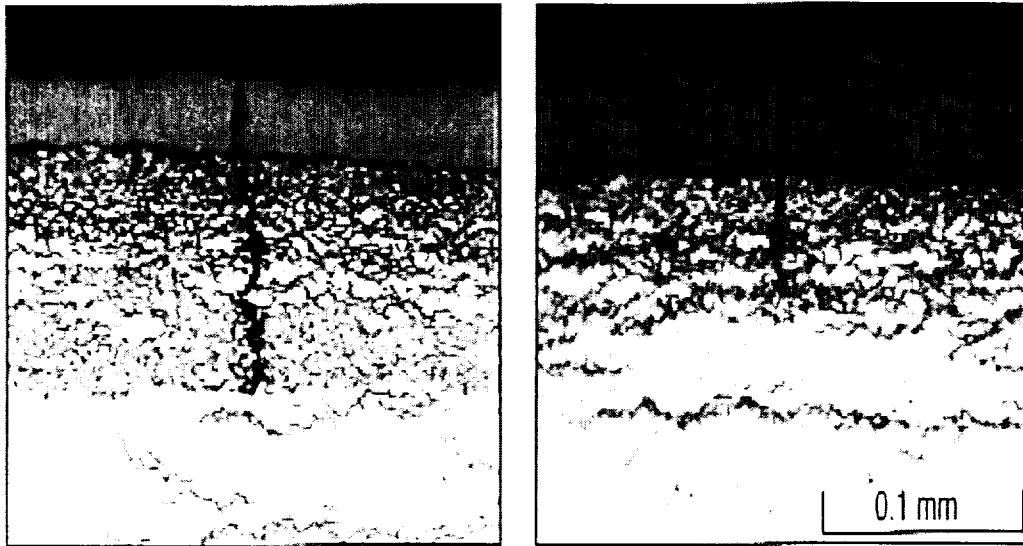


**Figure 3.8** Initiation of Crack in Hydride Rim and Termination in Ductile Ligament of Zircaloy-4 (Fuketa et al. 1996).

### 3.4. Summary of Findings

Zircaloy creep deformation and creep rupture databases were developed as a result of the present study. The creep deformation database contains 184 unirradiated and 180 irradiated data points with a tabulation of temperature, stress, fluence, and steady-state strain rate. The creep rupture database contains 29 data points with a tabulation of time-to-rupture, temperature, stress, and in most cases steady-state strain rates. Limited information was available on the level of hydriding and oxidation of the samples subjected to creep deformation and creep rupture tests.

Initial analyses of the new stress rupture data suggest that, for a given creep rate, the time-to-rupture (and failure strain) is similar for irradiated and unirradiated Zircaloy-4 cladding when hydrogen levels are low and oxide spalling is not present. Based on fast tensile tests of high burnup cladding, cladding oxidation and hydride rim thickness should not be considered as having load bearing capability in the determination of dry cask storage limits for high burnup fuel.

#### **4. REVISIONS TO CSFM METHODOLOGY BASED ON CURRENT DATA**

This section describes revisions to the CSFM Rev. 0 model, based on the data presented in Section 3, that resulted in CSFM Rev. 1. The CSFM methodology describes the deformation and fracture models. The DATING code applies the CSFM methodology to compute temperature limits for varying temperature and stress with time for dry cask storage. The revisions are based on new deformation theory, new experimental diffusion results, and new creep and stress rupture data for unirradiated Zr-4, unirradiated hydrided Zr-4, and Zr-4 SNF cladding with differing levels of burnup, corrosion and hydride contents. Extension of the model to high burnup SNF with spalled surface oxide requires applicable data, but no applicable creep or rupture data were found.

The data used to develop the CSFM Rev. 1 steady-state creep model include primary creep, steady-state creep, and tertiary creep to failure. The use of primary strain and tertiary creep strain along with steady-state creep strain to determine creep rates is conservative and bounding compared to using only the steady-state creep rates to determine steady-state creep rates. This is because creep rates based on either primary creep or tertiary creep strains are greater than those based on secondary creep strain only. However, the degree of conservatism introduced from using primary and tertiary creep strains is small compared to the variability in the creep rate data from the different cladding types used for SNF.

The following steps were used to develop the CSFM Rev. 1 equations:

- Identify those creep mechanisms that are active for dry cask storage based on those mechanisms that best fit the data trends.
- From the identified creep mechanisms develop equations that bound the majority of the creep data for commercial cladding types because there is a large variation in creep behavior for the different cladding types.
- Add primary creep model for strain calculation only.
- Examine data to determine if a creep reduction factor is justified for the effect of irradiation and hydriding for each relevant creep mechanism.

- Implement an alternative approach to model creep for high-stress climb/glide mechanisms using a hyperbolic sine function.
- Identify those creep rupture mechanisms that are active based on those mechanisms that best fit the trends of the new creep-rupture data.
- Provide best estimate and bounding creep-rupture equations based on the rupture data.
- Update the deformation and fracture maps based on new data and modeling.

#### 4.1. Description of Derivation of Revised CSFM Creep Coefficients

The following revisions and additions were made to CSFM Rev.0 to create the new CSFM Rev. 1 based on the new creep data. The evaluation of creep coefficients from the available data was based on the following definitions of hoop strain and hoop stress.

$$\epsilon_{hoop} = \frac{\Delta D_m}{D_{om}} = 1.06 \frac{\Delta D_e}{D_{oc}} \approx \frac{\Delta D_e}{D_{om}} \quad (4.1)$$

where

- $\epsilon_{hoop}$  = mid-wall hoop strain
- $D_{om}$  = mid-wall diameter at start of test
- $\Delta D_m$  = change in mid-wall diameter
- $D_{oc}$  = initial external diameter
- $\Delta D_e$  = change in external diameter
- 1.06 =  $1.06 \pm 0.005$  for PWR and for BWR cladding.

$$\sigma_{hoop} = \frac{PD_{om}}{2t} \quad (4.2)$$

where

- $\sigma_{hoop}$  = mid-wall hoop stress
- P = internal pressure
- $D_{om}$  = initial mid-wall diameter at start of test

$t$  = wall thickness.

The above equations ignore the external atmospheric pressure,  $P_{ext}$ , because  $P_{int} \gg P_{ext}$ . The observed steady-state creep mechanisms for unirradiated and irradiated cladding from the data in Section 3 are grain boundary sliding (GBS), Coble (not dominant for some unirradiated cladding with high creep rates), and low-temperature climb (LTC) or climb/glide. The mechanisms change depending on stress, temperature, creep rate, and grain size. The revised CSFM equations were selected to fit the data and to provide for consistency with theoretical mechanisms for deformation. The coefficients of the equations were adjusted to provide conservatism in relation to the data. A fluence dependence was required to correlate the observed decrease in creep rate of Zircaloy with irradiation. The mechanisms of GBS and LTC were found to be consistent with the observed creep behavior for unirradiated Zr-4. The high-temperature climb (HTC) mechanism was not observed for temperatures up to 420°C which was the upper temperature limit of the data. The GBS deformation was retarded by irradiation, thus enabling the slower Coble creep mechanism to become important at stresses below 100 MPa. For stresses above 100 MPa, irradiation significantly reduced the creep rate for the LTC deformation mechanism. The coefficients were altered to describe the effects of irradiation on the mechanisms. This model was identified as CSFM Rev. 1, model A (CSFM Rev. 1A).

To provide another option, a sinh term, similar to the model described by Murty (1999), was also used to describe the climb/glide deformation behavior at stresses above 150 MPa. The sinh term offers the feature of monotonically increasing stress dependence with increasing stress. This type of behavior is consistent with a stress exponent that increases with increasing stress, as is displayed by test results under conditions of the climb/glide creep phenomena. Effects of irradiation on the mechanisms were incorporated for consistency with the data for SNF cladding. This alternate model was identified as CSFM Rev. 1, model B (CSFM Rev. 1B). These two creep model options were developed and reviewed to determine if one provides a better fit to the data within the temperature and stress range for SNF dry cask storage.

Primary creep was not modeled or included in CSFM Rev. 0 because the methodology determines time-to-rupture based on steady-state creep rate and does not use primary creep

strain. For completeness, the Lagneborg (1978) primary creep equation as modified by Limback and Andersson (1996) was added to the CSFM Rev.1 models. It should be noted that both CSFM Rev. 1A and 1B methodologies do not require primary creep to calculate time-to-rupture, because creep rupture is only dependent on steady-state creep rate. The primary creep model will be described first, followed by a description of the steady-state creep models for unirradiated and irradiated zirconium alloys.

#### **4.1.1. Primary Stage Creep**

Primary stage creep is consistently observed for creep of unirradiated and irradiated Zircaloy cladding; however, it is considerably lower for irradiated cladding than unirradiated and the lower creep rates observed at dry cask conditions. Experimental creep data for both unirradiated and irradiated Zr-4 cladding show primary stage creep (Lagneborg 1978; Matsuo 1987; Limon et al. 2000) and Zr-2/-4 Sandvik cladding (Limback and Andersson 1996). A number of primary creep equations have been published. Primary creep in the high-stress climb/glide domain is associated with dislocation interactions. A theoretical basis for primary creep is provided by Burton and Reynolds (1995) when creep is controlled by diffusional mechanisms such as grain boundary sliding-grain boundary diffusion (GBS-GBD), and Coble creep. This theoretical basis suggests that primary creep is proportional to steady-state creep rate. Theory and experimental creep data from irradiated Zircaloy indicate that the saturated (terminal) primary creep strain is significantly lower than for unirradiated cladding below annealing temperatures. Theory and experimental data show that saturated primary creep strain is controlled by dislocation density such that Zircaloys with a low dislocation density will experience significantly higher primary strains than Zircaloys with a high dislocation density. The low dislocation density material requires a significant amount of strain and, therefore, strain hardening to create an equilibrium dislocation density before steady-state creep is achieved. High burnup spent fuel cladding has a very high dislocation density to start with, due to the significant amount of irradiation damage such that primary creep is very small compared to unirradiated Zircaloy.

The Lagneborg (1978) primary creep relationship provides reasonable agreement with primary creep data, is free of singularities, and is commonly used. A key feature of the Lagneborg

formulation is that the primary creep strain-time and saturation behavior is directly dependent on the steady-state creep rate as suggested by Burton and Reynolds (1985). Therefore, the steady-state strain rate is input to the primary creep equation. The primary creep term described by Lagneborg (1978) and revised by Limback and Andersson (1996) for Sandvik Zr-4 cladding was added to Rev. 1 of the CSFM model. As noted above, the CSFM Rev. 0 did not include a term for primary creep, because the methodology determined time-to-rupture based on steady-state creep rate only.

Limback and Andersson (1996) describe an empirical creep equation with a second power stress exponent for the steady-state strain rate for unirradiated Sandvik Zr-4 fuel cladding and then modified the model for in-reactor creep to account for irradiation hardening. The second power stress dependence for primary creep is consistent with the GBS-GBD deformation mechanism. This similarity in stress dependence implies that the deformation mechanism for steady-state creep is the same as for the primary stage. The saturated primary creep strain,  $\epsilon_p^s$ , is related to the steady-state strain rate,  $\dot{\epsilon}$ , in accordance with Limback and Andersson as follows:

The primary creep strain,  $\epsilon_p$ , from Limback and Andersson (1996) is:

$$\epsilon_p = \epsilon_p^s (1 - e^{-52\sqrt{\dot{\epsilon}}}) \quad (4.3)$$

The saturated primary creep strain by Limback and Andersson (1996) was found to increase with increasing steady-state creep rate,  $\dot{\epsilon}$  ( $\text{s}^{-1}$ ) (see Figure 3 in the reference), and used a tanh function to describe the dependence on the steady-state creep rate.

$$\epsilon_p^s = 0.0216 \times 3600^{0.109} \dot{\epsilon}^{0.109} [2 - \tanh(35500 \times 3600 \dot{\epsilon})]^{-2.05} \quad (4.4)$$

The saturated primary creep strain calculated using Equation 4.4 at a steady-state creep rate of  $10^{-10} \text{ sec}^{-1}$  (range for dry cask storage) is only 0.00105. Therefore, the impact of calculated primary creep strain on uniform creep strain to failure is very small for irradiated cladding.

The total strain,  $\epsilon$ , as a function of time,  $t$  (s), is shown by Equation (4.5) as the sum of Equation (4.3) and the product of time and the steady-state strain rate.

$$\epsilon = \epsilon_p + \dot{\epsilon}t \quad (4.5)$$

The steady-state creep rate for CSFM Rev. 1A is defined in Equations 4.6, 4.7 and 4.8, and for CSFM Rev. 1B (the alternative climb glide model) in Equation 4.9.

#### **4.1.2. Steady-State Creep of Unirradiated Cladding**

A model for steady-state creep of unirradiated Zircaloy was developed to account for annealing effects on irradiated SNF. The CSFM Rev. 1 annealing model is described in Section 4.3.4 and is expressed in terms of fraction annealing recovery. Therefore, if SNF is subjected to high temperatures the CSFM Rev. 1 methodology can model cladding creep with some of the irradiation damage annealed out. For example, for cladding with 100% recovery, the CSFM Rev. 1 methodology will calculate creep from the unirradiated CSFM Rev. 1A or 1B creep models. If only 50% recovery is experienced the CSFM methodology calculates steady-state creep rate by reducing the irradiated creep reduction factor (discussed in Section 4.3.1) by 50%. As noted previously, the CSFM Rev. 1 methodology determines time-to-rupture based on steady-state creep rate rather than a strain limit. The majority of simple creep rupture models described in the open literature, such as Larson-Miller or Monkman-Grant, calculate time-to-rupture based on an empirical correlation of either temperature and stress or creep rate rather than a strain limit.

Modifications were made to the steady-state creep models for GBS-GBD, LTC, HTC, and Coble creep of CSFM Rev. 0 to fit the trends in the data, to bound the majority of the unirradiated Zircaloy creep data, and to be consistent with newer theories for these mechanisms. The CSFM Rev. 0 creep models were revised for CSFM Rev. 1 because they did not bound the unirradiated steady-state creep data discussed in Section 3.1. These modifications are briefly discussed and then compared to unirradiated steady-state creep data in this section. Modifications to steady-state creep were also made for irradiated Zircaloy cladding and these are discussed in Section 4.4.1. The steady-state creep mechanisms of GBS-GBD, LTC, HTC and Coble creep will be

discussed briefly. A more thorough discussion of these mechanisms is provided by Chin et al (1986).

### Grain Boundary Sliding-Grain Boundary Diffusion

An illustration depicting deformation by the GBS-GBD mechanism is provided in Figure 4.1. Operation of the GBS-GBD mechanism requires concurrent operation of the climb/glide deformation mechanism that changes the shape of the grains to accommodate sliding of the grains by GBS-GBD. Irradiation can retard deformation by the GBS-GBD mechanism by the generation of point defect clusters and dislocations that interfere with dislocation slip. Without grain deformation, the GBS-GBD mechanism is restrained.

The revised formulation of GBS-GBD for CSFM Rev. 1A is

$$\dot{\epsilon}_{GBS} = A_{GBS} D_{oGBD} e^{-\frac{Q_{GBD}}{RT}} \frac{Eb}{kT} \left(\frac{b}{d}\right)^2 \left(\frac{\sigma}{E}\right)^2 \quad (4.6)$$

where

$$A_{GBS} = 30 \text{ s}^{-1}$$

$$\begin{aligned} D_{oGB} &= \text{frequency factor } (4.2 [+5.9/-2.5] \times 10^{-13} \text{ m}^3/\text{s}/\omega) \\ &= 4.2 \times 10^{-13} / 2b \\ &= 4.2 \times 10^{-13} / 6.46 \times 10^{-10} \\ &= 0.00065 \text{ m}^2/\text{s} \end{aligned}$$

$$\begin{aligned} \omega &= \text{grain boundary width} \\ &= 2b (6.46 \times 10^{-10} \text{ m}) \end{aligned}$$

$$b = \text{Burgers Vector } (3.23 \times 10^{-10} \text{ m})$$

$$Q_{GBD} = \text{activation energy for grain boundary self diffusion } (167 [\pm 7] \text{ kJ/mol})$$

$$R = \text{universal gas constant } (8.3144 \text{ kJ/mol})$$

$$T = \text{temperature (K)}$$

$$E = \text{Young's Elastic Modulus} = (11.09 - 11.61 \times T/T_m) * 10^4$$

- $T_m$  = melting temperature (2125 K)
- $k$  = Boltzmann's constant ( $1.38 \times 10^{-29}$  MJ/K)
- $d$  = volume average grain diameter = 1.776 L (m)
- $L$  = average grain intercept =  $6 \times 10^{-6}$  m
- 1.776 = metallographic grain linear intercept correction factor
- $\sigma$  = mid-wall hoop stress (MPa).

The CSFM Rev. 0 used the GBS-GBD mechanism described by Luthy et al. (1979). More recently, Langdon (1994, 2000a) presented a revised version that is substantiated with new creep data from unirradiated Zircaloy, and Vieregge and Herzig (1990) have provided new GBD coefficients. The primary differences between CSFM Rev. 0 and Rev.1 GBS-GBD are the values of the pre-exponential creep coefficient, the grain-size dependence, and the GBD coefficients. The theoretical value of  $\sim 30 \text{ s}^{-1}$  for  $A_{\text{GBS}}$  derived by Langdon (1994, 2000a) for the pre-exponential coefficient results in consistent creep rates with data for unirradiated Sandvik cladding by Limback and Andersson (1996) as shown in Figure 4.2. The CSFM Rev. 0 used an inverse-cube grain diameter dependence while Rev. 1 (Equation 4.6) used the Langdon derived inverse-square grain diameter dependence for the GBS-GBD mechanism.

CSFM Rev. 1 also uses the new diffusion coefficients ( $D_{\text{gb}}$  = frequency factor  $\{4.2 [+5.9/-2.5] \times 10^{-13} \text{ m}^3/\text{s}/\omega\}$  and  $Q_{\text{gb}}$  = activation energy for grain boundary self diffusion  $\{167 [\pm 7] \text{ kJ/mol}\}$ ) from subsequent GBD experiments (Vieregge and Herzig 1990), which were not available to Chin et al. (1986). Use of these experimental data for modeling the creep behavior of SNF cladding is consistent with recommendations by Hayes et al. (1999a and 1999b). The value for  $Q_{\text{gb}}$  of 158 kJ/mole used by Prasad et al. (1988) is near the lower uncertainty bound reported by Vieregge and Herzig (1990). The value of 166 KJ/mole for the activation energy from Limon et al. (2000) creep data in Figure 4.3 provides good agreement with the value of 167 KJ/mole for GBD measured in diffusion experiments by Vieregge and Herzig (1990). The Limon et al. creep data are from irradiated Zircaloy-4 that was tested at a constant stress of 150 MPa and temperatures of 379°C, 400°C, and 419°C (see Figure 1 of reference). The revised steady-state creep rate (CSFM Rev. 1) for the GBS-GBD creep mechanism is approximately an order of magnitude faster than the Luthy et al. (1979) formulation used by CSFM Rev. 0).

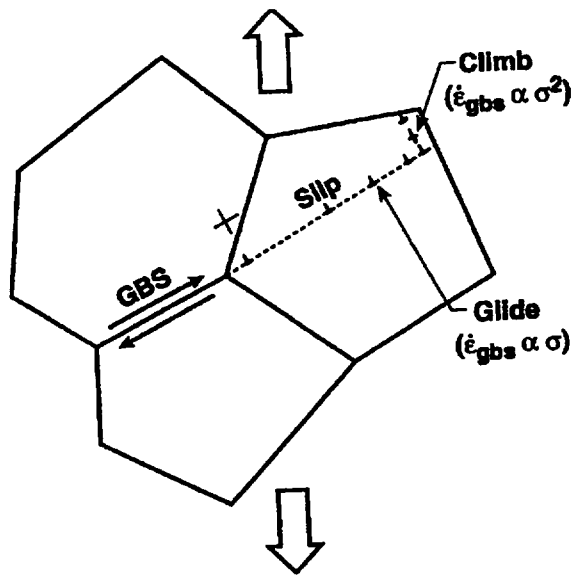


Figure 4.1 Deformation by the GBS-GBD Mechanism and Climb/Glide Mechanism.

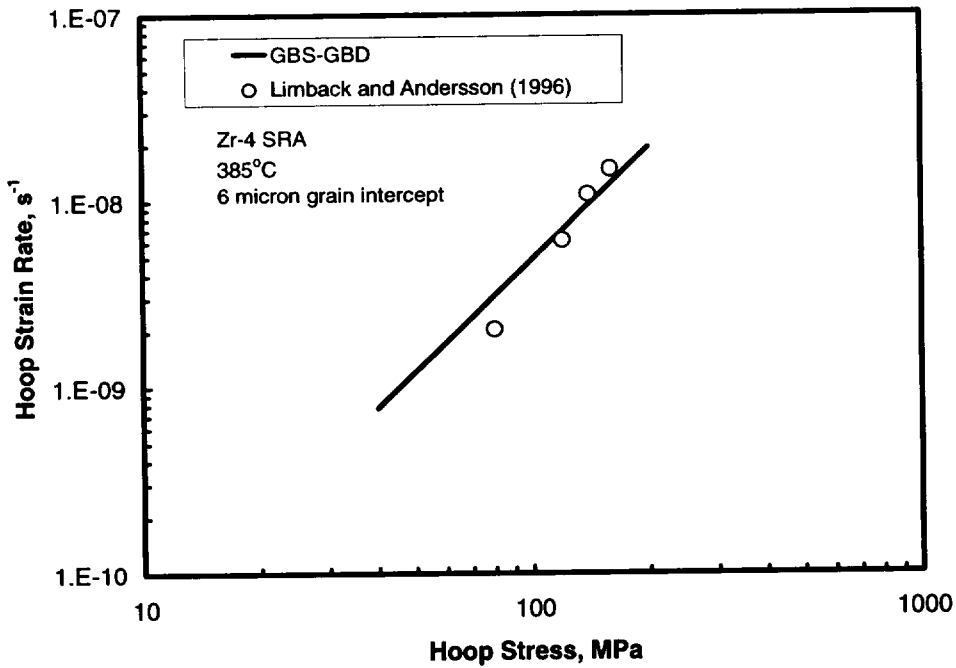


Figure 4.2 Comparison of Equation 4.6 for Deformation by GBS-GBD with Creep Results from Unirradiated Sandvik Cladding by Limback and Andersson (1996).

Langdon (2000b) indicated that Equation (4.6) uses the spatial grain size based on conversion from the average linear intercept grain size. Photomicrographs by Baty et al. (1984) show that the grains in CWSR Zr-4 are shaped like flat noodles with tapered edges or like stemless weeping willow leaves. A volumetric average intercept value of  $6 \times 10^{-6}$  m provides agreement between Equation (4.6) and the creep behavior of unirradiated Sandvik cladding by Limback and Andersson (1996). This value cannot be rigorously derived from the photomicrographs in Baty et al. (1984), however, a value on that order of magnitude appears credible.

### **Coble Creep**

The deformation mechanisms for creep in post-irradiated SNF cladding are believed to be Coble, GBS-GBD, climb/glide, and LTC in order of increasing stress, such that LTC is dominant at the highest stress levels. Coble creep has been reported for low-stress creep tests on unirradiated cladding conducted in the temperature range of 345 to 900°C (Bernstein 1967; Fiala and Cadek 1985; Prasad et al. 1988; Jones 1966; Murty 1999). Coble creep is not considered to be dominant below stresses of ~ 5 MPa for unirradiated cladding but the stress level for Coble creep to be dominant is increased to 30 MPa for irradiated cladding. The deformation mechanism for Coble creep is illustrated in Figure 4.4 and shows that the stress gradient promotes GBD resulting in grain deformation (creep).

The equation for Coble creep is described by Ruano et al. (1981) and Wadsworth et al. (1988), and applied by Chin and Gilbert (1989) and by Murty (1999). Their equations include the elastic Young's Modulus (E); however, to simplify units for the linear stress dependence of Coble creep, the value of E appears in both the numerator and denominator and is cancelled. Equation 4.7 for Coble creep is from Burton and Reynolds (1995).

$$\dot{\epsilon}_{\text{Coble}} = A_{\text{Coble}} D_{\text{oGBD}} e^{\frac{Q_{\text{GBD}}}{RT}} \frac{Eb}{kT} \left(\frac{b}{d}\right)^3 \frac{\sigma}{E} \quad (4.7)$$

where

- $\dot{\epsilon}_{\text{Coble}}$  = mid-wall hoop strain rate,  $\text{s}^{-1}$
- $A_{\text{Coble}}$  = pre-exponential creep coefficient,  
=  $150/\pi$
- $D_{\text{oGBD}}$  = pre-exponential GBD coefficient,  $\text{m}^2/\text{s}$   
=  $4.2 \times 10^{-13} (\text{m}^3/\text{s}) / 2b (\text{m})$   
=  $4.2 \times 10^{-13} / 2 / 3.23 \times 10^{-10}$   
=  $0.00065 \text{ m}^2/\text{s}$
- $b$  = Burgers Vector,  $3.23 \times 10^{-10} \text{ m}$
- $T$  = absolute temperature, K
- $k$  = Boltzmann Constant,  $1.38 \times 10^{-29} \text{ MJ/K}$
- $Q_{\text{GBD}}$  = activation energy for GBD, 167 kJ/mole
- $R$  = gas constant, 8.3144 J/mole
- $d$  = volume average grain diameter = 1.776 L (m)
- $L$  = average grain intercept =  $6 \times 10^{-6} \text{ m}$
- $\sigma$  = mid-wall hoop stress, MPa.

The primary microstructural variable for Coble creep is the spatial grain intercept (grain size),  $L$ , as determined by the intercept method in three dimensions for non-spherical grains in Zr-4 cladding.

Examination of some of the unirradiated and irradiated creep data (Figure 4.5) at stresses equal to or below 70 MPa with slow creep rates suggests that the stress dependence of the creep rate is approximately linear. This supports that Coble creep is the mechanism active at low creep rates.

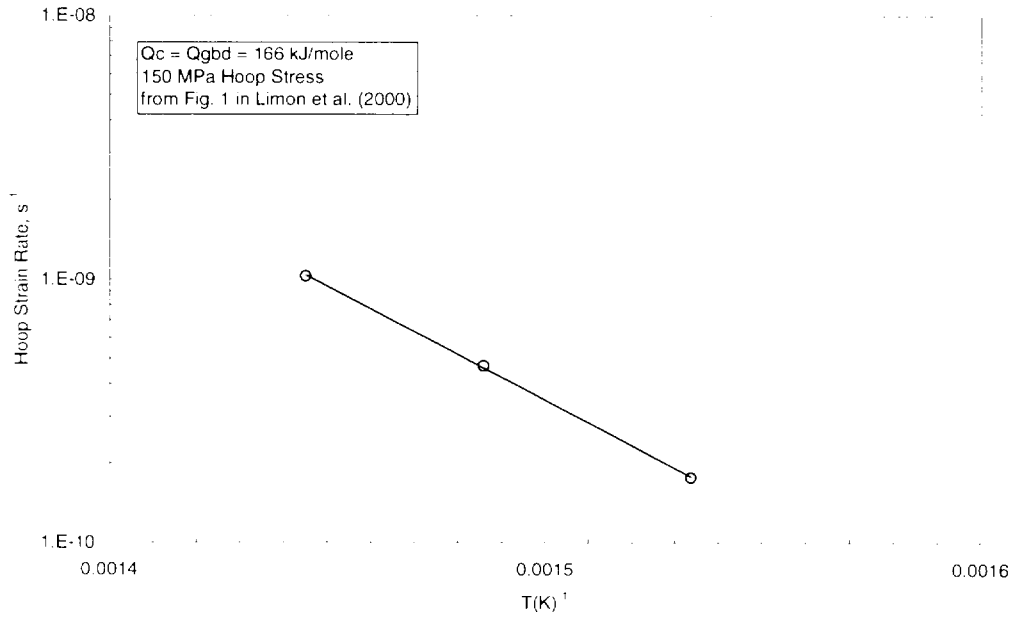


**Figure 4.3** Activation Energy of 166 KJ/mole for Creep of Irradiated Framatome Cladding is Consistent with Activation Energy of 167 KJ/mole Reported by Viergge and Herzig (1990) for GBD.

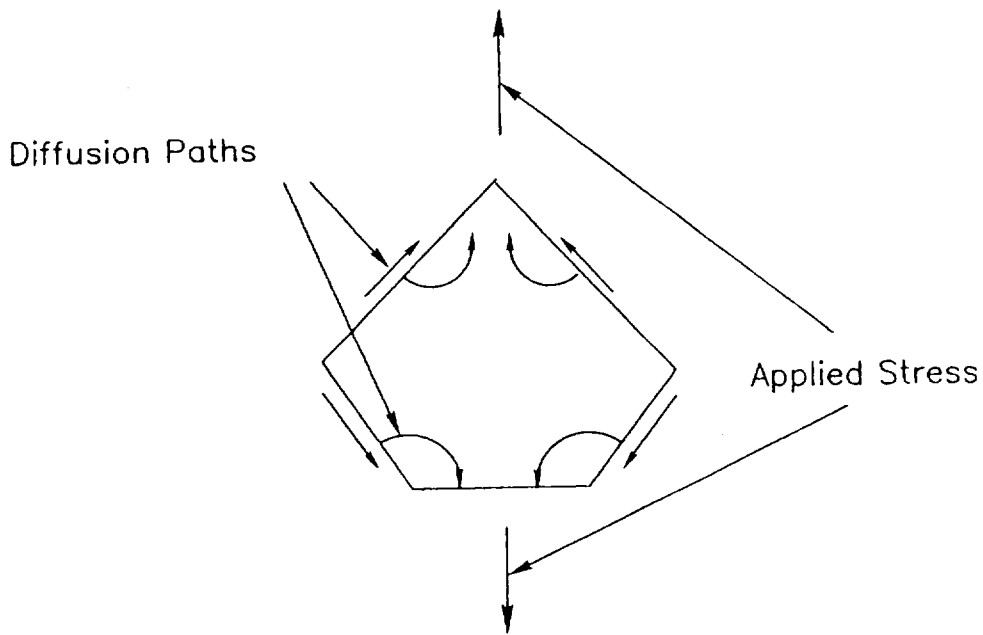


**Figure 4.4** Deformation by the Coble Mechanism.

The Coble and GBS-GBD creep mechanisms also bound most of the creep data for irradiated Siemens Zr-4 KWO cladding by Kaspar et al. (1985a) as illustrated in Figure 4.6 and unirradiated Framatome Zr-4 cladding by Cappelaere and Bouffioux in Figure 4.7. A comparison of the stress dependence for creep by GBS-GBD (Equation 4.6) and for creep by the Coble mechanism (Equation 4.7) with unirradiated and irradiated creep rate data at a test temperature of 350°C is also provided in Figure 4.5. This figure illustrates that the steady-state creep rate appears to have a linear stress dependence below 70 MPa but increases to a second power dependence between 70 to 150 MPa. Therefore, to conservatively bound most of the creep data for unirradiated cladding (Schäffler et al. 2000; Limback and Andersson 1996; Spilker et al. 1999), GBS-GBD was assumed to be the dominant creep mechanism for unirradiated cladding at stresses below 150 MPa. At stresses above 150 MPa a higher power (5 to 7) dependence is observed due to low temperature climb or climb/glide. For dry cask storage this means that cladding stress has a significant impact on clad temperature limits at stresses above 70 MPa.

The CSFM Rev. 1 methodology assumes that the Coble and GBS-GBD creep mechanisms are always active and the creep from each mechanism is added to obtain a total creep strain and strain rate for a given temperature and stress. This results in the methodology bounding the majority of the unirradiated and irradiated creep data as illustrated in Figures 4.6, 4.7, and 4.8.

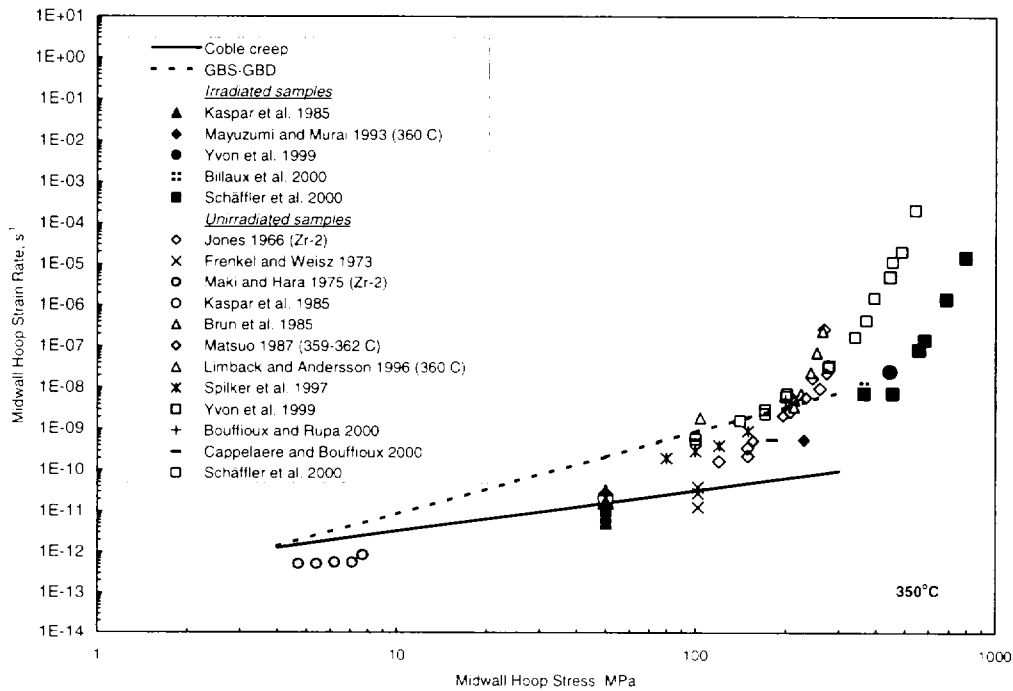


Figure 4.5 Comparison of the Stress Dependence for the Unirradiated GBS-GBD and Coble Creep Equations with Experimental Data at 350°C.

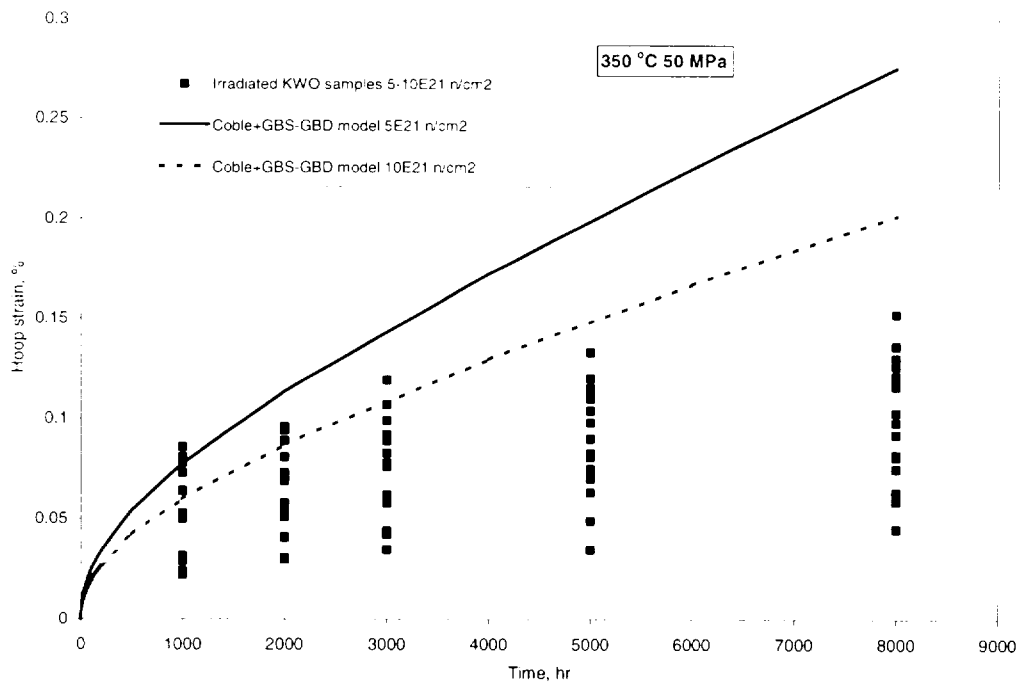
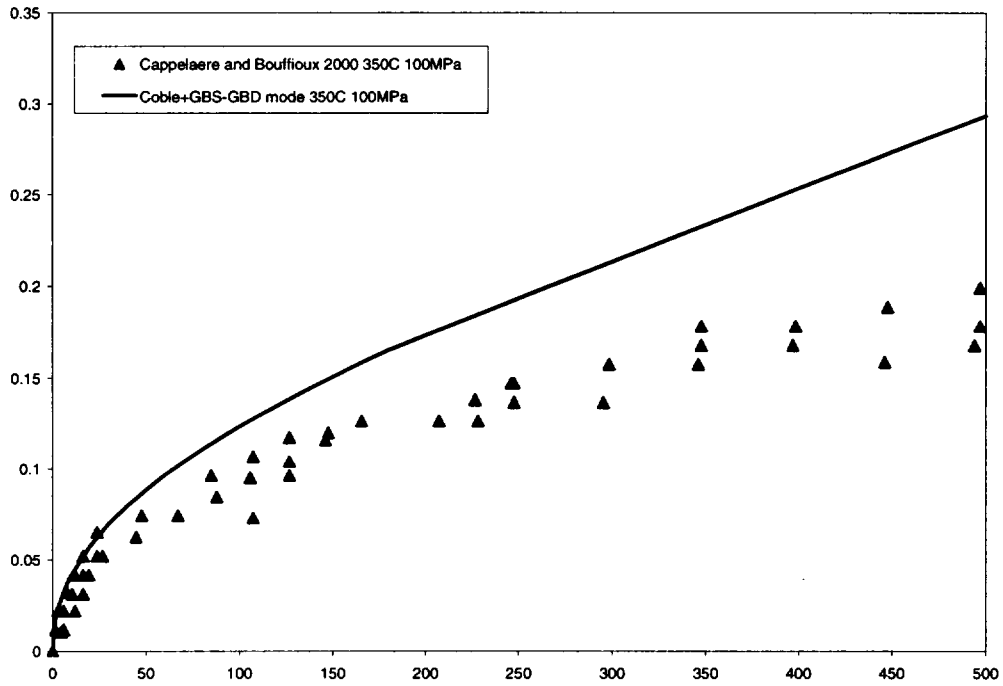
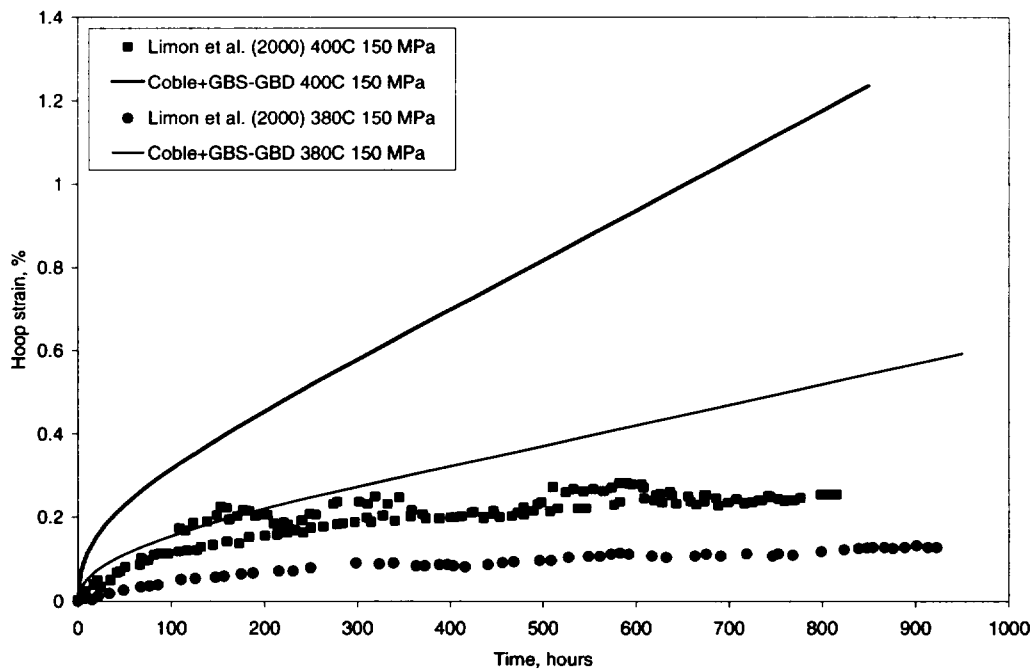


Figure 4.6 The Coble and GBS-GBD Creep Models Bound Irradiated KWO Siemens Cladding Creep Data by Kaspar et al. (1985a and 1985b).



**Figure 4.7** The Coble and GBS-GBD Creep Models Bound Unirradiated Cladding Creep Data by Cappelaere and Bouffioux (2000).



**Figure 4.8** Coble and GBS-GBD Creep Models Compared with Irradiated Creep Data for Framatome SNF Cladding by Limon et al. (2000).

## Low-Temperature Climb

The LTC model is used for the CSFM Rev. 1A model. The coefficients for the LTC mechanism were selected to bound the majority of the unirradiated and irradiated cladding creep data for hoop stress above ~150 MPa. A comparison of Equation (4.8) with unirradiated and irradiated steady-state creep rate data at 350°C is provided in Figure 4.9. The LTC model is defined as:

$$\dot{\epsilon}_{LTC} = A_{LTC} e^{-\frac{Q_{CD}}{RT}} \frac{Eb}{kT} \left( \frac{\sigma}{E} \right)^7 \quad (4.8)$$

where

- $\dot{\epsilon}_{LTC}$  = midwall hoop strain rate,  $s^{-1}$
- $A_{LTC}$  = product of pre-exponential creep and diffusion coefficient  
= 200,000,  $s^{-1}$
- $E$  = Young's elastic modulus, MPa =  $(11.09 - 11.61 \times T/T_m) \times 10^4$
- $T$  = absolute temperature, K
- $T_m$  = melting temperature, 2125K
- $b$  = Burgers Vector,  $3.23 \times 10^{-10}$  m
- $k$  = Boltzmann Constant,  $1.38 \times 10^{-29}$  MJ/K
- $Q_{CD}$  = activation energy for dislocation core diffusion, 185 kJ/mole
- $R$  = gas constant, 8.3144 J/mole
- $\sigma$  = midwall hoop stress, MPa.

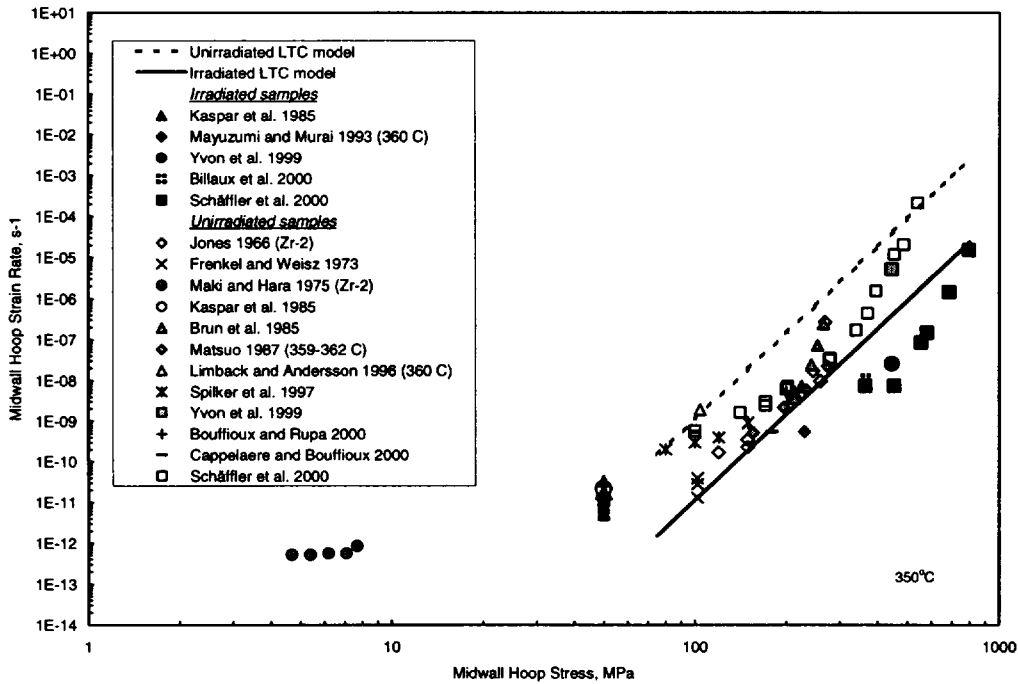


**Figure 4.9 Comparison of LTC Mechanism Model with Unirradiated and Irradiated Zr-2/-4 Cladding Creep Data at 350°C.**

### Climb/Glide

This creep model replaces LTC in the CSFM Rev. 1B model. The coefficients for the climb/glide mechanism were selected to bound the majority of the unirradiated and irradiated cladding creep data at very high stresses (> 150 MPa). The equation for the climb/glide model follows.

$$\dot{\epsilon}_{\sinh} = A_{\sinh} \frac{E}{T} \left( \sinh \frac{420\sigma}{E} \right)^5 e^{-\frac{Q_{CG}}{RT}} \quad (4.9)$$

where

$\dot{\epsilon}_{\sinh}$  = mid-wall hoop strain rate,  $s^{-1}$

$A_{\sinh}$  = product of pre-exponential creep coefficient and diffusion coefficient  
 $= 2.4 \times 10^5 s^{-1}$

$E$  = Young's elastic modulus, MPa  
 $= (11.09 - 11.61 \times T/T_m) \times 10^4$

- T = absolute temperature, K
- T<sub>m</sub> = melting temperature, 2125K
- b = Burgers Vector,  $3.23 \times 10^{-10}$  m
- k = Boltzmann Constant,  $1.38 \times 10^{-29}$  MJ/K
- Q<sub>CG</sub> = activation energy for climb-glide dislocation core diffusion  
= 185 kJ/mole
- R = gas constant, 8.3144 J/mole
- σ = mid-wall hoop stress, MPa

A comparison of Equation (4.9) with unirradiated and irradiated creep rate data for 350°C is provided in Figure 4.10. Examination of the unirradiated steady-state creep rate data at 350°C and a stress of 100 MPa (Figures 4.9 and 4.10) shows that the data varies by up to two orders of magnitude (factor of 100). This large variation is attributed to differences in fabrication that affect the microstructure and the dislocation climb/glide and GBS mechanisms. This large variation in creep rates for different cladding types that are used for commercial fuel provides a difficult task for cask designers to determine temperature limits for their casks for all possible designs and cladding types. The CSFM Rev. 1 creep coefficients were chosen to conservatively bound the majority of the creep data so that cask designers could be assured that the CSFM methodology applies to the majority of cladding types in SNF.

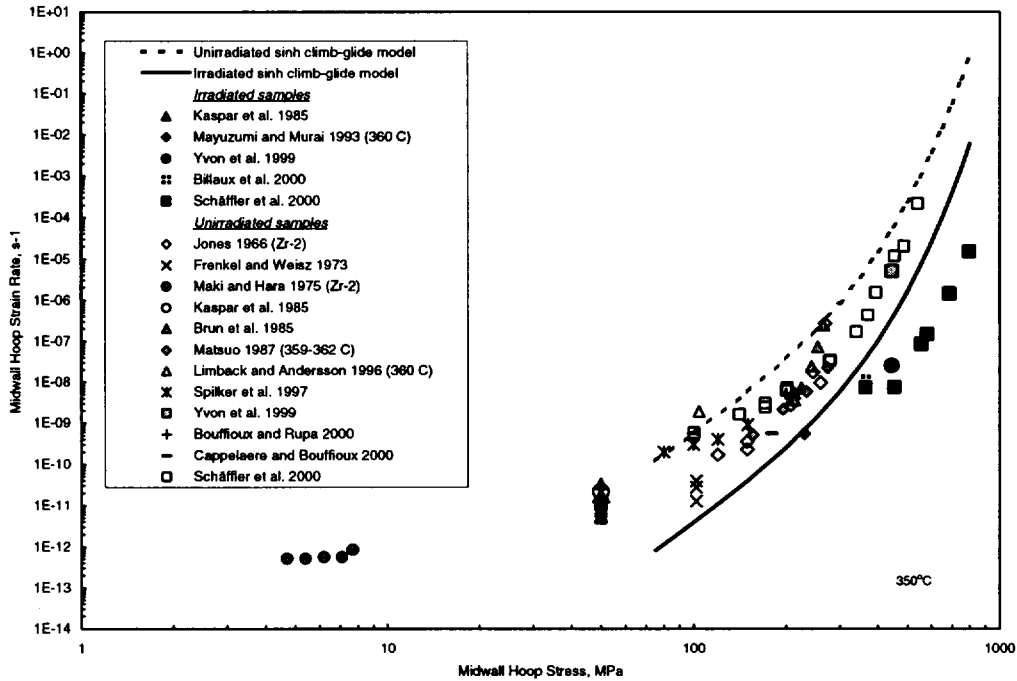


**Figure 4.10 Comparison of the Climb/Glide Mechanism Model with Zircaloy Cladding Creep Data at 350°C.**

### Effect of Hydrogen

Bouffieux and Rupa (2000) have demonstrated that hydrogen retards the creep of unirradiated Zr-4. Their results are summarized in Figure 4.11 with a function that saturates as the hydrogen concentration increases. A single data point at 386 MPa does not follow the trend established by data points at lower stress levels. While these results illustrate an effect of hydrogen on creep, that effect was not adopted as part of the CSFM Rev. 1 model because the creep reduction factor attributed to irradiation implicitly includes the effect due to the hydrogen increase that occurs during irradiation. At this point, the effects of hydrogen and irradiation are not separated in the CSFM Rev. 1 model because it is difficult to separate the effects in high burnup cladding. A reduction in creep rate generally results in an increase in dry cask storage temperatures unless there is a mechanism that reduces the strain or time-to-rupture. It should also be noted that the Bouffieux and Rupa Zircaloy test samples were uniformly hydrided and not prototypical of high burnup cladding where the majority of hydrogen is at the clad outer-diameter surface rim under the oxide layer.

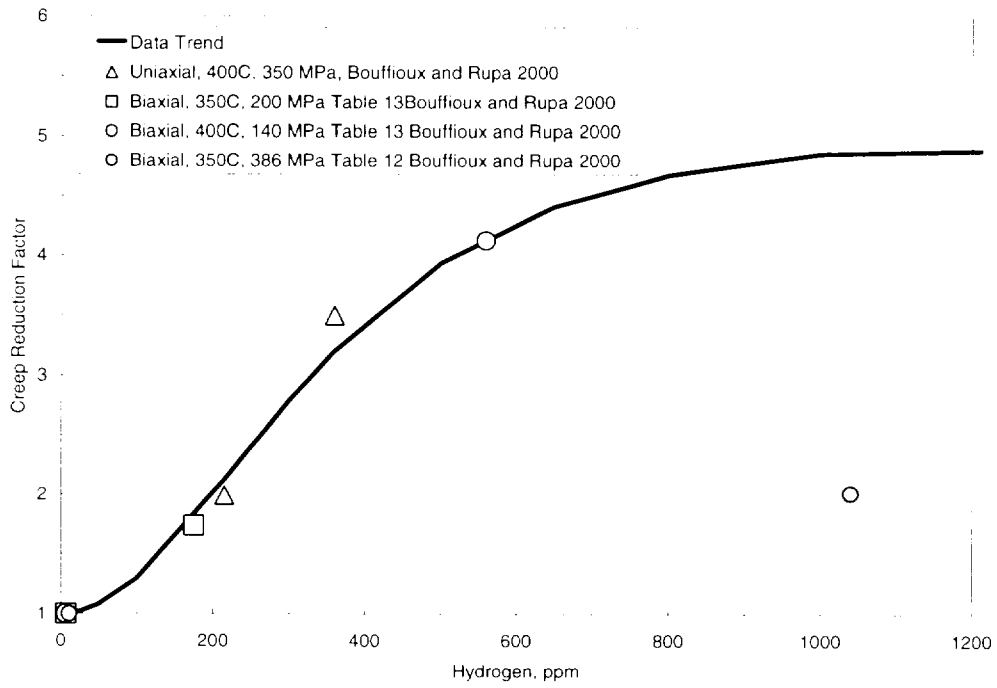


**Figure 4.11 Effect of Hydrogen on Steady-State Creep Rate for Unirradiated Zr-4.**

## 4.2. Derivation of Creep Rupture Coefficients

The fracture mechanisms at high stresses in the CSFM Rev. 0 modeling are triple-point cracking, transgranular fracture, and shear at stresses approaching the theoretical strength. Because the stresses associated with these fracture mechanisms are beyond the peak design stress of 150 MPa for dry storage, resources were not applied toward reviewing the application of these mechanisms for developing the revised CSFM Rev. 1 model. The CSFM Rev. 0 modeling assumed that the fracture mechanisms applicable for SNF cladding during dry storage (at stresses below 150 MPa) were power law cavitation and DCCG. The Monkman-Grant relationship was used for the power law cavitation and its form was also be used for transgranular fracture at higher stresses (above 200 MPa) with a different Monkman-Grant coefficient for CSFM Rev. 0. A Monkman-Grant relationship can also be used for some cases of triple-point cracking (within a narrow stress range). Cavitation is the predominant fracture mechanism observed for both power law cavitation and DCCG mechanisms. It is generally necessary to nucleate cavities to initiate fracture, and it is well established that creep cavitation occurs by the nucleation, growth, and coalescence of intergranular cavities (Nix 1983). The difference between power law cavitation and DCCG is that the former depends on deformation rate only to initiate cavities (created by dragging precipitates through the matrix) while DCCG creates cavities by diffusion that are functions of temperature, stress, and creep rate.

The following sections on creep rupture will show that the Zircaloy rupture data collected in this report are consistent with the Monkman-Grant relationship while the DCCG mechanism is inconsistent within the stress and temperature ranges of the rupture data presented in this report. The stress rupture data were generated by tests in the stress range of 226 to 630 MPa and temperature range of 288 to 420°C. The exception to this is a couple of data points at 138 and 172 MPa at 400°C that are from unirradiated Zr-2 (15% cold-worked) samples by Pankaskie (1962). With the exception of the Pankaskie data the majority of the rupture data are at much higher stresses than the 120 to 150 MPa design basis range for dry storage. Testing in the stress range where DCCG may be applicable (below 100 MPa) has not been conducted. Argonne National Laboratory plans to conduct lower-stress, long-term creep rupture testing using low (30 GWd/MTU) and high (60 GWd/MTU) burnup SNF cladding from Westinghouse and Siemens

Power Corporation (presently Framatome ANP), to provide additional assessment of the creep-rupture behavior for both low- and high-burnup SNF.

It should also be mentioned that the rupture data in this report suggest that the Monkman-Grant coefficient changes within different temperature ranges. The Monkman-Grant relationship will be discussed at the higher temperature range (350 to 420°C) first and secondly within the broader temperature range (288 to 420°C) of the data.

#### 4.2.1. Creep Rupture Data Between 350°C and 420°C

Comparison of creep rupture data with CSFM Rev. 0, is presented in Figure 4.12. These data were from Zircaloy fuel cladding, and tubing that is representative of fuel cladding, but are at a higher stress than the design basis application for dry cask storage. These creep rupture data span a narrow temperature range of 350 to 420°C and include tests for SNF cladding with burnup levels to 64 GWd/MTU and neutron fluence levels to  $12.1 \times 10^{21}$  n/cm<sup>2</sup> (E > 1MeV). Two test data are from samples with average hydride contents between 600 to 660 ppm with no oxide spallation (Goll et al 2001). The steady-state strain rate dependence with time-to-rupture observed from this plot demonstrates that the Monkman-Grant model provides a very good fit to this data.

The Monkman-Grant correlation is

$$t_r = \frac{C_{MG}}{\dot{\epsilon}} \quad (4.10)$$

where

- $t_r$  = rupture time, s
- $C_{MG}$  = Monkman-Grant coefficient
- $\dot{\epsilon}$  = steady-state strain rate, s<sup>-1</sup>.

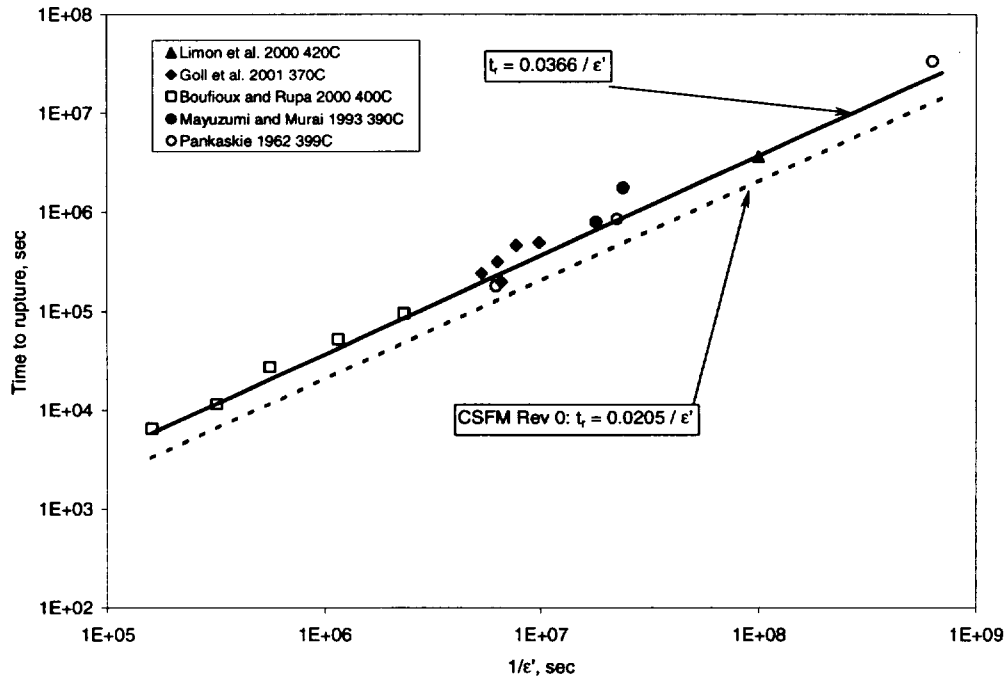


**Figure 4.12 Comparison of Creep Rupture Data with CSFM Rev. 0, T = 350 - 420°C.**

Considering the diversity of the test conditions, the data are remarkably consistent. There are no apparent differences between results from unirradiated and irradiated tests. The strain rates for the Goll et al. (2001) data appear on the high side, but the strain rates are expected to be high because they are based on measured uniform fracture strain (primary plus steady-state) divided by the time-to-rupture. Furthermore, the Goll et al. data were generated by oil pressurization. The time-to-rupture for creep tests conducted with oil pressurization is commonly longer than for tests with gas pressurization and results in higher measured strains. These data yield a mean value of  $\sim 0.0366$  for the Monkman-Grant strain rate coefficient for temperatures between 370°C and 420°C. There appears to be a dependence of decreasing uniform strain to failure with decreasing temperature when the lower temperature rupture data are examined in Figure 4.13b. (see section below).

#### 4.2.2. Temperature Dependence of Creep Rupture Between 280°C and 420°C and Development of Bounding Monkman-Grant Coefficient

Validity of the Monkman-Grant correlation is further demonstrated using a broader set of experimental data obtained over the temperature range of 288°C to 420°C, where the Monkman-Grant coefficient appears to be temperature dependent. To describe the effect of temperature, the following dependence for the Monkman-Grant coefficient was established:

$$C_{MG} = Ce^{\left(6.2 - \frac{4300}{T}\right)} \quad (4.11)$$

where

- T = temperature, K
- C = a constant.

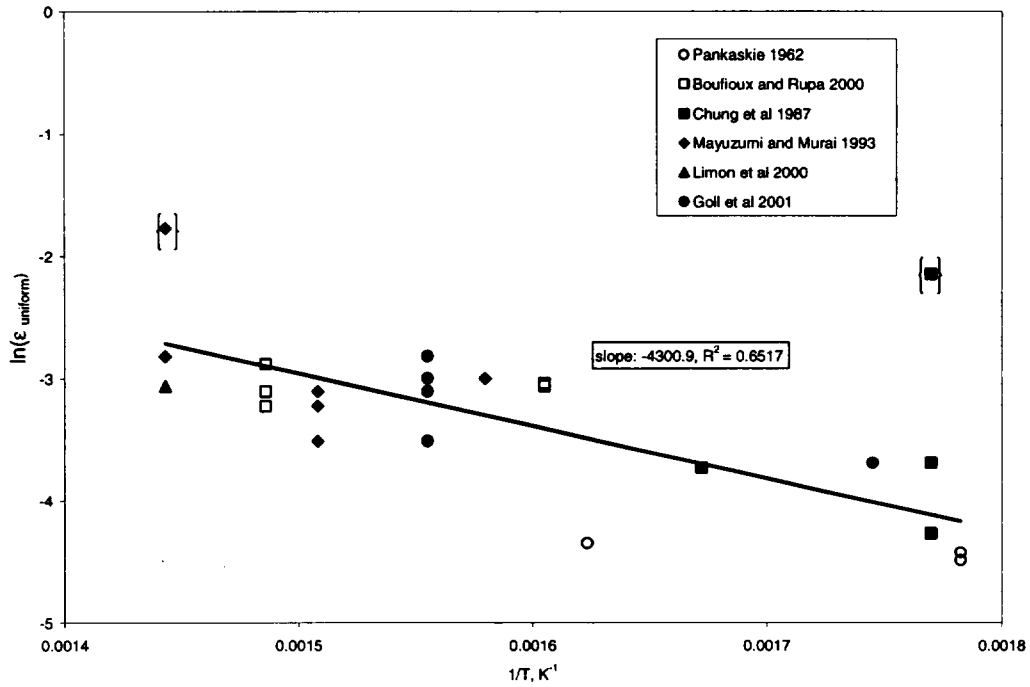
Equation (4.11) was obtained using a regression analysis of the data illustrated in Figure 4.13. Figures 4.13a and 4.13b contain logarithmic and linear scales, respectively, and filled points represent irradiated data. Figure 4.13b includes values of hoop stress shown next to the experimental data points. The data points shown in brackets in Figure 4.13 were not included in the regression analysis. The temperature exponent of 4300 was determined as the slope in the relationship between the logarithm of the uniform strain and the reciprocal temperature. The intercept of 6.205 was chosen so that Equation (4.11) becomes  $C_{MG} = C$  at a temperature of 420 °C. The mean Monkman-Grant relationship becomes:

$$t_r = \frac{0.0366e^{\left(6.2 - \frac{4300}{T}\right)}}{\dot{\epsilon}} \quad (4.12)$$

There are no rupture data in the design basis stress and temperature range for dry storage of 120 to 150 MPa and 340 to 380°C, respectively. Therefore, a bounding relationship was chosen for use in the CSFM Rev. 1 modeling of rupture strain. The conservative Monkman-Grant relationship becomes:

$$t_r = \frac{0.02e^{\left(6.2 - \frac{4300}{T}\right)}}{\dot{\epsilon}} \quad (4.13)$$

a)



b)

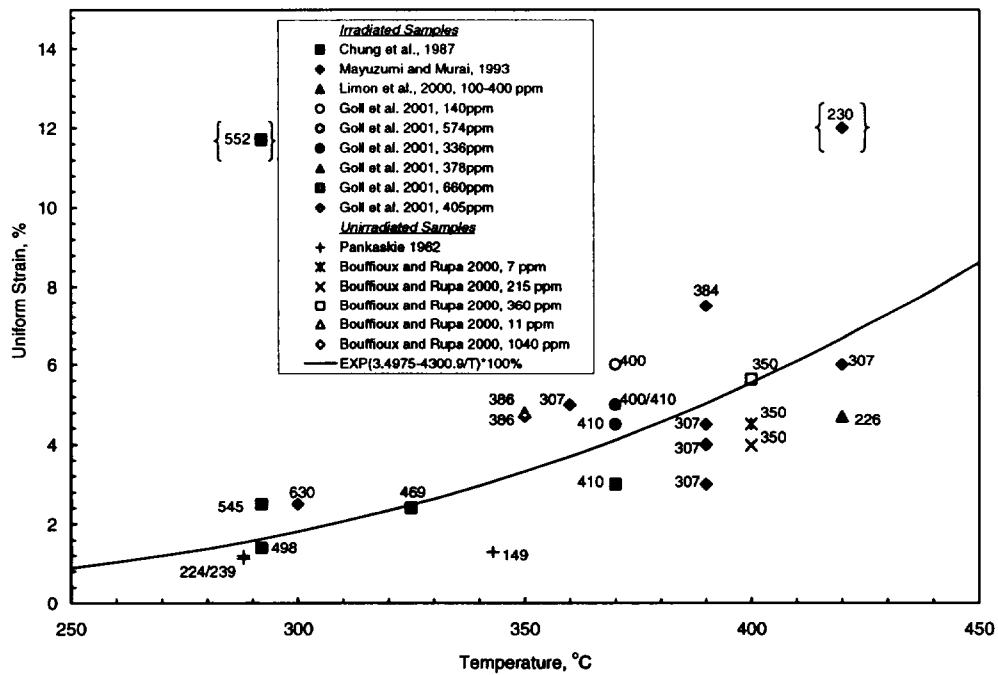


**Figure 4.13 Regression Analysis of the Experimental Data to Determine the Temperature Exponent in Equation (4.11).**

A comparison of the mean and conservative temperature-dependent Monkman-Grant relationships (Equations. 4.12 and 4.13) to the creep rupture data is shown in Figure 4.14. The x-axis has normalized out the effect of temperature on the Monkman-Grant coefficient as defined in Equation 4.11. This normalization allows a two dimensional plot of the Monkman-Grant relationship compared to the data rather than the three dimensions of time-to-rupture, steady-state strain rate, and temperature used in the correlation.

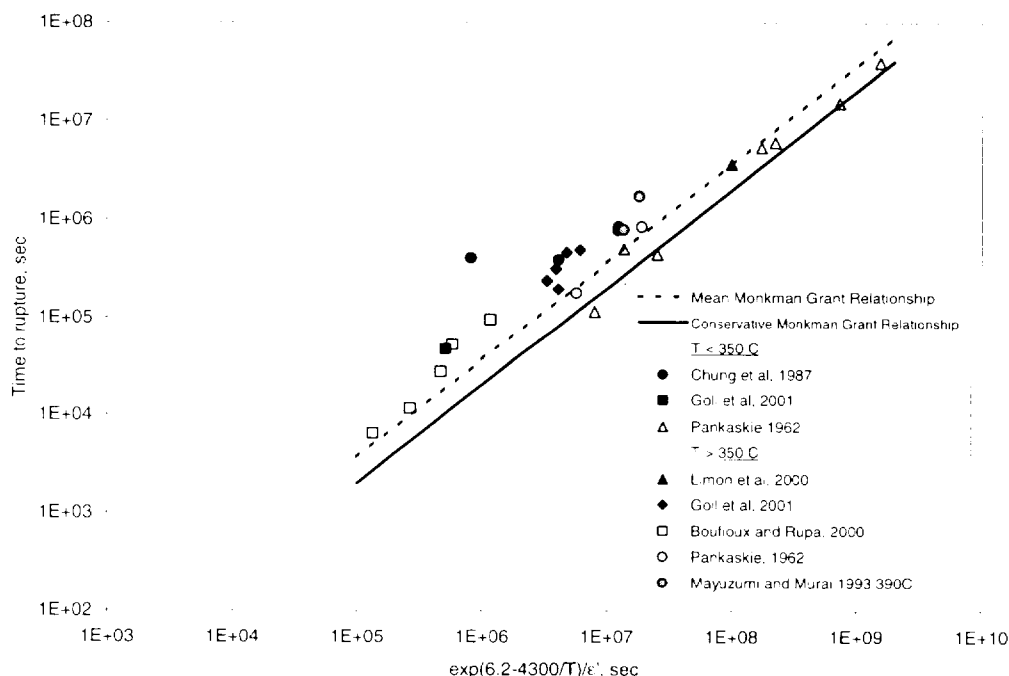


**Figure 4.14 Stress Rupture Data Correlated on a Monkman-Grant Plot of Rupture Time vs. Strain Rate, Irradiated Samples are Shown as Filled Points.**

A plot of the ratio of the measured time-to-rupture to the CSFM Rev.1 predicted time-to-rupture versus the measured time-to-rupture data using the mean Monkman-Grant correlation (equation 4.12) is shown in Figure 4.15. The average of the measured/predicted ratio for irradiated samples is 7.2. This indicates that on average the CSFM Rev. 1 methodology predicts a time-to-rupture that is 7 times shorter than measured for these data using the best-estimate Monkman-Grant relationship in Equation 4.12. However, this plot also shows that for two data points, one from Mayuzumi and Murai (1993) and the other from Pankaskie (1962), the methodology predicts less than a factor of two (conservatism) of the measured time-to-rupture. A plot of

measured versus predicted time-to-rupture is also shown in Figure 4.16 using the same best-estimate Monkman-Grant relationship and the CSFM Rev. 1 creep models.

A plot of the ratio of the measured time-to-rupture to the calculated time-to-rupture versus the measured time-to-rupture using the conservative Monkman-Grant correlation (Equation 4.13) is shown in Figure 4.17. The average of the measured/predicted ratio for irradiated samples is 13.1. This indicates that on average the CSFM Rev. 1 methodology predicts a time-to-rupture that is 13 times shorter than measured for these data using the conservative Monkman-Grant relationship in Equation 4.13. This plot also shows that for two data points, one from Mayuzumi and Murai (1993) and the other from Pankaskie (1962), the methodology predicts less than a factor of three (conservatism) of the measured time-to-rupture. A plot of measured versus predicted time-to-rupture is also shown in Figure 4.18 using the same best-estimate Monkman-Grant relationship and the CSFM Rev. 1 creep models.

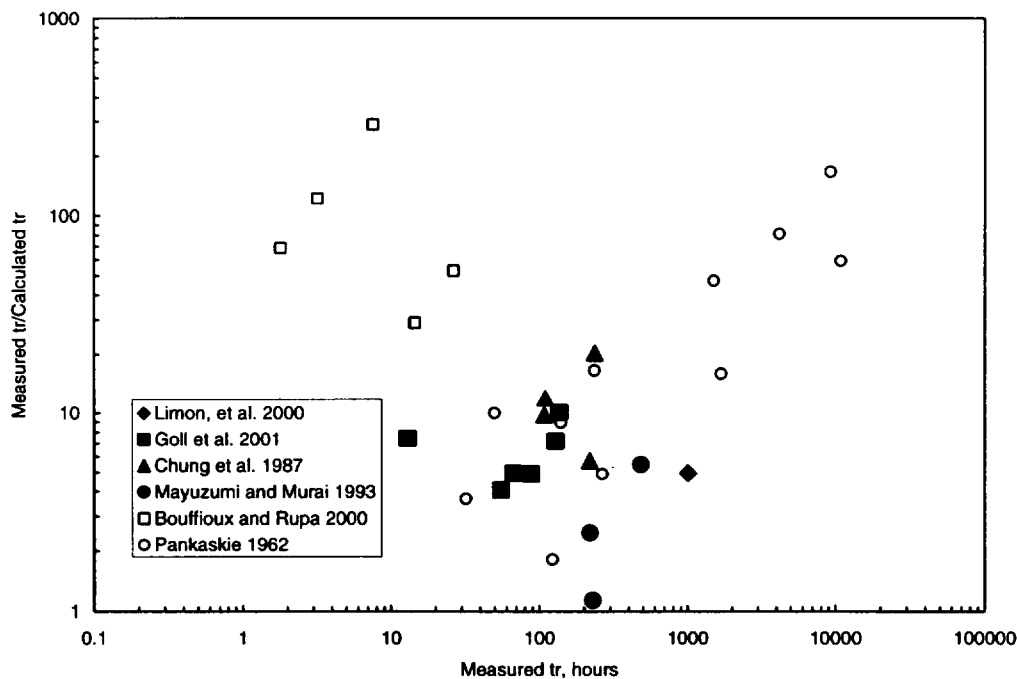


**Figure 4.15 Ratio of Measured versus Calculated Rupture Time Using the Mean Monkman-Grant Relationship (Equation 4.12).**

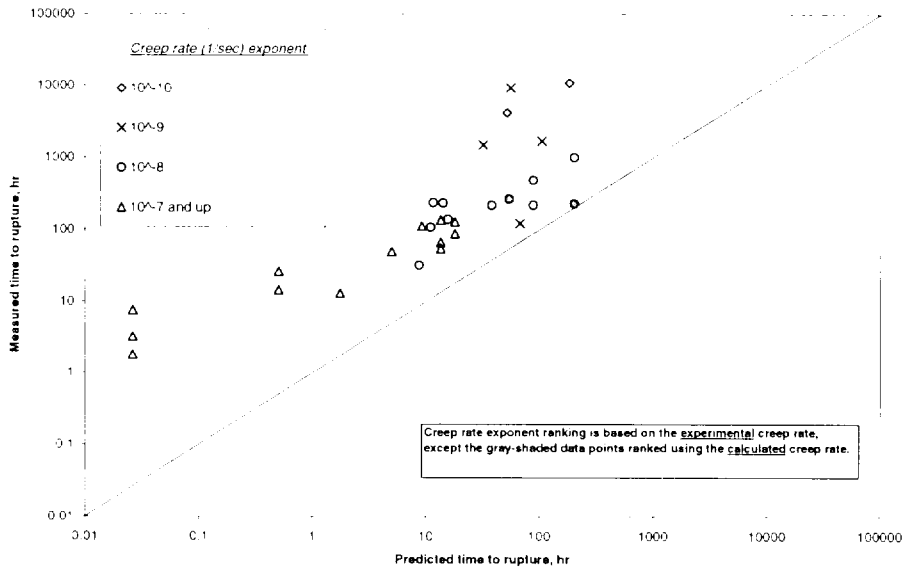


Figure 4.16 Measured vs. Calculated Rupture Time Using the Mean Monkman-Grant Relationship (Equation 4.12).

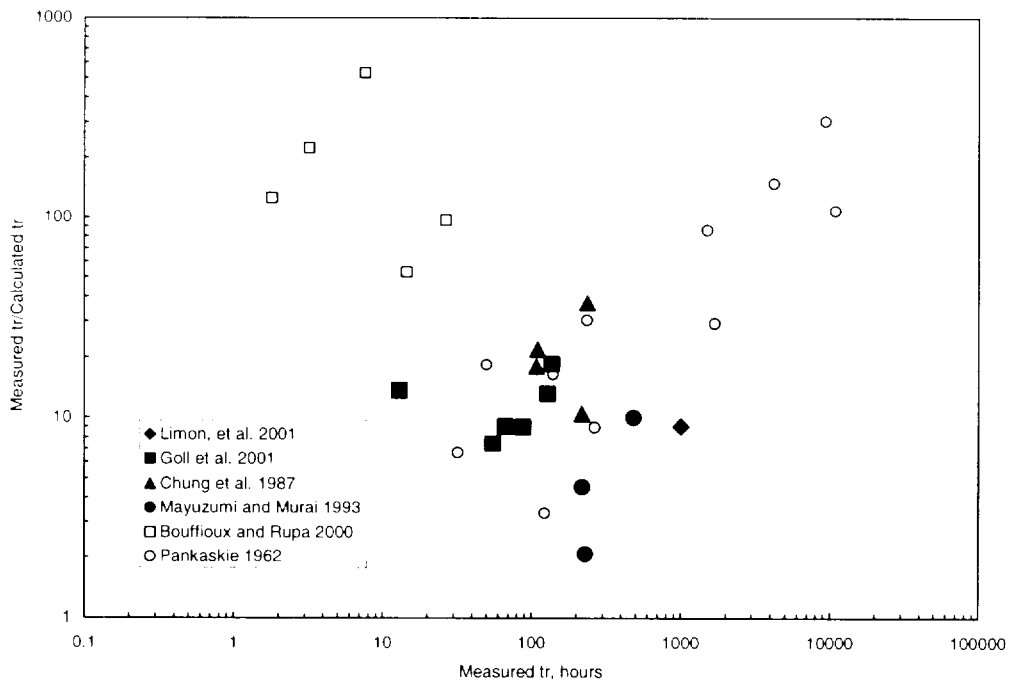
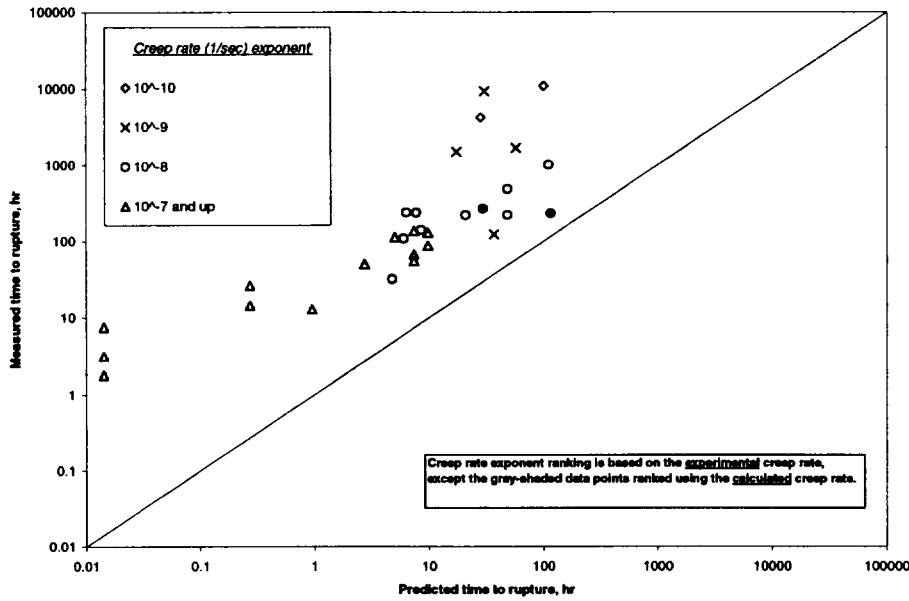


Figure 4.17 Ratio of Measured vs. Calculated Rupture Time Using the Conservative Monkman-Grant Relationship (Equation 4.13).



**Figure 4.18 Measured versus Calculated Rupture Time Using the Conservative Monkman-Grant Relationship (Equation 4.13).**

#### 4.2.3. Comparison of Creep Rupture Data to Various DCCG Rupture Models

The CSFM Rev. 0 methodology included a DCCG model as a rupture mechanism at stresses below ~ 100 MPa in addition to the Monkman-Grant rupture model at stresses between 100 to 200 MPa. A report by Schwartz and Witte (1987) (Lawrence Livermore National Laboratory) for NRC provided an independent review of the CSFM Rev. 0 rupture methodology. This report considered DCCG to be the primary creep rupture mechanism for all dry storage conditions and proposed changes to the DCCG model coefficients from those proposed by CSFM Rev. 0. Even though the coefficients were changed the Schwartz and Witte DCCG model predicted similar temperature limits for dry cask storage as those predicted by CSFM as illustrated in Figure 4.19. A second report by Hayes et al. (1999) (also from Lawrence Livermore National Laboratory) provided a second review of CSFM Rev. 0 methodology for creep rupture and evaluated the coefficients recommended by Schwartz and Witte. This report also concluded that DCCG was the primary failure mechanism for all dry cask storage conditions but recommended more conservative values for some of the coefficients than those proposed by Schwartz and Witte and also used in the CSFM Rev. 0 DCCG model. However, the Hayes et al. model was not compared to any creep rupture data to verify its validity or level of conservatism. The

Hayes et al. recommended coefficients resulted in significantly lower predicted temperature limits for dry storage than those predicted by either Schwartz and Witte or CSFM Rev. 0.

The Schwartz and Witte (1987) and Hayes et al. (1999a and 1999b) recommended DCCG creep rupture models are both compared with the creep rupture data in Figure 4.20. The Hayes et al. recommended model is shown to be overly conservative (Figure 4.20b); for example, the model predicts that the Limon et al. (2000) creep test of irradiated cladding at 420°C and 226 MPa stress should have failed in  $5 \times 10^{-4}$  hours while the test required over 1,000 hours to rupture. The Schwartz and Witte (1987) DCCG model provides a better fit to the time-to-rupture data (Figure 4.20a), but it still is not nearly as good as that provided by the Monkman-Grant correlation. For example, Schwartz and Witte (1987) predict that the creep test for the Limon et al. (2000) irradiated cladding should have failed in 8.5 hours. The CSFM Rev. 0 DCCG model would predict a similar result as that provided by the Schwartz and Witte (1987) model. Therefore, the DCCG models do not provide a good representation of the rupture times, nor the correct functional dependence of these rupture data.

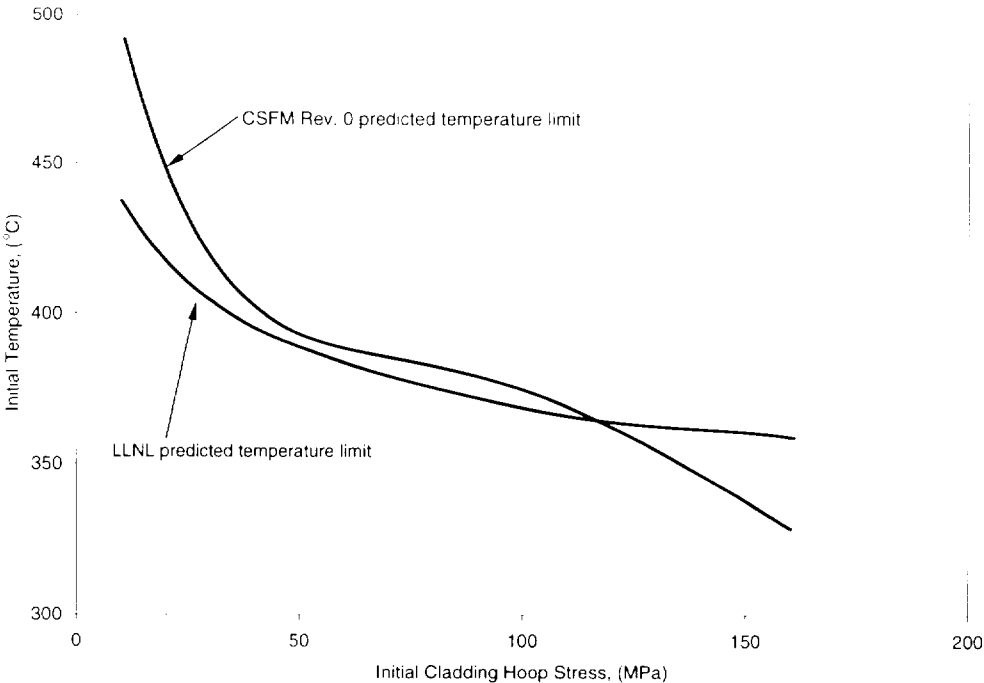
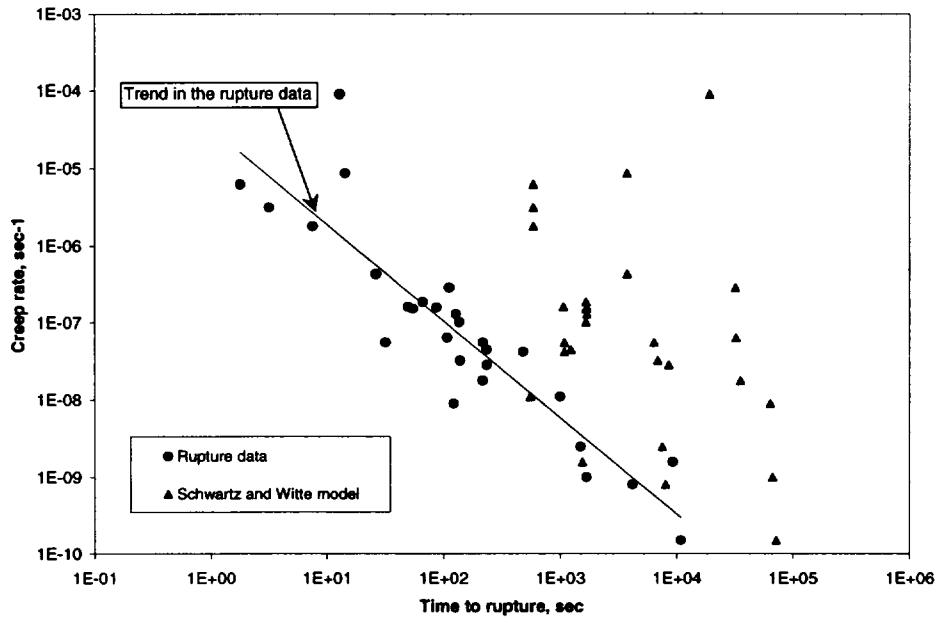


**Figure 4.19 Comparison of Predicted Temperature Limits by CSFM Rev. 0 and Schwartz and Witte DCCG Model.**

a)



b)

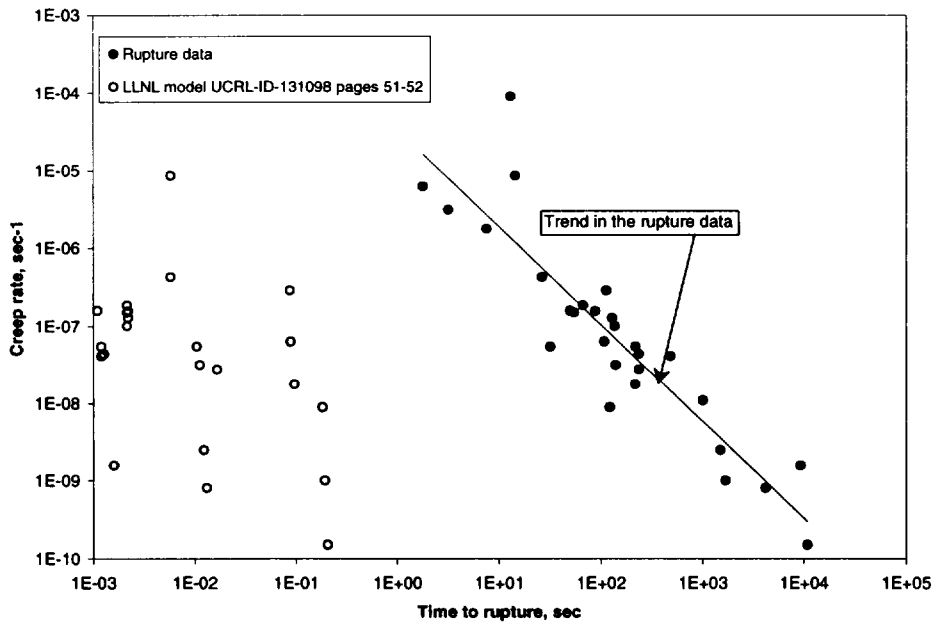


**Figure 4.20 Comparison of LLNL DCCG Fracture Mechanisms with Creep Rupture Data for Zircaloy Cladding.**

It should be noted that removal of the CSFM Rev. 0 DCCG model from CSFM Rev. 1 and use of the Monkman-Grant relationship for all stress levels in Rev. 1 results in lower temperature limits than Rev. 0 for dry cask storage at stresses below 100 MPa where DCCG was assumed to be active.

### **4.3. Effects of Irradiation, Hydrogen, and Annealing on Creep and Rupture Strains of Zircaloy**

#### **4.3.1. Effects of Irradiation on Creep**

Investigations have shown that microstructures of irradiated Zr alloys consist of point defects, small dislocation loops, and precipitates. The density of these defect features increases with neutron fluence and appears to saturate as the fluence approaches  $10 \times 10^{21}$  n/cm<sup>2</sup> ( $E > 1$  MeV). It has been hypothesized that the irradiated microstructure may reduce the creep rates of SNF cladding.

The irradiated and unirradiated steady-state creep strain rate data, where GBS-GBD, LTC and climb/glide creep mechanisms are believed to be active, show that strain rate is reduced due to irradiation. This is evident in Figures 4.9 and 4.10 for LTC and climb/glide mechanisms, respectively, at stresses above 150 MPa. The ratio of unirradiated to irradiated Zircaloy creep rate is referred to in this report as a creep reduction factor, CRF. The effect irradiation has on the CRF appears to be dependent on the stress and creep mechanism as illustrated in Figure 4.21. This figure provides the CRF from Cappelaere and Bouffieux (2000) unirradiated and irradiated data at a stress of only 130 MPa, within the GBS-GBD regime, as a function of fast neutron fluence. Also included on this figure are similar CRF data at 400°C from Yvon et al. (1999) at a stress of 445 MPa and from Schäffler et al. (2000) at a stress of 334-450 MPa that are both in the high stress LTC and climb/glide regimes. This figure shows that the CRF begins to saturate to a value of 10 for the GBS-GBD mechanism and to a value of 200 to 1000 for LTC and climb/glide mechanisms when fluences are greater than  $10 \times 10^{21}$  n/cm<sup>2</sup>.

The CRF relationship for GBS-GBD as a function of fluence is:

$$CRF_{GBS-GBD} = 11 - \frac{10}{\cosh(2 \times 10^{-22} \Phi)} \quad (4.14)$$

where  $\Phi$  = neutron fluence, n/cm<sup>2</sup> (E > 1MeV)

This empirical relationship was developed to provide a best fit to the Cappelaere and Bouffioux (2000) data at a stress of 130 MPa and is shown as a dashed line in Figure 4.21.

The CRF relationship for LTC or climb/glide as a function of fluence is:

$$CRF_{climb/glide} = 201 - \frac{200}{\cosh(2 \times 10^{-22} \Phi)} \quad (4.15)$$

This empirical relationship was developed to provide a bounding fit to the Yvon et al. (1999) and Schäffler et al. (2000) data at high stress (> 400 MPa) and is shown as a solid line in Figure 4.21.

This relationship provides a reasonably good fit to Schäffler et al. (2000) data at stresses between 334 to 368 MPa.

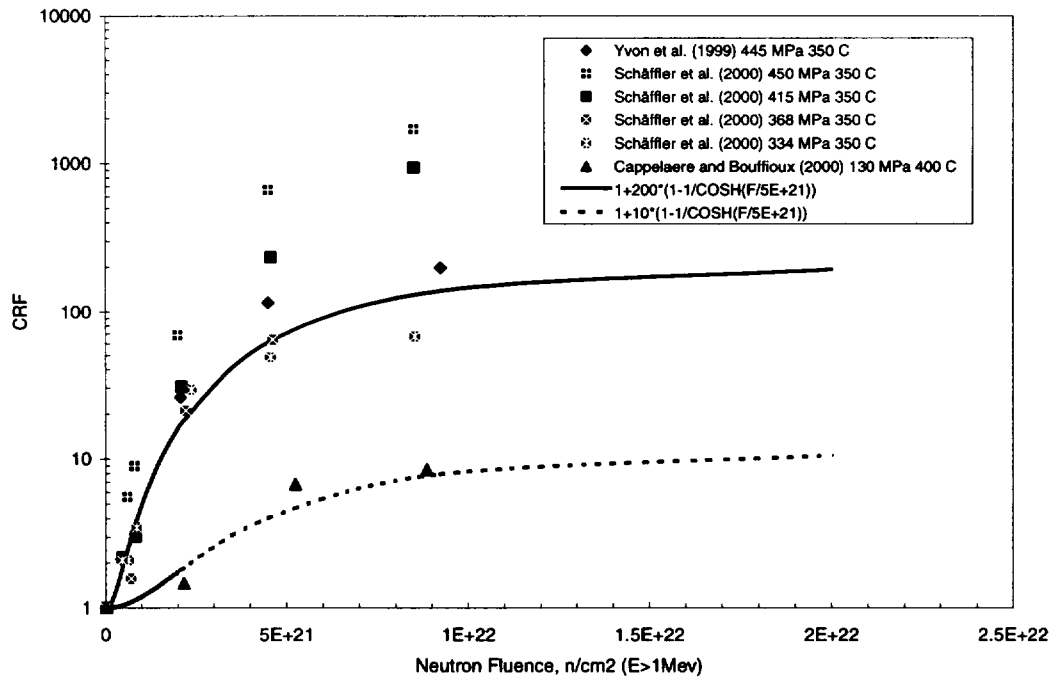


**Figure 4.21** Creep Reduction Factor for Framatome Cladding Data in the Regimes for the High-Stress LTC or Climb/Glide Creep Mechanisms, and the Low-Stress GBS-GBD Creep Mechanism.

Examination of the creep rate data in the stress range where Coble creep is active does not show a significant decrease in creep rate due to irradiation. This is demonstrated in Figure 4.5 at stresses less than 70 MPa. Consequently, no CRF is used in the CSFM Rev. 1 methodology to calculate Coble creep rates for irradiated Zircaloy.

As noted earlier, the creep mechanisms are assumed to be additive because it is likely that all mechanisms are active with some more dominant than others within a given temperature and stress range. For CSFM Rev. 1A option, steady-state creep is calculated for irradiated cladding using Equations 4.6, 4.7, 4.8, 4.14, 4.15 and the following:

$$\dot{\epsilon}_{\text{Rev. 1A}} = \dot{\epsilon}_{\text{Coble}} + \dot{\epsilon}_{\text{GBS-GBD}} \cdot \text{CRF}_{\text{GBS-GBD}} + \dot{\epsilon}_{\text{LTC}} \cdot \text{CRF}_{\text{LTC}} \quad (4.16)$$

For CSFM Rev. 1B option, steady-state creep is calculated for irradiated cladding using Equations 4.6, 4.7, 4.9, 4.14, 4.15 and the following:

$$\dot{\epsilon}_{\text{Rev. 1B}} = \dot{\epsilon}_{\text{Coble}} + \dot{\epsilon}_{\text{GBS-GBD}} \cdot \text{CRF}_{\text{GBS-GBD}} + \dot{\epsilon}_{\text{climb/glide}} \cdot \text{CRF}_{\text{climb/glide}} \quad (4.17)$$

Equations 4.16 and 4.17 are plotted as a function of hoop stress in Figure 4.22 and 4.23, respectively, for a temperature of 350 °C and fast neutron fluence of  $10 \times 10^{21}$  n/cm<sup>2</sup>.

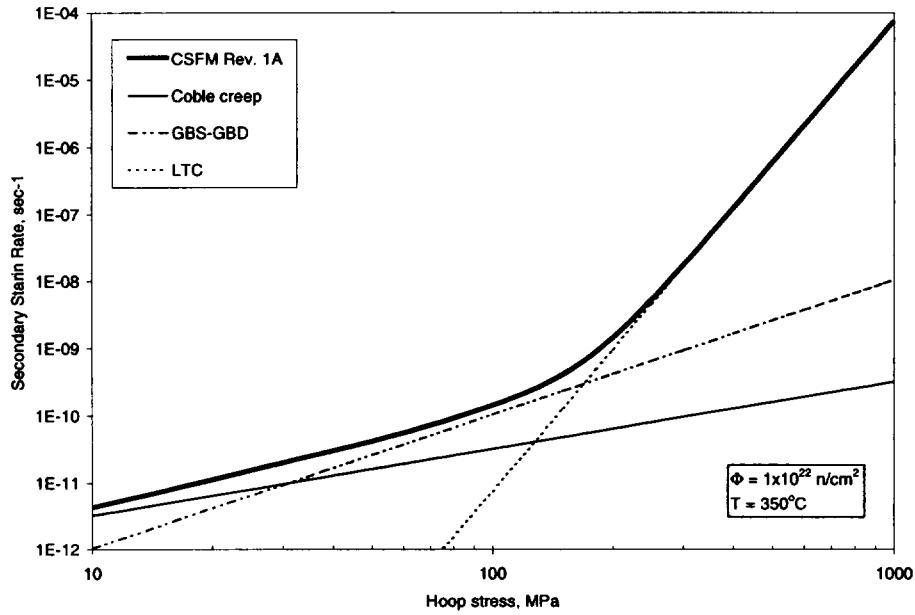


**Figure 4.22** Graphic Representation of Equation 4.16 as a Function of Hoop Stress.

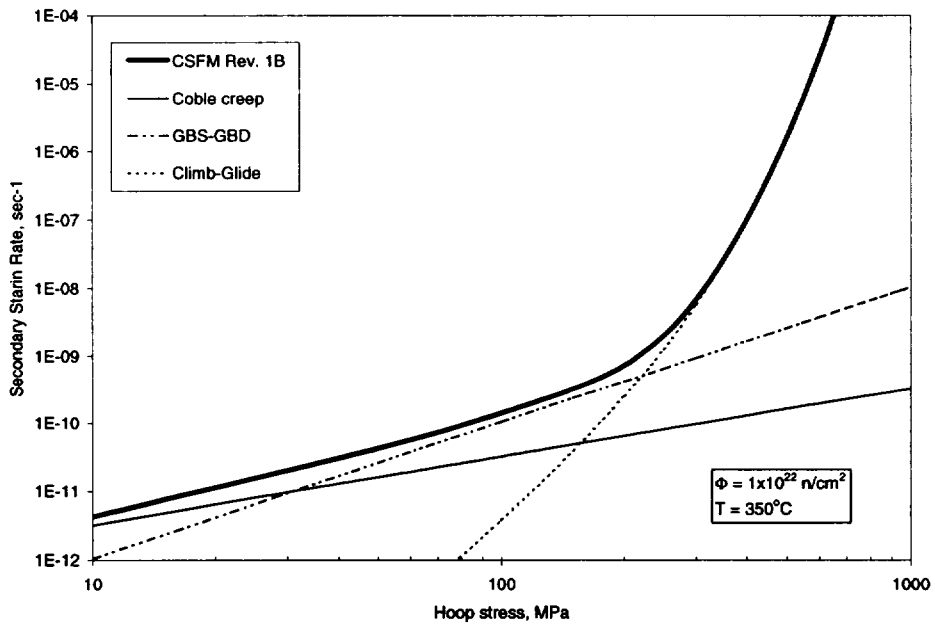


**Figure 4.23** Graphic Representation of Equation 4.17 as a Function of Hoop Stress.

### **4.3.2. Effects of Irradiation on Creep to Rupture**

The Monkman-Grant strain criterion (based on uniform strain) for rupture has not been found to be dependent on irradiation from the limited rupture data collected in this report (see Section 4.2). The hydride levels of this database extend to 660 ppm with no oxide spallation (see Section 4.3.3).

### **4.3.3. Effects of High Burnup and Hydrided Microstructures on Creep and Rupture**

Bouffieux and Rupa (2000) demonstrated that the presence of uniform hydride precipitates (1,040 ppm of hydrogen) in unirradiated Zr-4 resulted in a reduction of the creep strain rate at a temperature of 400°C and a hoop stress of 140 MPa. Creep tests conducted to rupture at 350°C and a hoop stress of 386 MPa for the sample hydrided to 1,040 ppm, and at 400°C with a uniaxial stress of 350 MPa for the sample hydrided to 360 ppm, demonstrated a reduction of the creep strain rate and an increase of the time-to-rupture without an impact on the total strain to failure. Bell (1963) reported that up to 1,075 ppm of uniform hydrogen reduced the creep strain rate in annealed Zr-2 tested at 300 and 400°C for uniaxial stresses of 138 and 69 MPa, respectively. These creep tests were uniaxial (as opposed to pressurized). The uniform hydrogen distribution of these test samples was not prototypical of the hydrogen distribution in high burnup cladding.

Irradiating fuel to high burnup results in high corrosion layer thickness (> 60 µm) and hydrogen concentration levels in the cladding. The hydrogen is present in the form of brittle zirconium hydrides near the cladding outer surface (creating a dense hydride rim) at the oxide-metal interface. The hydrogen level and local hydride rim thickness is dependent on corrosion thickness, the amount of oxide spallation at the local cladding location, and any localized cold spots on the cladding such as at spacer grid locations. Consequently, high burnup cladding does not have a uniform distribution of hydrides axially or radially through the clad thickness because the majority of the hydrides are on the outer surface with little hydriding on the inner surface. If the local oxide thickness is relatively uniform, without oxide spallation, the hydride rim (with high density hydrides) thickness is generally 50 to 70% of the oxide thickness. If localized spallation or a cold spot exists on the cladding, a hydride blister (of high density hydrides) may

penetrate anywhere from 30 to nearly 100% of the cladding thickness, depending on the size of the spallation or cold spot area.

The hydride rim (with a high density of hydrides) appears to result in crack growth starting on the outer surface of high burnup fuel cladding with high hydrogen levels, as shown in the photomicrograph (Figure 3.8). Garde et al. (1996) and Herman (1999) have performed uniaxial and biaxial stress tests on high burnup cladding and shown significantly reduced rupture strains due to cracking at the outer cladding surface with average hydrogen levels of less than 800 ppm. One test sample from Garde et al. had localized oxide spallation and hydride blisters, and experienced a uniform rupture strain of only 0.05% at a test temperature of 315 °C. Garde et al. have proposed that the high density of hydrides near the surface (rim) contributes to the crack initiation observed at the cladding surface. Therefore, the rupture tests performed by Bouffioux and Rupa (2000) and Bell (1963) on unirradiated cladding with uniform hydrogen (at similar hydrogen levels) do not appear to be applicable to high burnup cladding.

The impact of stress and hydrogen level on creep rupture strain data has been examined. Examination of Figure 4.13b shows no general trend between uniform rupture strain and hoop stress (values next to data points). Examination of the Bouffioux and Rupa (2000) uniform rupture strains and uniform hydrogen level in these unirradiated test specimens in Figure 4.13b shows no obvious dependence between these variables. However, examination of uniform rupture strains and non-uniform hydrogen levels in the Goll et al. (2001) test specimens from high burnup fuel shows that the specimen with the lowest hydrogen level of 140 ppm (smallest and less dense hydride rim) resulted in the highest measured uniform strain of 6%. The test sample with the highest hydrogen level of 660 ppm resulted in the lowest measured strain of 3% at test temperatures above 350 °C. The Goll et al. high burnup cladding creep results are the only data with significant hydrogen levels (> 400 ppm) and only three data points above 400 ppm.

The uniform strain results from Goll et al. (2001) plotted versus measured oxide thickness in Figure 4.24 indicate that those five test specimens with corrosion thicknesses equal to or greater than 50 µm all failed, while all but one of the 14 test specimens with corrosion thickness below 50 µm did not fail. This also suggests that the strain limit or time-to-rupture may be lower for

higher levels of hydrogen and hydride rim thickness. It is also noted that hydride content increases with increasing corrosion thickness and oxide spallation in high burnup fuel rod cladding.

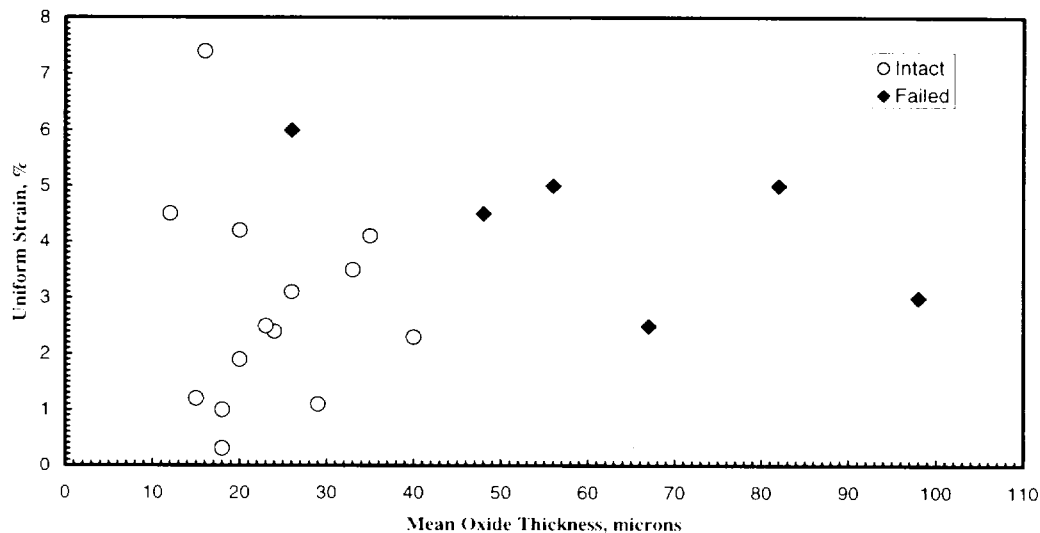


**Figure 4.24 Effect of Corrosion on Creep Rupture from Results by Goll et al. (2001).**

The dependence of rupture on hydrogen level could not be quantitatively determined because of the small amount of SNF data with known hydrogen levels and the large scatter observed in the data (see Section 4.2.2 and Figure 4.13b). This is one of the primary reasons why a conservative Monkman-Grant relationship was developed from the rupture data. The irradiated cladding rupture data presented in this report were generated for cladding with burnup levels to 64 GWd/MTU, neutron fluence levels to  $12.1 \times 10^{21}$  n/cm<sup>2</sup> (E > 1MeV), and mean hydride contents up to 660 ppm with no oxide spallation. Therefore, the effects of hydrides are implicitly included in the creep and rupture models for the range of hydrogen, up to 660 ppm with no oxide spallation, in the irradiated cladding data. Note that hydride levels greater than 660 ppm can be experienced in high-burnup/corrosion fuel rods and can significantly exceed 700 ppm levels when oxide spalling is experienced. It is possible that higher hydrogen levels (> 700 ppm) may significantly reduce the strain to failure in high burnup rods below those assumed in the Monkman-Grant correlation by the CSFM Rev. 1 model. Currently, there is insufficient creep rupture data to quantitatively model rupture for cladding at high hydrogen levels. Very low burst

and tensile fracture strains due to cracking have been observed for cladding with oxide spallation (Garde et al. 1996, Herman 1999).

Due to a lack of creep-to-failure data from cladding with high hydride levels, and based on low fracture strains observed on cladding with oxide spallation, it cannot be precluded that this cladding may have lower creep rupture strains than those predicted by the CSFM Rev. 1 Monkman-Grant rupture model. Therefore, it cannot be precluded that cladding with high hydrogen levels may fail during dry cask storage. ANL researchers will conduct tests with pressurized gas in high burnup cladding and higher levels of corrosion/hydrides, near design stresses and temperature for dry storage, to determine the continued applicability of these correlations to higher corrosion and hydride levels.

Based on the discussions in Section 4.3, it is recommended that the oxide layer and hydride rim not be included as load bearing material in determining cladding stress and dry cask storage limits. For example, SNF with 100  $\mu\text{m}$  of corrosion and 70  $\mu\text{m}$  of hydride rim should reduce the clad thickness to account for metal loss from oxidation plus discount the 70  $\mu\text{m}$  hydride rim. Because the volume of zirconium oxide is 1.5 times that of zirconium metal this represents a reduction in clad thickness of  $(100/1.5 + 70)$   $\mu\text{m}$  or 0.137 mm. For an initial clad thickness of 0.5461 mm the thickness is reduced to 0.409 mm which means the stress on the cladding will increase by a factor  $(0.5461/0.399)$  of 1.33.

#### **4.3.4. Effects of Annealing and Hydride Reorientation on Creep and Rupture (Temperatures Above Dry Cask Storage Conditions)**

The NRC is interested in temperatures above normal dry storage conditions that may result in thermal annealing of SNF because some cask vendors have proposed cask drying temperatures significantly above 400°C. Also, the NRC would like to evaluate the consequences of accidents that increase the fuel rod temperatures. Thermal annealing of the cladding can increase creep rates and the likelihood of failure.

Bouffieux and Legras (2000) and Bauer and Lowry (1978) have performed thermal testing on SNF cladding. These tests suggest that cask drying operations that do not exceed 400°C will not

result in significant annealing of the SNF cladding and, therefore, should not impact post-irradiation creep. Temperature limits for dry cask storage above 400°C should be examined more thoroughly before being found acceptable for short-term drying operations or for off-normal and accident conditions. For example, for an off-normal transient provided by NRC, with a temperature increase up to 608°C and stress of 184 MPa, CSFM Rev. 1 predicted failure to occur within less than an hour.

Hydride reorientation from the as-fabricated circumferential orientation to the radial orientation in Zircalloys has been found to significantly reduce cladding ductility resulting in a decrease in stress for fracture (Louthan and Marshall 1963). The degree of hydride reorientation has been found to be dependent on circumferential (hoop) tensile stress of the Zircaloy cladding when the hydride platelets precipitate during cooldown. The reorientation begins at stress levels between 50 to 120 MPa depending on fabrication history of the Zircaloy cladding (Louthan and Marshall 1963; Hindle and Slattery 1971; and Pickman 1972). Therefore, it is possible that hydride reorientation may occur in high burnup fuel during cooling following the cask drying operation or an off-normal temperature transient. Higher drying or off-normal temperatures could be detrimental because this will allow more hydrogen in solution and, therefore, more hydride platelets may precipitate in the radial orientation during cooling. The hydride reorientation in the radial direction will decrease ductility, strength, fracture toughness and brittle cladding fracture. An increase in the density of radial hydrides appears to increase the likelihood of crack formation from these hydrides. The result would be to lower the dry cask storage temperature limits for high burnup fuel.

Another concern is for failed rods from in-reactor operation that may be present in fuel assemblies that are subjected to the cask drying operation such that moisture associated with drying does not react with exposed the uranium dioxide to form low density  $U_3O_8$  at cladding breach sites. The formation of  $U_3O_8$  increases the fuel volume that can in turn result in clad splitting and alteration of fuel geometry. Therefore, it is recommended that cask drying temperatures not exceed 400°C for high burnup fuel until further data is obtained in these subject areas.

Bouffieux and Legras (2000) have summarized experimental annealing results for as-fabricated and irradiated Zircaloy cladding tubes. Thermal recovery and recrystallization for irradiated and hydrided tubes require more thermal exposure than as-fabricated tubes. The degree of recrystallization is increased by increasing temperature-time thermal exposure and reduced for increasing hydride content. Combined irradiation exposure and the associated increased hydride levels appear to retard recrystallization. The Bouffieux and Legras (2000) analysis indicates that for cask drying temperatures of 400°C and below, a time period approaching one year may be required for significant recovery and recrystallization of SNF cladding.

The annealing recovery equation used for the CSFM Rev. 1 model is

$$A_F = \text{Fraction recovered} = \frac{1}{1 + (5 \times 10^{21}) e^{-\frac{46440}{T_i} \Delta t_i}} \quad (4.18)$$

where  $\Delta t_i$  (seconds) is time spent at the  $i^{\text{th}}$  temperature  $T_i$ .

The fraction recovered as determined by Equation 4.18 is applied to the creep reduction factor in the CSFM Rev. 1 model to allow for recovery of the irradiation damage. This results in an increase in the creep rate as thermal recovery reduces the creep reduction factor from the value for irradiated Zr-4 cladding toward the value of unity for unirradiated cladding.

For the  $i^{\text{th}}$  time step the steady-state creep is calculated for irradiated cladding with annealing based on the following equations for CSFM Rev. 1A

$$\dot{\epsilon}_{\text{Rev.1A}}^i = \dot{\epsilon}_{\text{Coble}}^i + A_F^i \cdot (\dot{\epsilon}_{\text{GBS-GBD}}^i \cdot \text{CRF}_{\text{GBS-GBD}}^i + \dot{\epsilon}_{\text{LTC}}^i \cdot \text{CRF}_{\text{LTC}}^i) \quad (4.19)$$

and for CSFM Rev. 1B

$$\dot{\epsilon}_{\text{Rev.1B}}^i = \dot{\epsilon}_{\text{Coble}}^i + A_F^i \cdot (\dot{\epsilon}_{\text{GBS-GBD}}^i \cdot \text{CRF}_{\text{GBS-GBD}}^i + \dot{\epsilon}_{\text{climb/glide}}^i \cdot \text{CRF}_{\text{climb/glide}}^i) \quad (4.20)$$

The superscript  $i$  denotes the strain rate, annealing fraction, and creep rate reduction factor at the temperature  $T_i$  for the  $i^{\text{th}}$  time step.

ANL plans an investigation of the effect of annealing during creep of high burnup SNF cladding. Dynamic annealing during deformation may be a concern during cask drying at temperatures above 400°C. The very large stress exponent of 12.5 for the creep of Zr-2 at 425°C as reported by Jones (1966) is difficult to rationalize in terms of published creep mechanisms. Creep concurrent with dynamic recrystallization results in an unstable microstructure that may have an unusually low resistance to deformation. A consequence may be an unusually large value for the stress exponent.

#### **4.4. Validation of CSFM Rev. 1 Methodology with Creep Data**

##### **4.4.1. Validation of CSFM Rev. 1A with Unirradiated and Irradiated Zircaloy Creep Data.**

A comparison of measured versus predicted steady-state creep rate using CSFM Rev. 1A for all of the unirradiated and irradiated data creep data is provided in Figure 4.25. A perfect fit of the data would lie on the 45° diagonal line. Data above the 45° line are overpredicted and data below the line are underpredicted. This shows that all but six of the irradiated creep data are bounded by the Rev. 1A methodology with three of the six only slightly underpredicted. A bounding creep curve is used because 1) there are several different cladding types in the SNF inventory, and 2) there is very little irradiated creep data within the design basis temperature and stress range for dry cask storage.

Comparisons of the predictions of the proposed CSFM Rev. 1A equations with data for unirradiated and irradiated Zr-2/-4 at the different test temperatures of 300, 325, 350, 380, 400, and 420°C are presented in Figures 4.26 through 4.31. This provides an indication of the level of conservatism that exists at the different test temperatures. Most of the irradiated data were irradiated to neutron fluence levels of  $\sim 8.5$  to  $12 \times 10^{21}$  n/cm<sup>2</sup> ( $E > 1\text{MeV}$ ). Consequently, the irradiated curve in these figures is for a fluence of  $10 \times 10^{21}$  n/cm<sup>2</sup> ( $E > 1\text{MeV}$ ). Note that some of the Framatome cladding data, such as from Bouffioux and Rupa (2000) and from Limon et al.

(2000) at 380 °C and 400 °C, appear similar and may be the same data reported in the two different publications, but this could not be confirmed.

Examination of Figures 4.26 to 4.31 shows that there is considerable scatter in the creep rate data with the Einziger and Kohli (1984) data showing the largest scatter of two orders of magnitude variation in SNF cladding creep rate. The four data points that are significantly underpredicted are one of the Einziger and Kohli data points at 325 °C and ~150 MPa; a Chung et al. (1987) data point at 292 °C and 552 MPa; and two Goll et al. (2001) data points at 300 °C and 552 MPa, and at 370 °C and 320 MPa.

#### **4.4.2. Validation of CSFM Rev. 1B with Unirradiated and Irradiated Zircaloy Creep Data**

A second creep model was also developed based on a hyperbolic sine function similar to that proposed by Murty (1999) for creep by climb/glide; this model has been identified as CSFM Rev. 1B.

A comparison of measured versus predicted steady-state creep rate using CSFM Rev. 1B for all of the irradiated data creep data is provided in Figure 4.32. A perfect fit of the data would lie on the 45° diagonal line. Data above the 45° line are overpredicted and data below the line are underpredicted. This shows that all but four of the irradiated creep data are equal to or bounded by the Rev. 1B methodology. A bounding creep curve is used because 1) there are several different cladding types in the SNF inventory, and 2) there is very little irradiated creep data in the design basis temperature and stress range for dry cask storage. Therefore, conservatism is provided for all SNF cladding types and those yet to be tested in the range for dry cask storage.

A comparison of the CSFM Rev. 1A predictions to the creep data in Figure 4.25 and the CSFM Rev. 1B predictions to creep data in Figure 4.32 shows that the latter model (CSFM Rev. 1B) provides a slightly better fit and less scatter relative to the 45° diagonal than the CSFM Rev. 1A predictions for measured creep rates between  $10^{-7}$  to  $10^{-10}$  sec<sup>-1</sup>. The CSFM Rev. 1A predictions provide a better fit to the 45° diagonal at creep rates greater than  $10^{-7}$  sec<sup>-1</sup>. The slower creep rates are of interest for dry cask storage; therefore, this suggests that CSFM Rev. 1B provides a

slightly better prediction to the irradiated data in the range of interest. The CSFM Rev. 1B creep model also underpredicts fewer of the irradiated creep data than CSFM Rev. 1A. Therefore, it is recommended that CSFM Rev. 1B creep equations be used rather than the Rev. 1A equations; even though, within the temperature and stress range for dry cask storage of  $< 380\text{ }^{\circ}\text{C}$  and  $\leq 150\text{ MPa}$  respectively, the CSFM 1A and 1B creep equations predict the same temperature limits within  $\pm 2\text{ }^{\circ}\text{C}$ .

Comparisons of predictions using the CSFM Rev. 1B equations with data for unirradiated and irradiated Zr-2/-4 at the different temperatures of 300, 325, 350, 380, 400, and  $420\text{ }^{\circ}\text{C}$  are presented in Figures 4.33 through 4.38. The comparison of predictions and data in these figures shows that the CSFM Rev. 1B equations bound most of the unirradiated and irradiated creep rate data. Most of the irradiated data were irradiated to neutron fluence levels of  $8.5\text{ to }12 \times 10^{21}\text{ n/cm}^2$  ( $E > 1\text{ MeV}$ ). Consequently, the irradiated curve in these figures is for a fluence of  $10 \times 10^{21}\text{ n/cm}^2$  ( $E > 1\text{ MeV}$ ). The four data that are underpredicted with CSFM Rev. 1B are two of the Einziger and Kohli (1984) data points at  $325\text{ }^{\circ}\text{C}$  and  $\sim 150\text{ MPa}$ ; a Goll et al. (2001) data point at  $370\text{ }^{\circ}\text{C}$  and  $320\text{ MPa}$ , and a Mayuzumi and Murai (1993) data point at  $420\text{ }^{\circ}\text{C}$  and  $154\text{ MPa}$ .

An important observation from Figures 4.26 to 4.31 and Figures 4.33 to 4.38 is that there is a large scatter in the measured creep rates for different cladding types at similar temperature and stress conditions. The largest range of creep rates for unirradiated cladding, a factor of over 200 range in rate, is observed at the  $350\text{ }^{\circ}\text{C}$  (Figure 4.28 or 4.35) and at a stress of  $100\text{ MPa}$ . The largest range of creep rates for irradiated cladding, a factor of  $\sim 100$  range in rate, is observed at  $325\text{ }^{\circ}\text{C}$  (Figure 4.27 or 4.34) and at a stress of  $\sim 150\text{ MPa}$ . This data is from Einziger and Kohli (1984) and part of the reason for the large scatter are the very low creep rates measured on SNF cladding. The next largest range of creep rates for irradiated cladding, a factor of 20 range in rate, is observed at  $420\text{ }^{\circ}\text{C}$  (Figure 4.31 or 4.38) and a stress of  $\sim 150\text{ MPa}$ . Creep rates measured by the same experimenter and similar cladding types show a factor of 5 to 7 variation in creep rates. This illustrates the wide range of possible creep rates for SNF cladding and the difficulty in predicting creep rates and temperature limits for dry cask storage. This is further complicated

by the large scatter in the creep rupture data and the lack of creep or rupture data in the temperature and stress range of interest.

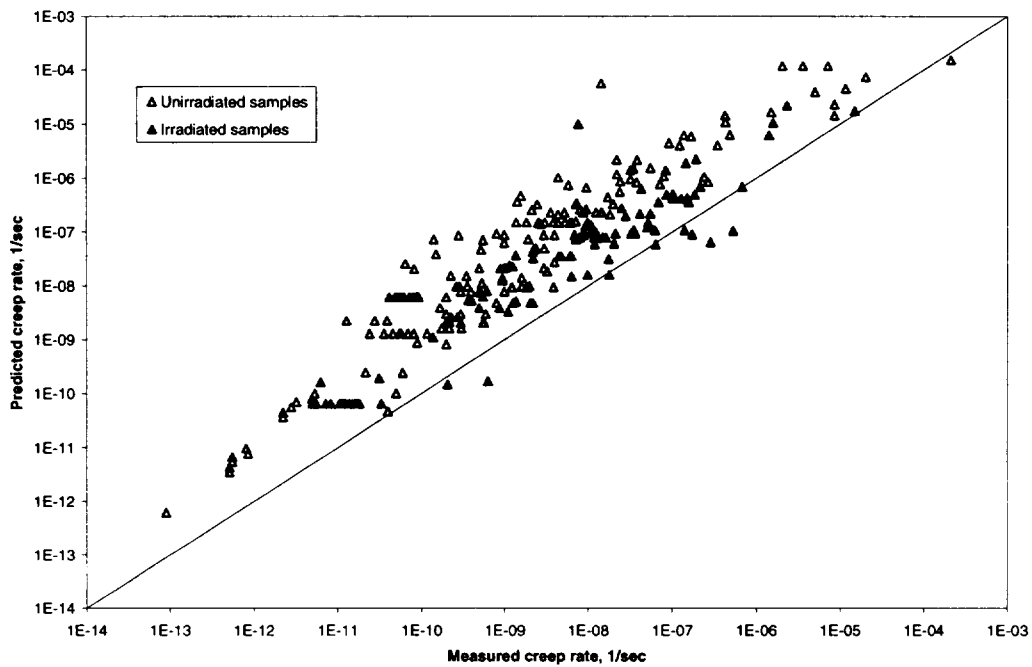


Figure 4.25 Predicted Versus Measured Creep Rate Using CSFM Rev. 1A for All Data.

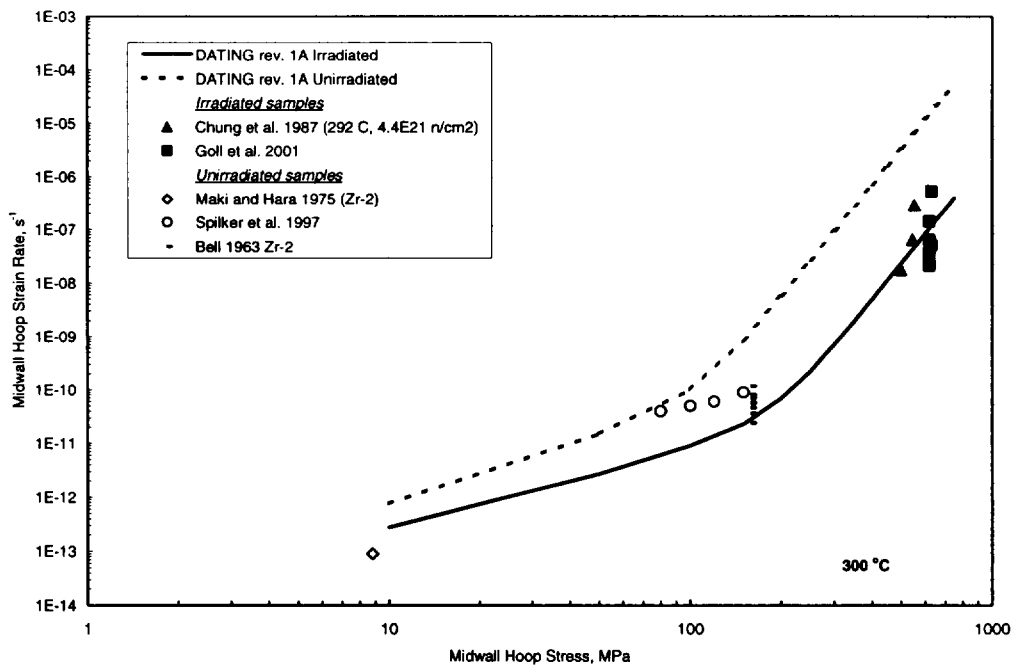


Figure 4.26 Comparison of CSFM Model 1A with Unirradiated and Irradiated Zr-2/-4 Cladding Creep Data at 300°C.

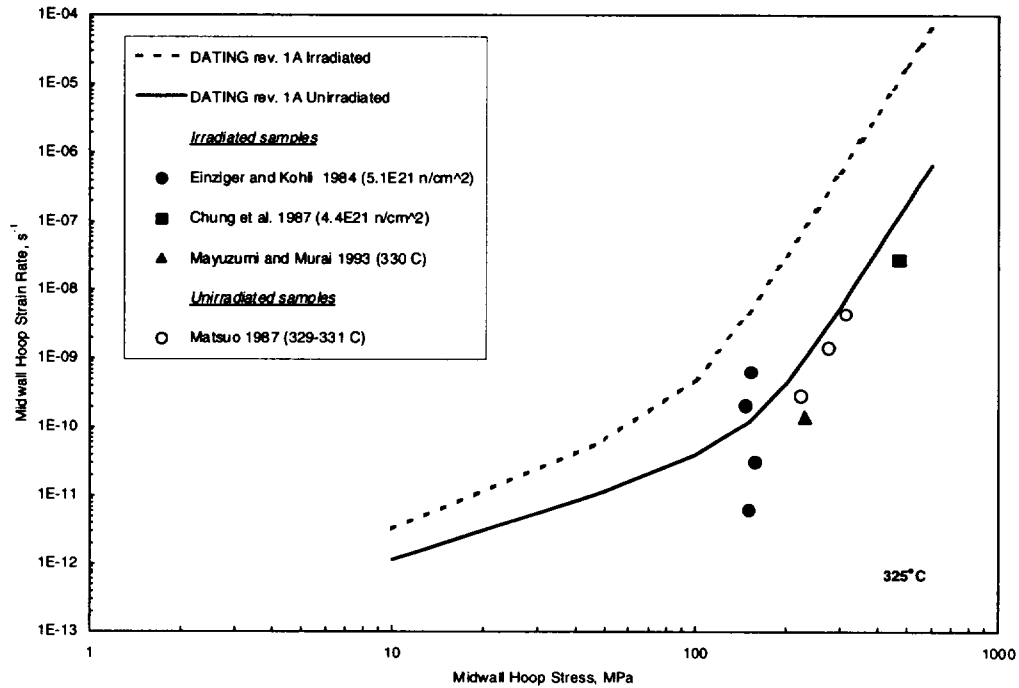


Figure 4.27 Comparison of CSFM Model 1A With Unirradiated and Irradiated Zr-2/-4 Cladding Creep Data at 325°C.

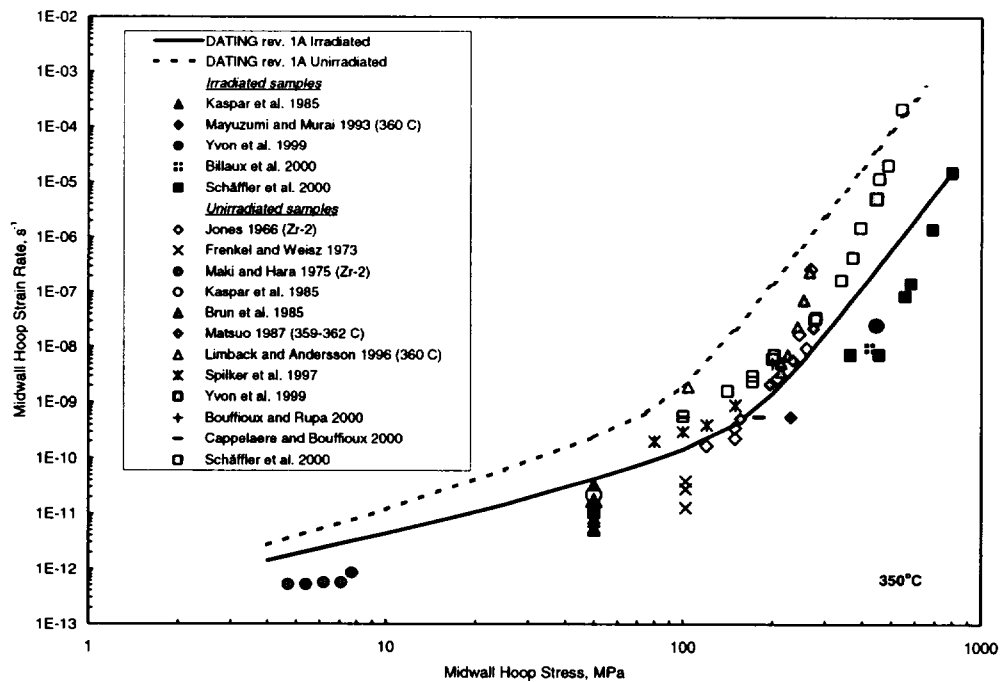
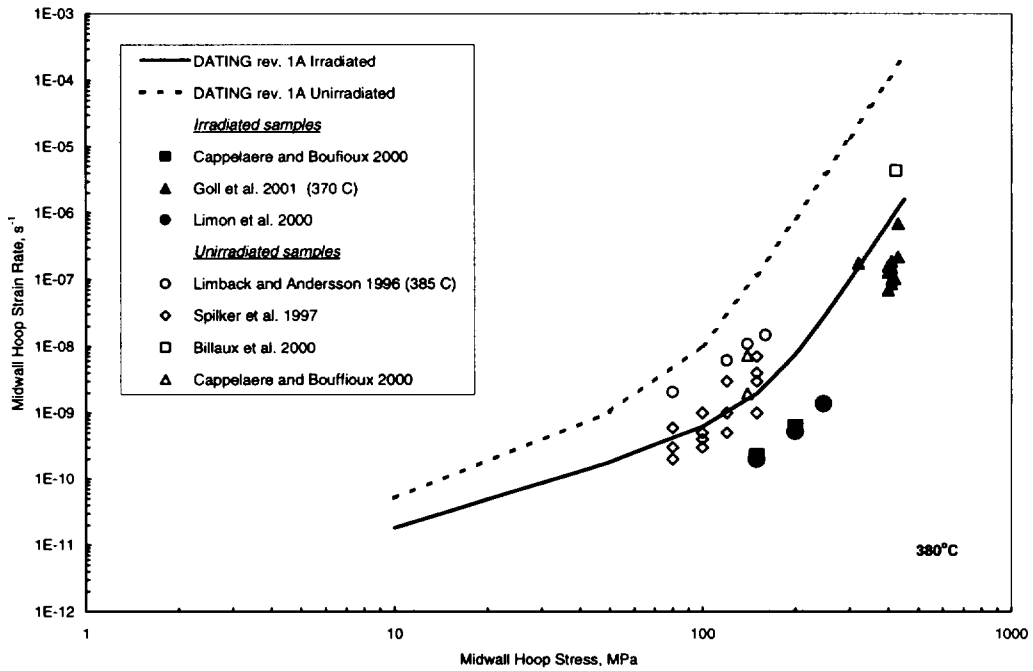
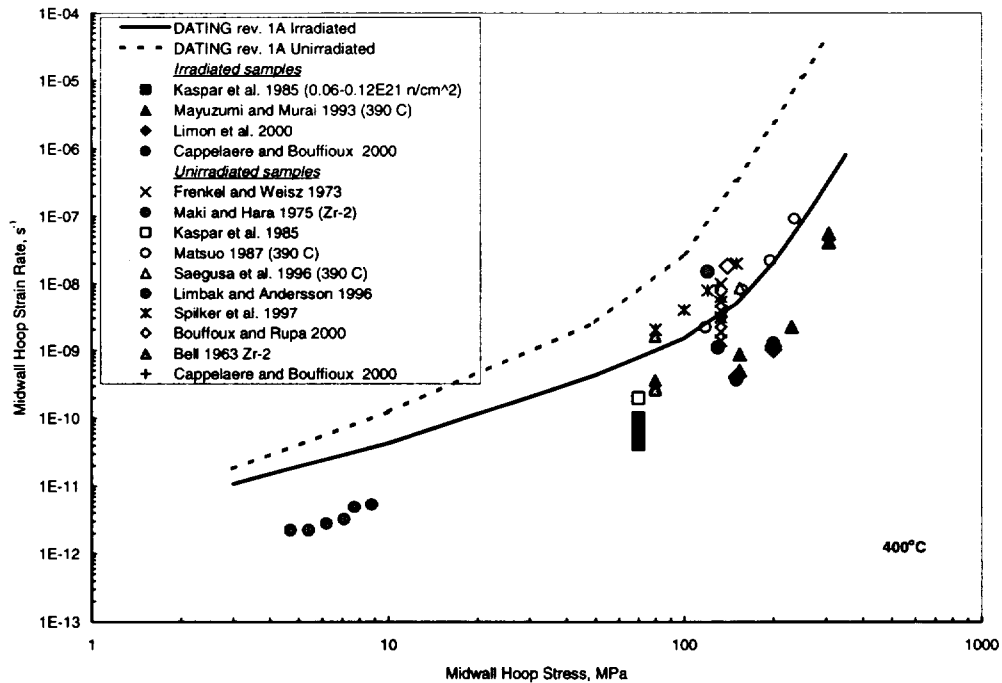


Figure 4.28 Comparison of CSFM Model 1A with Unirradiated and Irradiated Zr-2/-4 Cladding Creep Data at 350°C.



**Figure 4.29 Comparison of CSFM Model 1A with Unirradiated and Irradiated Zr-2/-4 Cladding Creep Data at 380°C.**



**Figure 4.30 Comparison of CSFM Model 1A with Unirradiated and Irradiated Zr-2/-4 Cladding Creep Data at 400°C.**

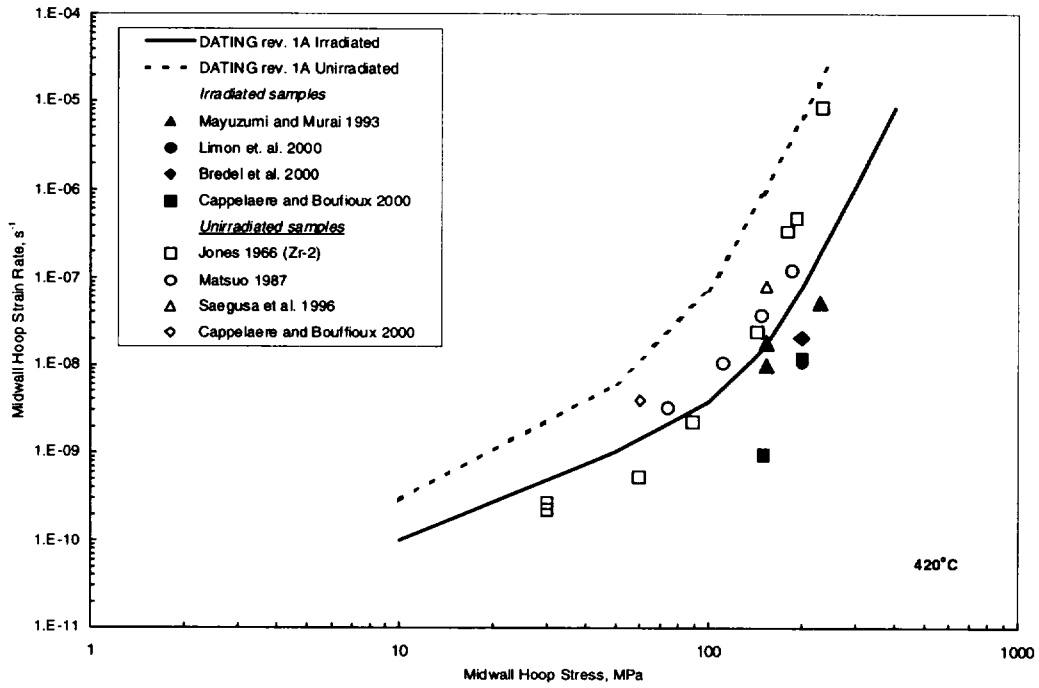


Figure 4.31 Comparison of CSFM Model 1A with Unirradiated and Irradiated Zr-2/-4 Cladding Creep Data at 420°C.

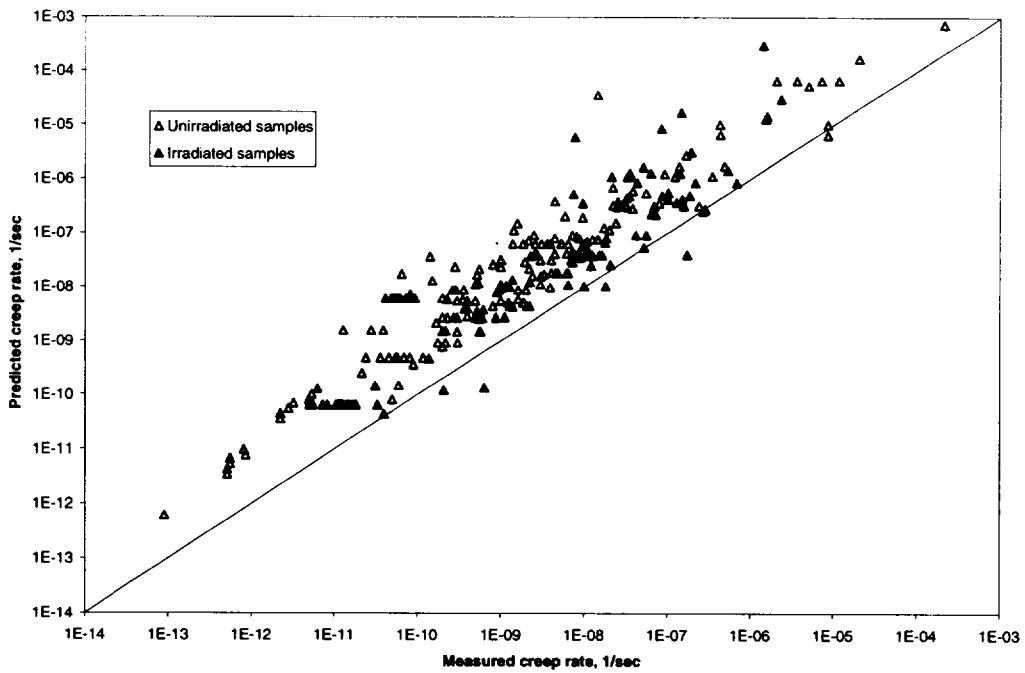
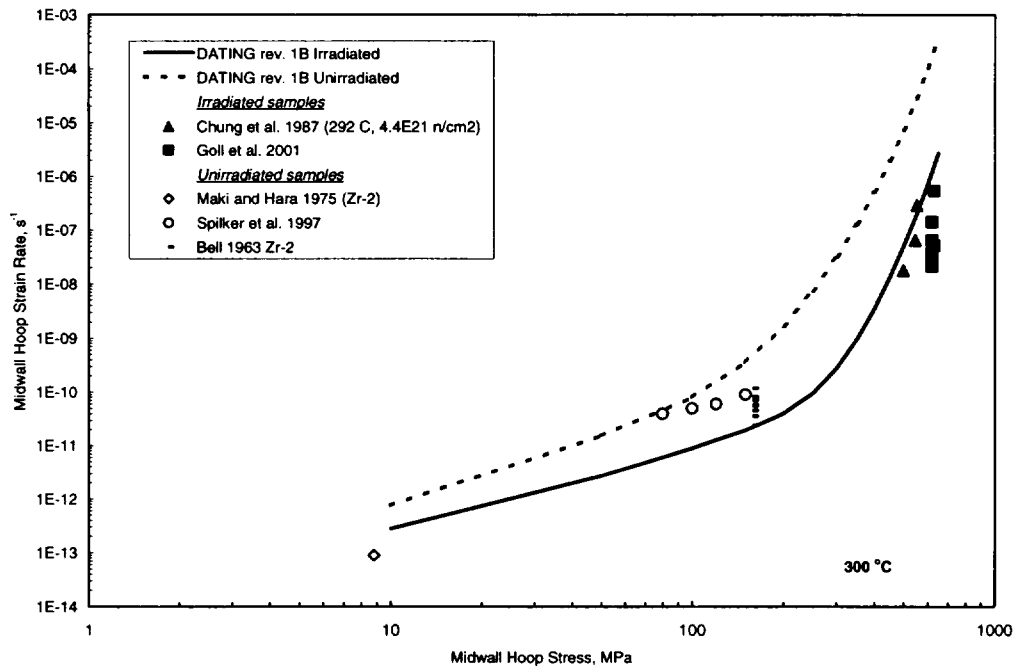
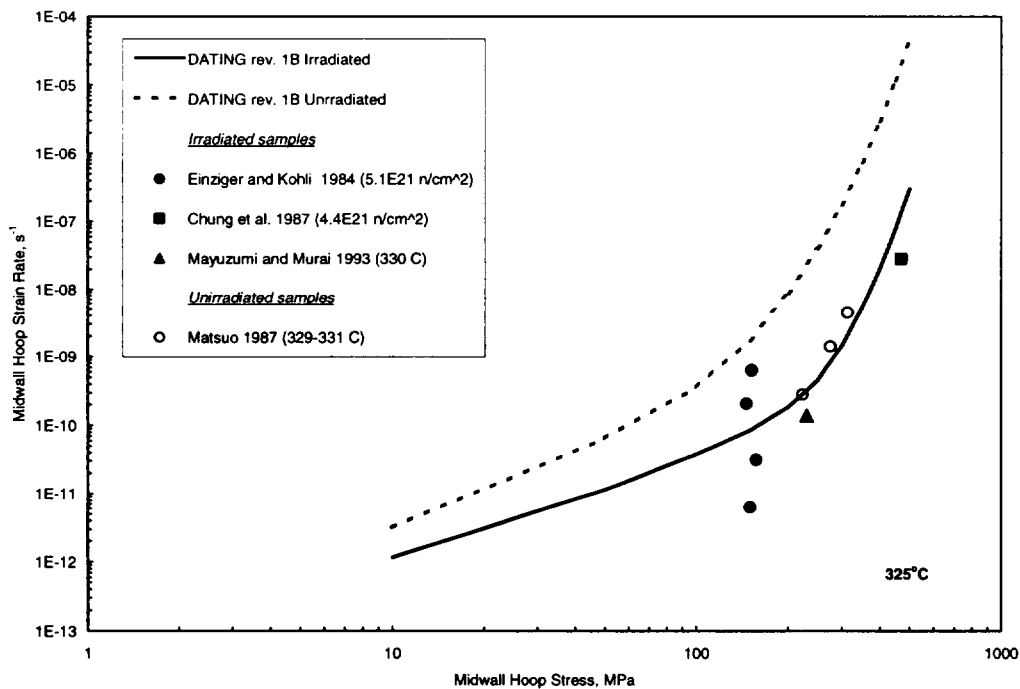


Figure 4.32 Predicted Versus Measured Creep Rate Using CSFM Rev. 1B for All Data.



**Figure 4.33 Comparison of CSFM Model 1B with Unirradiated and Irradiated Zr-2/-4 Cladding Creep Data at 300°C.**



**Figure 4.34 Comparison of CSFM Model 1B with Unirradiated and Irradiated Zr-2/-4 Cladding Creep Data at 325°C.**

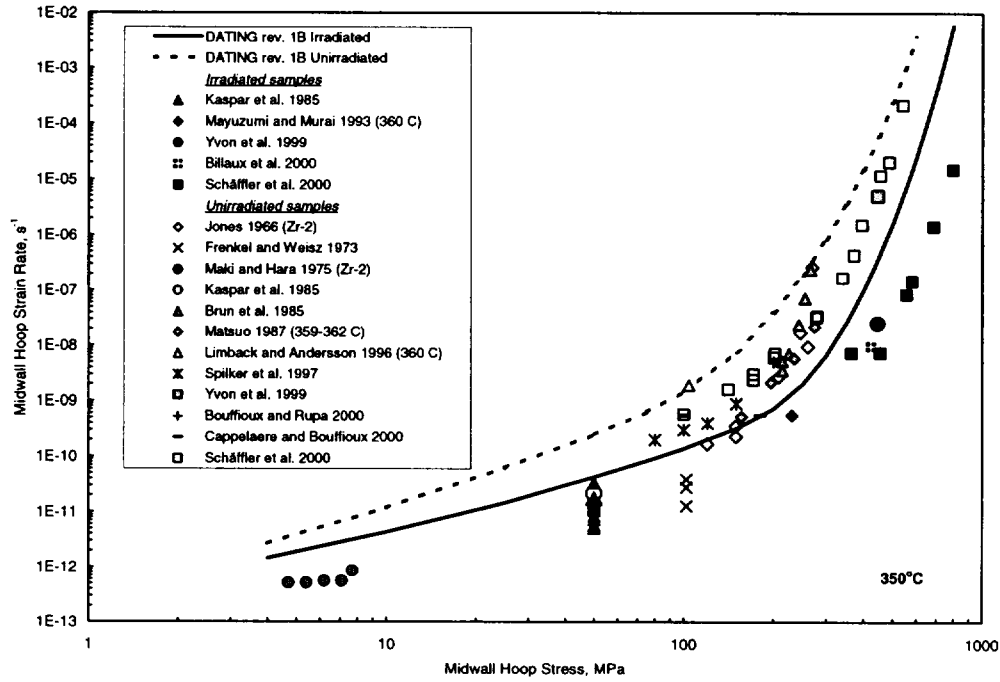


Figure 4.35 Comparison of CSFM Model 1B with Unirradiated and Irradiated Zr-2/-4 Cladding Creep Data at 350°C.

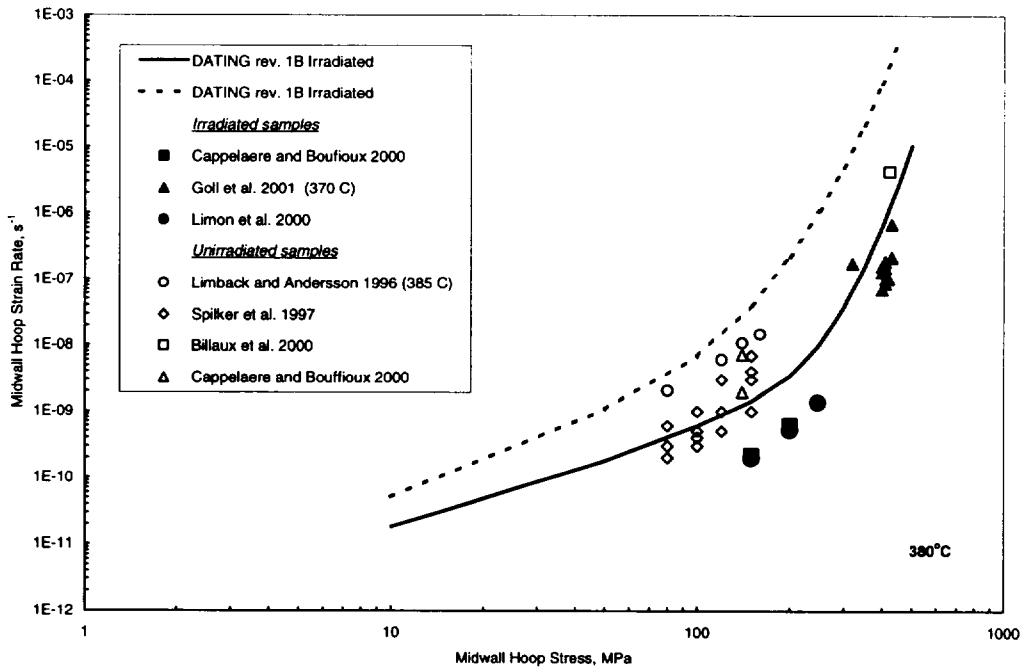
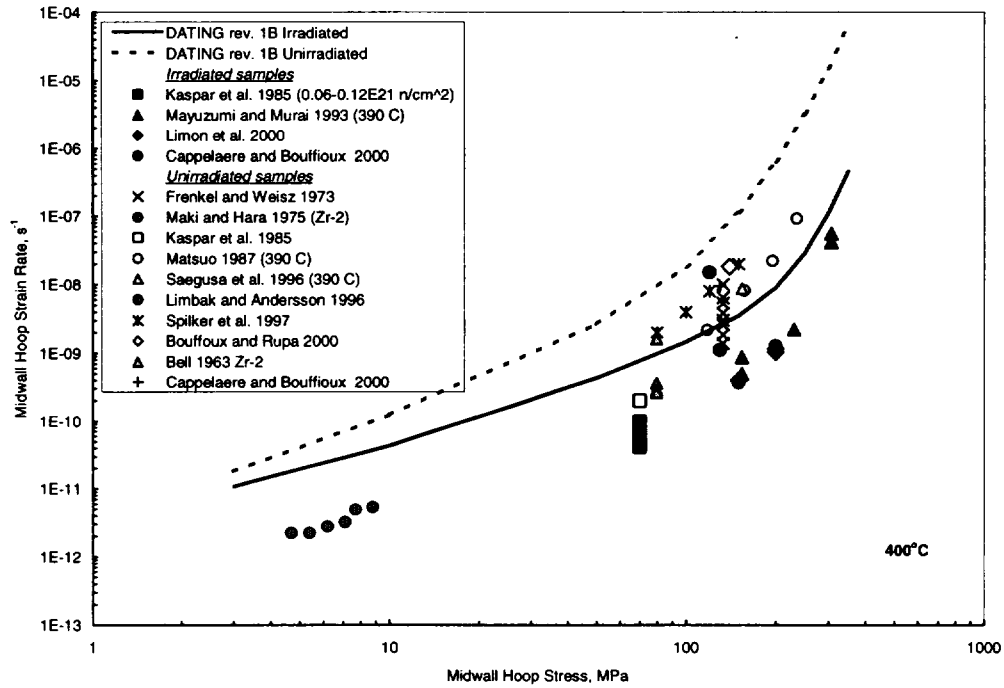
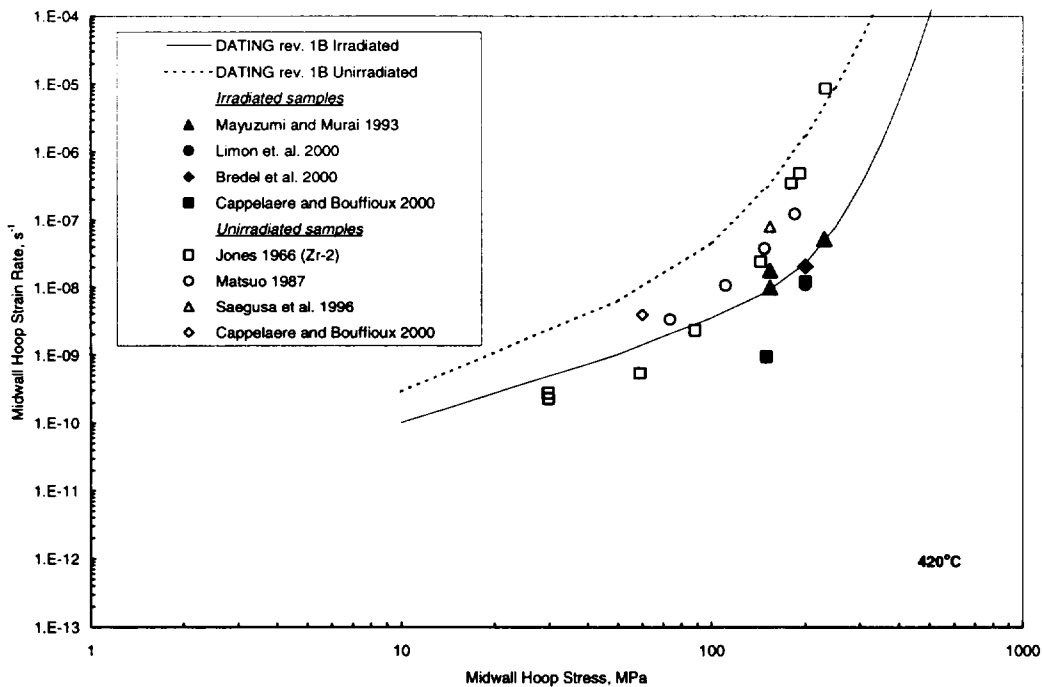


Figure 4.36 Comparison of CSFM Model 1B with Unirradiated and Irradiated Zr-2/-4 Cladding Creep Data at 380°C.



**Figure 4.37 Comparison of CSFM Model 1B with Unirradiated and Irradiated Zr-2/-4 Cladding Creep Data at 400°C.**



**Figure 4.38 Comparison of CSFM Model 1B with Unirradiated and Irradiated Zr-2/-4 Cladding Creep Data at 420°C.**

#### 4.5. Deformation Mechanism Maps

The deformation maps in Figures 4.39 and 4.40 are presented for unirradiated and irradiated ( $\Phi = 1 \times 10^{22} \text{ n/cm}^2$ ) Zircaloy, respectively in the CSFM Rev. 1A and Rev. 1B models. The stress-temperature boundaries characteristic for the model describing creep of unirradiated cladding are shown as dashed lines. Solid lines portray boundaries of the model describing creep of irradiated cladding. Also included in Figures 4.39 and 4.40 are the published experimental data used in the present study. The stress-temperature area characteristic for dry cask storage of SNF is shown as a solid box.

No fracture map is provided because the CSFM Rev. 1 methodology assumes only the Monkman-Grant model is active within the range of the data and the dry storage application. The Monkman-Grant model can be used to describe more than one fracture mechanism, but due to the limited amount of creep rupture data, it was not possible separate the different fracture mechanisms. Therefore, the Monkman-Grant relationship proposed for the CSFM Rev. 1 methodology may be a composite of different fracture mechanisms.

#### 4.6. Life Fraction Rule

CSFM Rev. 1 continues to use the life fraction rule that was employed for CSFM Rev. 0 for changing stress and temperature, as is the case for dry cask storage. The life fraction rule assumes that damage from all mechanisms is independent and additive. The life fraction rule can be expressed as

$$1 = \sum_{i=1}^n \frac{\Delta t_i}{\tau_i} = \frac{\Delta t_1}{\tau_1} + \frac{\Delta t_2}{\tau_2} + \frac{\Delta t_3}{\tau_3} + \dots + \frac{\Delta t_n}{\tau_n} \quad (4.21)$$

where

$\Delta t_i$  = time spent at the  $i^{\text{th}}$  temperature,

$\tau_i$  = period required to fracture a specimen under the  $i^{\text{th}}$  temperature (isothermal) and stress (isostress) conditions.

When the cumulative fraction, the summation of the life fractions ( $\Delta t_i/\tau_i$ ), reaches one, failure is assumed. The time period required for rupture,  $\tau_i$ , is calculated using the Monkman-Grant correlation (Equation 4.13) and the calculated steady-state creep rate (Equation 4.19 or 4.20).

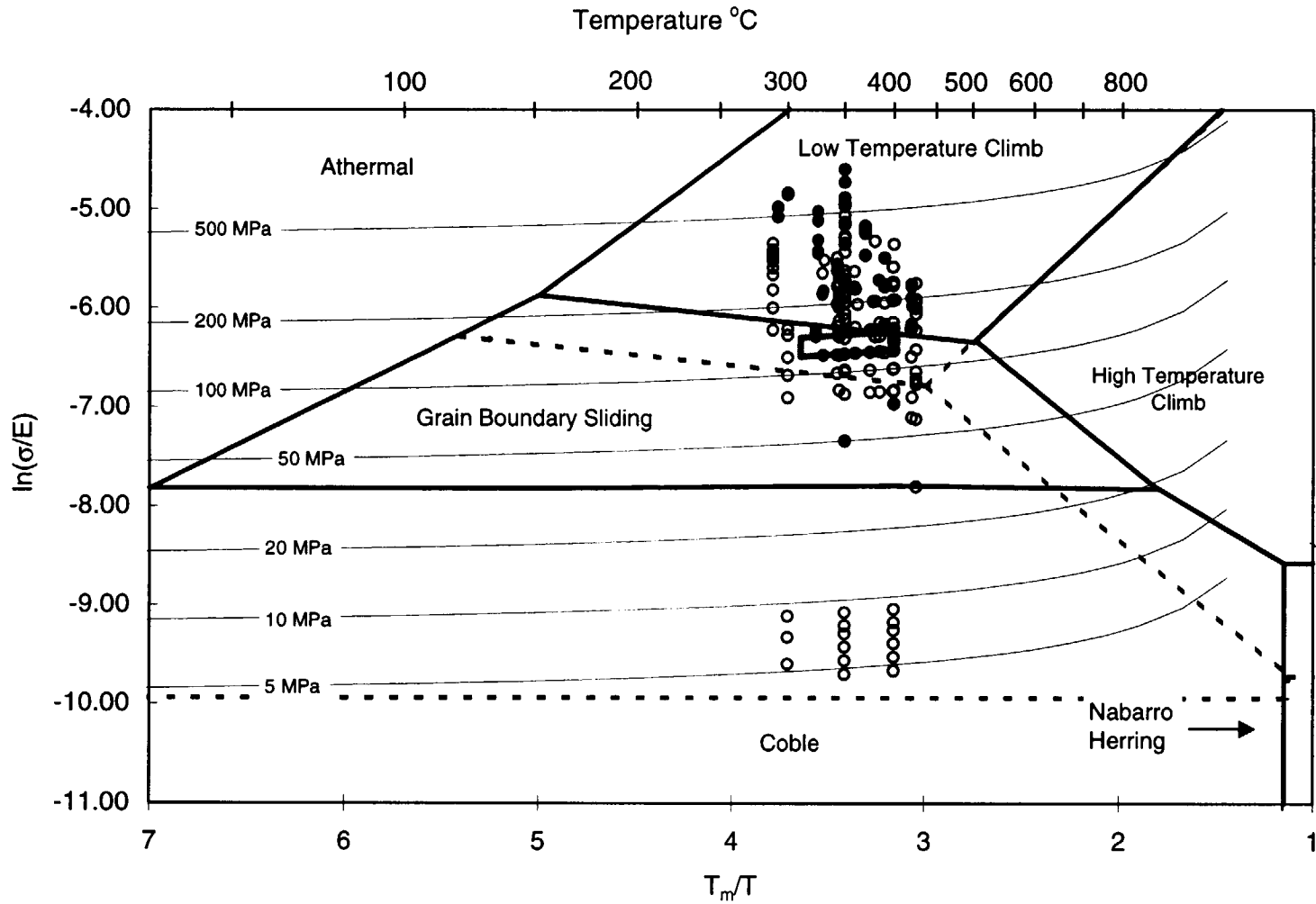


Figure 4.39 Deformation Mechanism Map for the CSFM Rev. 1A Model for Zircaloy Cladding.

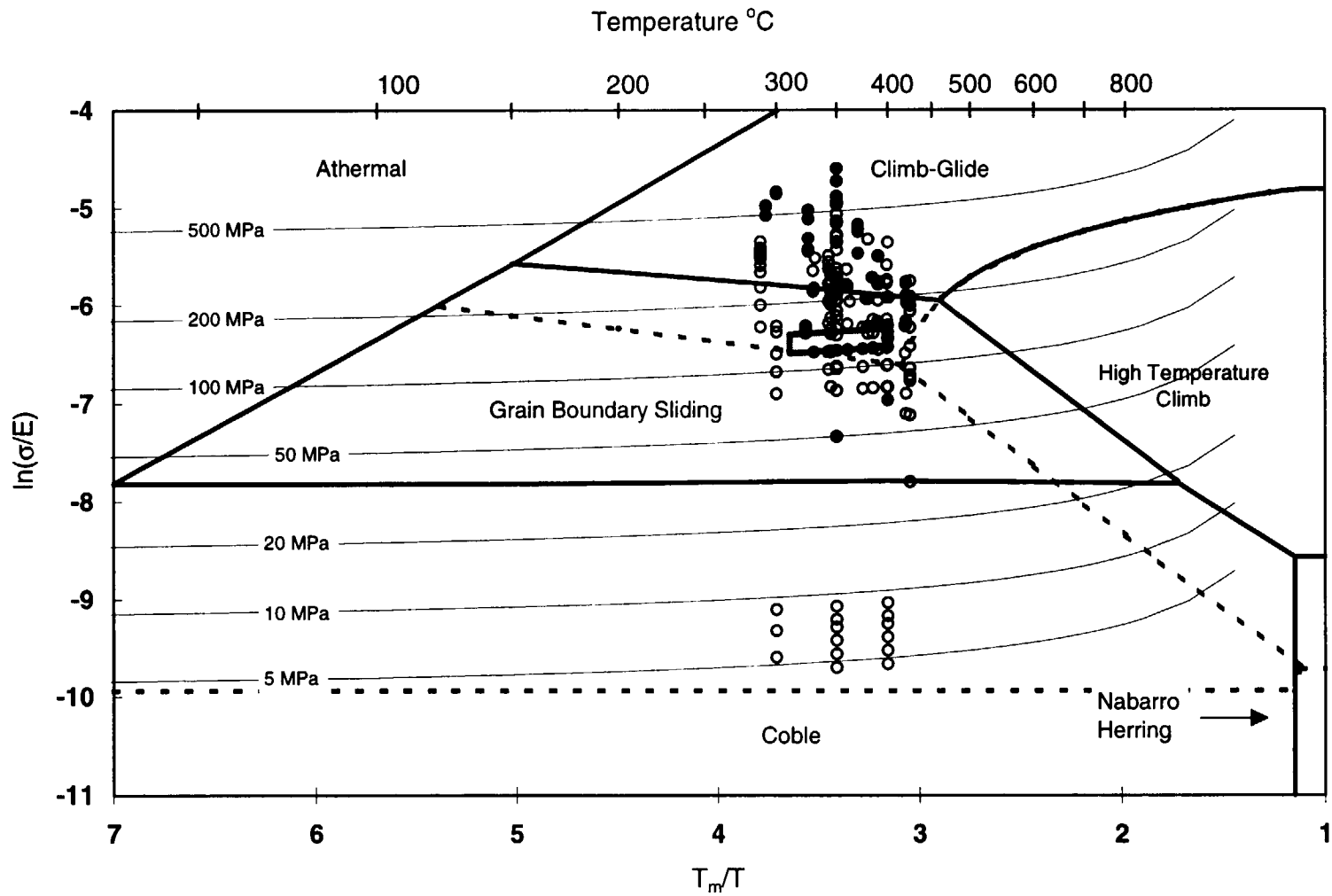


Figure 4.40 Deformation Mechanism Map for the CSFM Rev. 1B Model for Zircaloy Cladding

## **5. CSFM REV. 1 CALCULATED TEMPERATURE LIMITS**

### **5.1. Comparison of CSFM Rev. 1 and Rev. 0 Calculated Temperature Limits**

Temperature limits as a function of stress were calculated using both CSFM Rev. 1 and Rev. 0 models in DATING and are shown in Figures 5.1 and 5.2 for low and high burnup fuel, respectively. The comparisons made in this section are for cooling times of 5 and 10 years for both low and high burnup fuel. As will be shown in this section, fuel age, i.e., cooling time after reactor discharge, at the time of storage has the strongest impact on the allowable temperature limit with the second strongest impact being stress, and the third strongest burnup. Consequently, the difference in calculated temperature limits between CSFM Rev. 1 and Rev. 0 will significantly change for different cooling times. The low burnup cooling curve used for these calculations is the helium cooling curve from CSFM Rev. 0 that was calculated using ORIGEN-2 for PWR fuel at a burnup of 30 GWd/MTU (Levy et al. 1987). The high burnup cooling curve used for these calculations is based on ORIGEN-ARP calculations for PWR fuel at a burnup of 60 GWd/MTU.

As evidenced in Figures 5.1 and 5.2, both cooling time before storage and fuel burnup have an impact on dry storage temperature limits. High burnup fuel has a higher initial heat load for the same cooling time as low burnup fuel so that less high burnup fuel can be loaded in the same cask. However, for determining fuel temperature limits, the heat load for high burnup fuel decays faster, such that a cask loaded only with high burnup fuel can withstand an initially higher temperature limit than can a cask loaded with low burnup fuel for the same cooling time.

The DATING Rev. 1 and Rev. 0 results indicate that the largest difference in calculated temperature limits between the two models is ~ 20°C for low burnup fuel and ~ 15°C for high burnup fuel, with Rev. 1 predicting the lower limit at a stress of 110 MPa and 10 year cooling time. Between stresses of 130 to 150 MPa the predicted temperature limits are similar for high burnup fuel with 10 year cooling and similarity is not achieved for low burnup fuel with 10 year cooling until stresses are between 160 to 170 MPa.

For low burnup fuel with 5 year cooling CSFM Rev. 1 predicts only a 5 to 7°C lower temperature limit than Rev. 0 for stresses between 80 to 120 MPa, and similar temperature limits at stresses between 130 to 140 MPa. For stresses above 150 MPa, Rev. 1 predicts increasingly higher temperature limits than Rev. 0 models. For high burnup fuel with 5 year cooling, Rev. 1 and Rev. 0 predict similar temperature limits for stresses between 80 to 120 MPa, while Rev. 1 predicts increasingly higher temperature limits than Rev. 0 for stresses above 120 MPa.

Examination of the Rev. 0 results shows a significant inflection in the temperature limit curves while there is no similar inflection in the curve for Rev. 1. The inflection in Rev. 0 exists because Rev. 0 assumed that the failure mechanism below a stress of 110 MPa was DCCG while above 110 MPa the failure mechanism was power law cavitation, i.e., modeled using the Monkman-Grant correlation. The lack of inflection in Rev. 1 is because only the Monkman-Grant approach is used for estimating rupture times, which is in contrast to the two mechanisms used for Rev. 0. The differences in predicted temperature limits above 110 MPa between Rev. 0 and Rev. 1 where both use Monkman-Grant approach are due to differences in the creep equations and the Monkman-Grant coefficient between Rev. 0 and Rev. 1.

The higher temperature limits for Rev. 0 compared to for Rev. 1 in the stress range of 60 to 110 MPa are due to the presence of the DCCG rupture mechanism in this stress range. As noted earlier, the DCCG rupture model is not included in the temperature limit calculations for the Rev. 1 methodology.

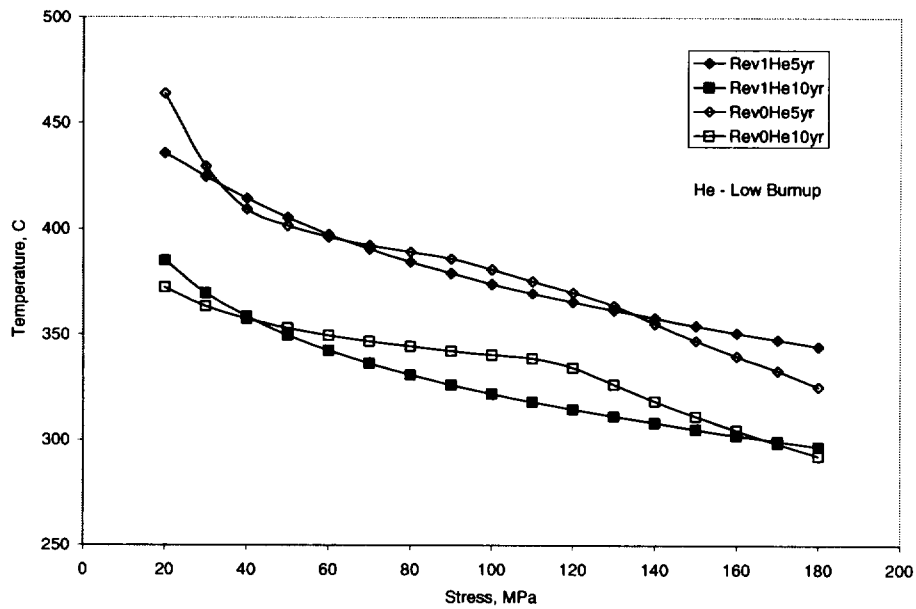


**Figure 5.1 Comparison of CSFM Rev. 1 and Rev. 0 Calculated Temperature Limits as a Function of Stress for Low Burnup Fuel (30 GWd/MTU) with 5 and 10 year Cooling (Using the Helium Cooling Curve from CSFM Rev. 0).**

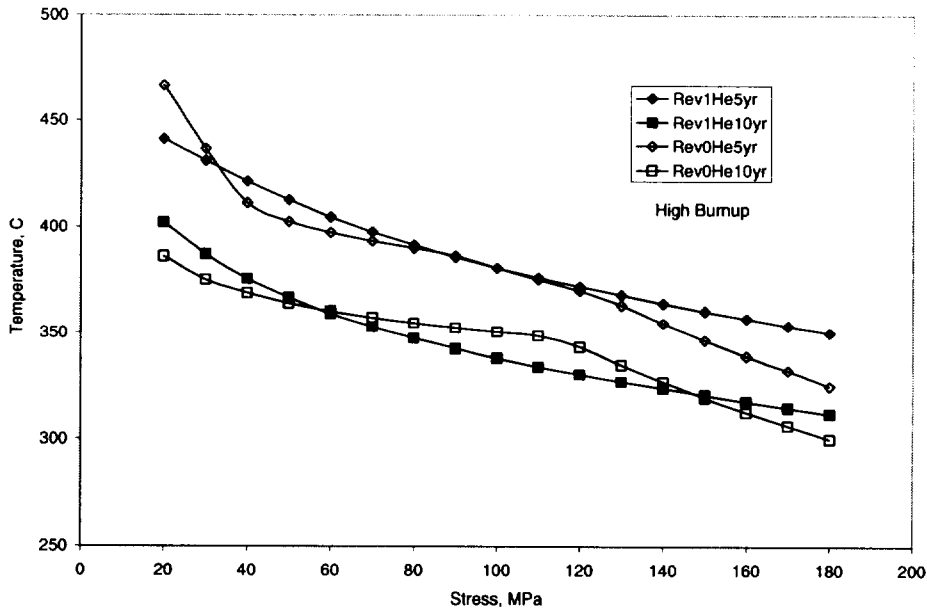


**Figure 5.2 Comparison of CSFM Rev. 1 and Rev. 0 Calculated Temperature Limits as a Function of Stress for High Burnup Fuel (60 GWd/MTU) with 5 and 10 year Cooling.**

## 5.2. Sensitivity and Uncertainty Analyses on Temperature Limits

In order to evaluate the sensitivity of the creep and rupture models to predicted temperature limits, these models were modified to increase or decrease the respective model predictions by a specified amount. The impact of varying the new CSFM Rev. 1 creep and rupture models by a factor of 2 on calculated cladding temperature limits is provided in Figure 5.3 for high burnup fuel with 10 year cooling. A similar plot of varying creep and rupture models by a factor of 2 is provided in Figure 5.4 for low burnup fuel with 10 year cooling. Examination of Figure 5.3 for high burnup fuel with 10 year cooling demonstrates that a variation of a factor of 2 in creep and creep time-to-rupture (conservative Monkman-Grant coefficient) changes the calculated temperature limits by  $\sim \pm 15\text{ }^{\circ}\text{C}$  at a stress of 150 MPa and  $\sim \pm 16\text{ }^{\circ}\text{C}$  at a stress of 110 MPa, respectively. Examination of Figure 5.4 for low burnup fuel with 10 year cooling demonstrates that the same factor of 2 variation in creep and creep rupture strain changes the calculated temperature limits by  $\sim \pm 15\text{ }^{\circ}\text{C}$  at stresses between 110 to 150 MPa. In both Figure 5.3 and 5.4 the points for a factor of 2 increase in creep rate fall on top of the factor of 2 decrease in the Monkman-Grant coefficient. This means that increasing the creep rate by a factor of 2 is equivalent to a factor of 2 decrease in rupture time.

It should be noted that the difference between the conservative Monkman-Grant coefficient and the best-estimate (mean) coefficient is approximately 1.8 so that using the best-estimate coefficient in DATING will result in approximately 11 to 12 $^{\circ}\text{C}$  higher SNF temperature limits. It is also noted the use of the best-estimate coefficient still results in a bounding prediction of the creep rupture data collected in this work (Figures 4.15 and 4.16) because the creep equations used for CSFM Rev. 1 are bounding and conservative. This leaves it up to the user on the level of conservatism they feel comfortable with in determining temperature limits.

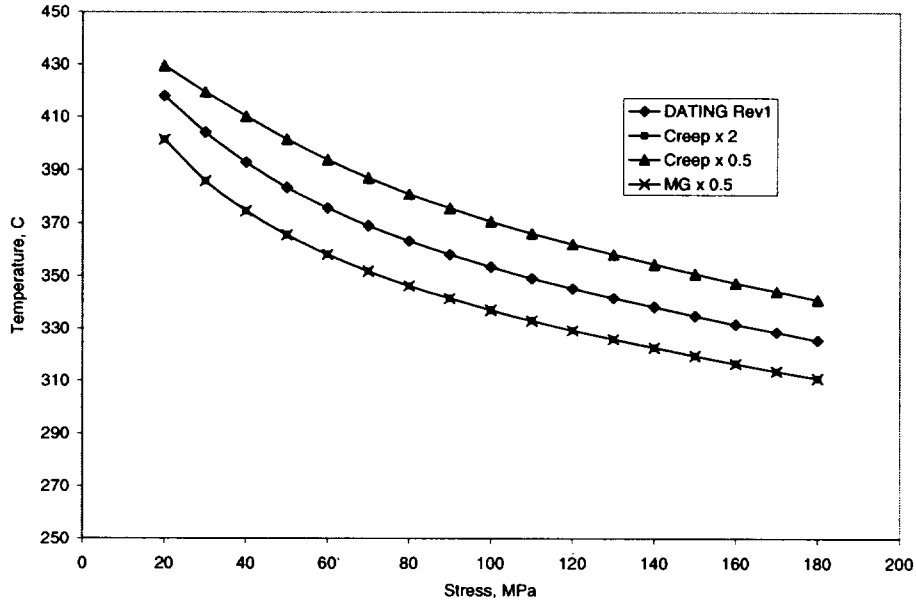


**Figure 5.3 Sensitivity of Varying Rev. 1 Creep Rates and Rupture Time (Monkman-Grant Coefficient) by a Factor of 2 on Calculated Temperature Limits for High Burnup (60 GWd/MTU) Fuel Cooled for 10 Years.**

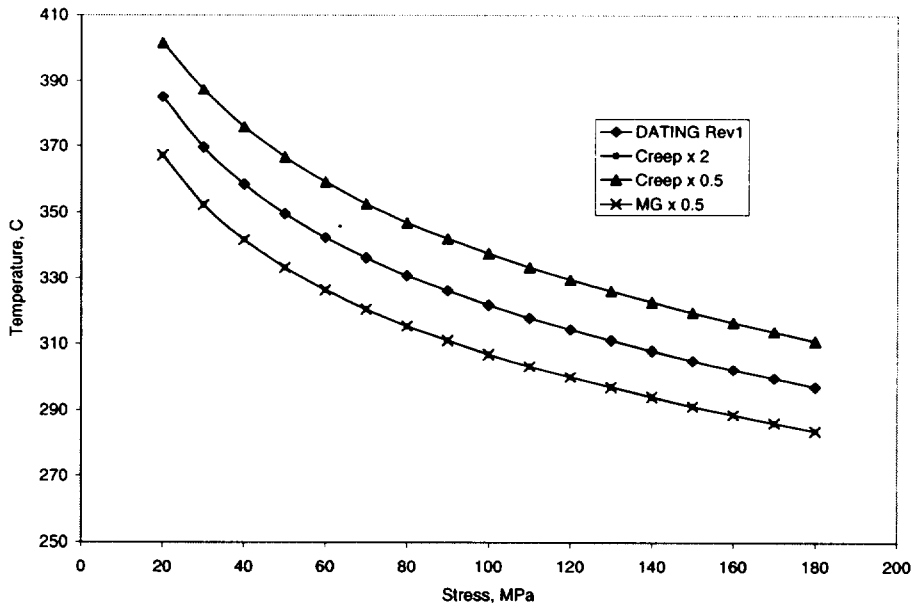


**Figure 5.4 Sensitivity of Varying Rev. 1 Creep Rates and Rupture Strain (Monkman-Grant Coefficient) by a Factor of 2 on Calculated Temperature Limits for Low Burnup (30 GWd/MTU) Fuel Cooled for 10 years.**

### **5.3. Comparison of CSFM Rev.1 Temperature Limits to Those Calculated with Other Methodologies**

A comparison of calculated temperature/stress limits using CSFM Rev. 1 models (conservative Monkman-Grant coefficient) in DATING to those calculated using two recently proposed methodologies by Spilker et al. 1996 and Siegmann 2000 for determining SNF temperature limits, is provided in Figures 5.5 to 5.10 for low (30 GWd/MTU) and high (60 GWd/MTU) burnup fuel. For both low and high burnup fuel only one cooling time of 10 years is assumed.

The comparison of calculated temperature limits from CSFM Rev. 1 to those calculated with the Spilker et al. (1996) methodology (assumes a 1% strain limit for failure) is shown in Figures 5.5 and 5.6 for high and low burnup fuel, respectively. For high burnup fuel (Figure 5.5) the Spilker et al. predicted temperature limits are lower than those predicted by CSFM Rev.1 at all stresses. For low burnup fuel (30 GWd/MTU) the Spilker et al. model predicts higher temperature limits at stresses equal to or below 110 MPa and similar to CSFM Rev. 1 temperature limits between stresses of 120 to 130 MPa. The CSFM Rev. 1 predicted temperature limits then become higher at stresses above 135 MPa.

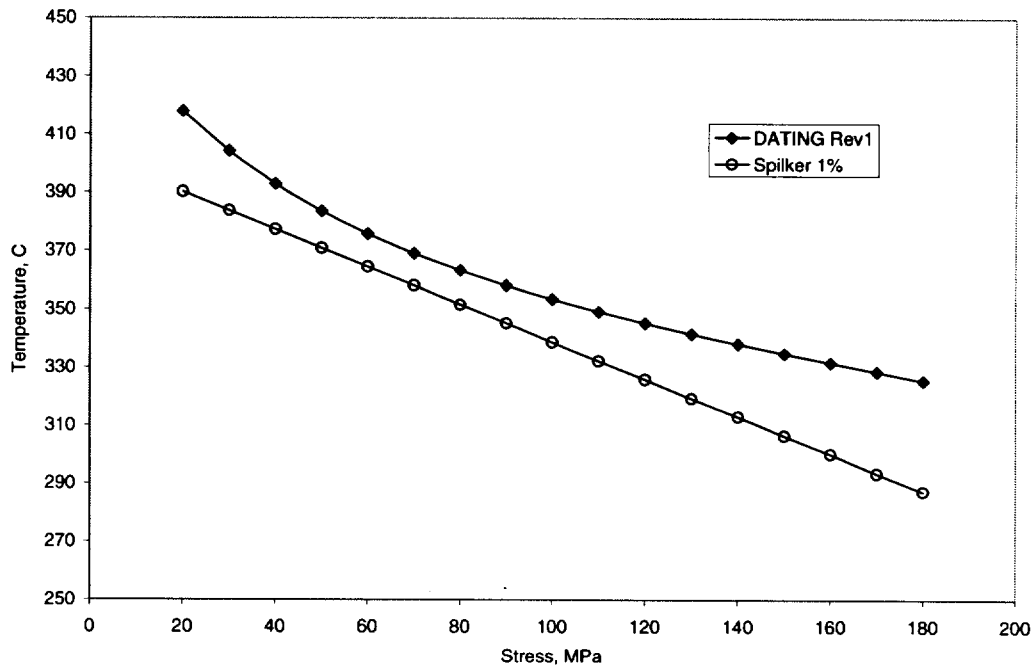


**Figure 5.5 Comparison of Calculated Temperature Limits from CSFM Rev. 1 (conservative Monkman-Grant) and Spilker et. al 1996 Model (1% Strain Limit) for High Burnup Fuel (60 GWd/MTU and 10 Year Cooled).**

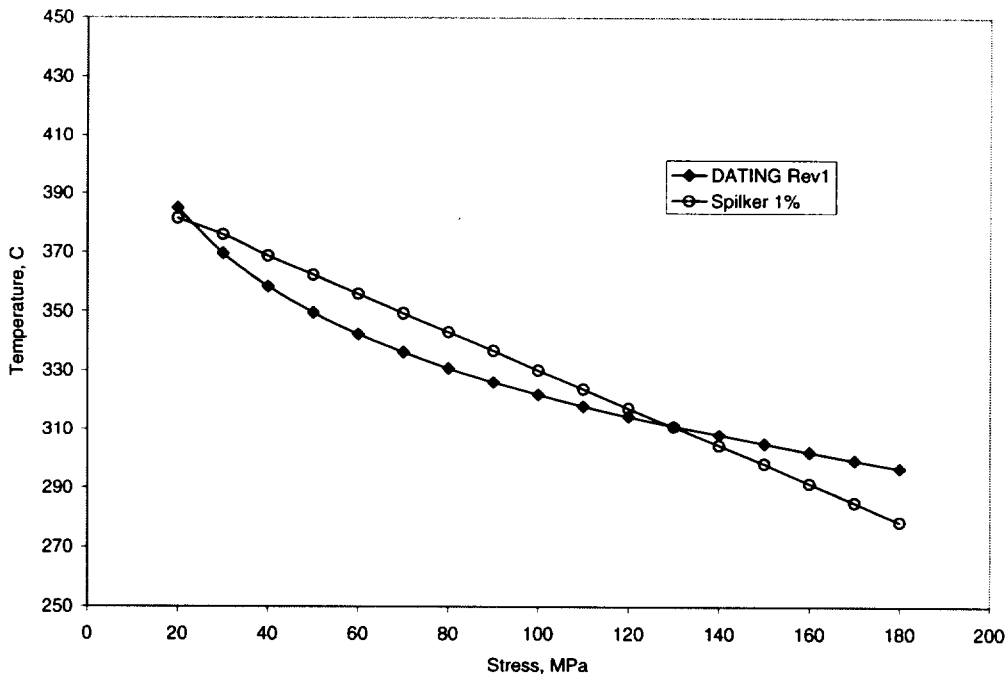


**Figure 5.6 Comparison of Calculated Temperature Limits from Conservative CSFM Rev. 1 (Bounding Monkman-Grant) and Spilker et. al 1996 Model (1% Strain Limit) for Low Burnup Fuel (30 GWd/MTU and 10 Year Cooled).**

The Siegmann (2000) methodology is based on a best estimate creep model but the failure strain limit is based on a complementary cumulative distribution function (CCDF). The CCDF has been developed to determine the probability of failure at a specific strain for a given population of SNF. It should be noted that this methodology does not consider the uncertainty in the Siegmann creep model predictions and, therefore, the Siegmann failure probability does not account for the creep variability among fuel rods using this methodology. In Sections 3 and 4, the creep variability among the different cladding fabrication types is shown to be significant.

The comparison of calculated temperature limits from CSFM Rev. 1 to those calculated with the best-estimate Siegmann model (assumes a 2.86% strain limit based on the median of the failure strain data) is shown in Figures 5.7 and 5.8 for high and low burnup fuel, respectively. The Siegmann best-estimate model implies that 50% of SNF rods may fail at the temperature and stress conditions selected. As expected, the best-estimate Siegmann model predicts significantly higher temperature limits (~30°C) for the high burnup fuel (Figure 5.7) between stresses of 110 to 150 MPa. For low burnup fuel the best-estimate Siegmann model also predicts higher temperature limits (~40°C) for the low burnup fuel (Figure 5.8) between stresses of 110 to 150 MPa. The lower temperature limits calculated with CSFM Rev. 1 are expected because both the creep and failure strain models used for Rev. 1 are bounding in relation to their data, while the best estimate Siegmann model is a mean of their data.

A conservative Siegmann prediction is provided in Figures 5.9 and 5.10 by assuming a 2% probability for failure from Siegmans CCDF, i.e., 98% of the SNF rods will not fail, that yields a failure strain limit of 0.499%. The conservative Siegmann model predicts lower temperature limits (~10°C) for high burnup fuel than the conservative CSFM Rev. 1 (Figure 5.9) between stresses of 110 to 150 MPa. For low burnup fuel (Figure 5.10) the two conservative models predict nearly the same temperature limits (< 3°C difference).

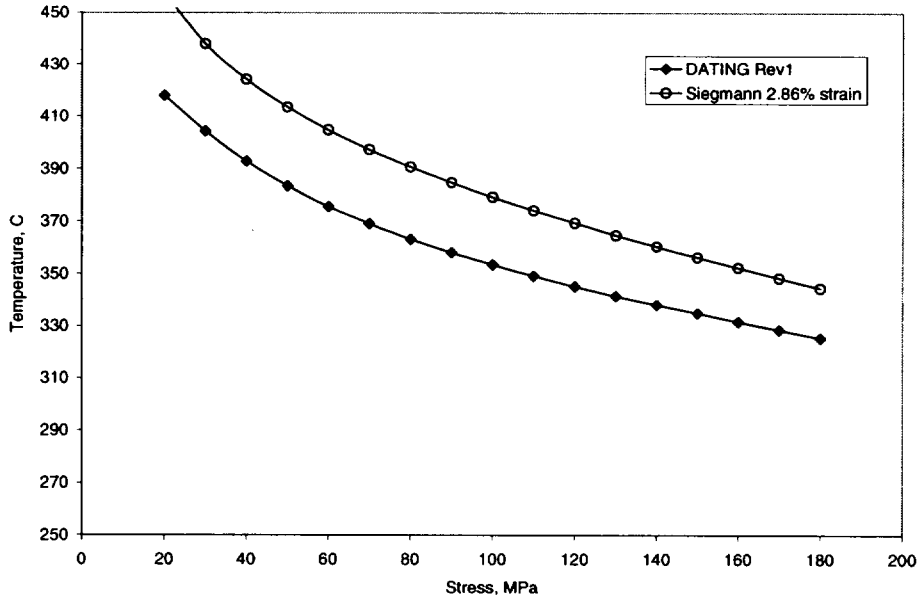


**Figure 5.7 Comparison of Calculated Temperature Limits from CSFM Rev. 1 (Conservative Monkman-Grant) and Siegmann 2000 Model Using Best Estimate Creep and Failure Strain for High Burnup Fuel (60 GWd/MTU and 10 Year Cooled).**

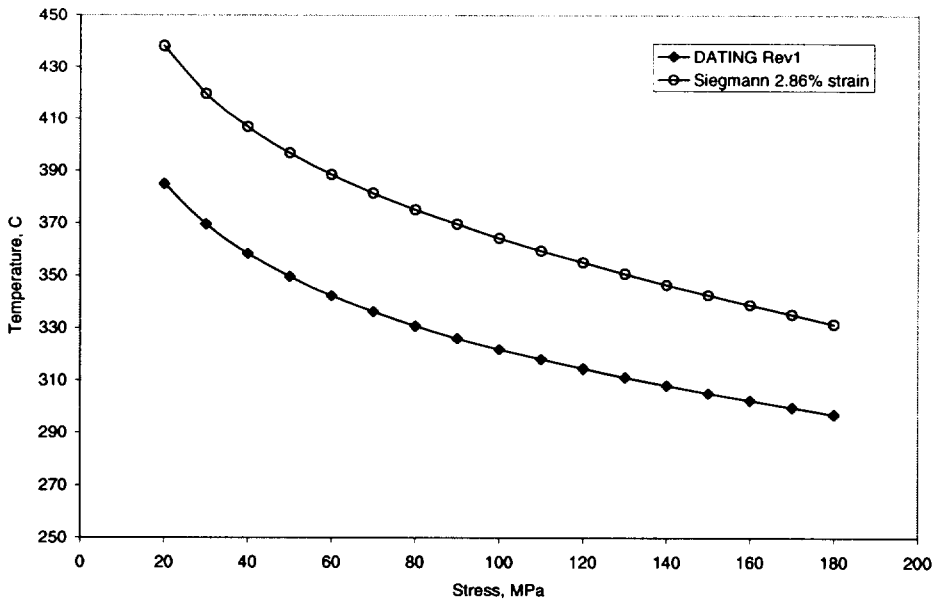


**Figure 5.8 Comparison of Calculated Temperature Limits from CSFM Rev. 1 (Conservative Monkman-Grant) and Siegmann 2000 Model Using Best Estimate Creep and Failure Strain for Low Burnup Fuel (30 GWd/MTU and 10 Year Cooled).**

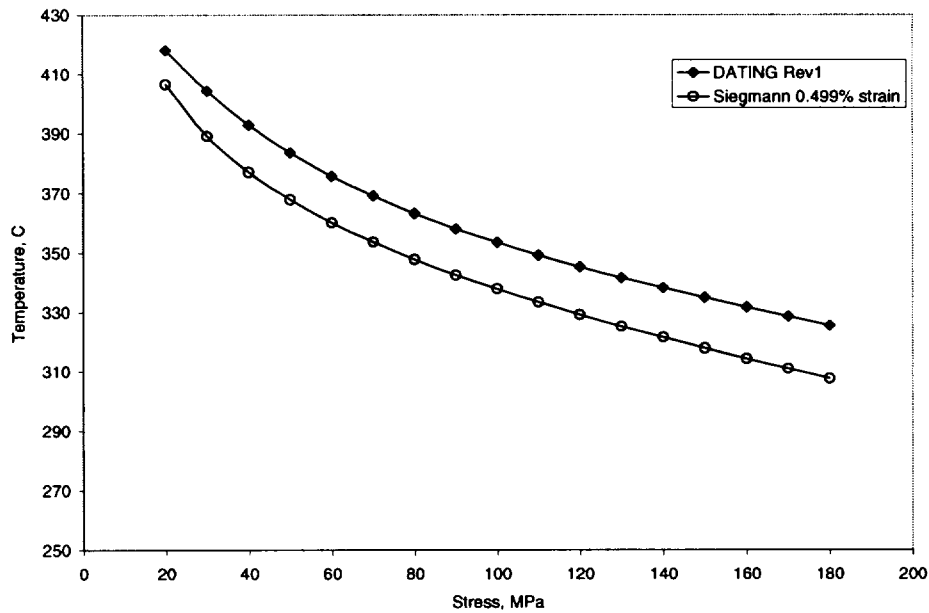


**Figure 5.9** Comparison of Calculated Temperature Limits from CSFM Rev. 1 (Conservative Monkman-Grant) and Siegmann 2000 Model Using Best Estimate Creep and Conservative Failure Strain (0.499% at 2% Probability) for High Burnup Fuel (60 GWd/MTU and 10 Year Cooled).

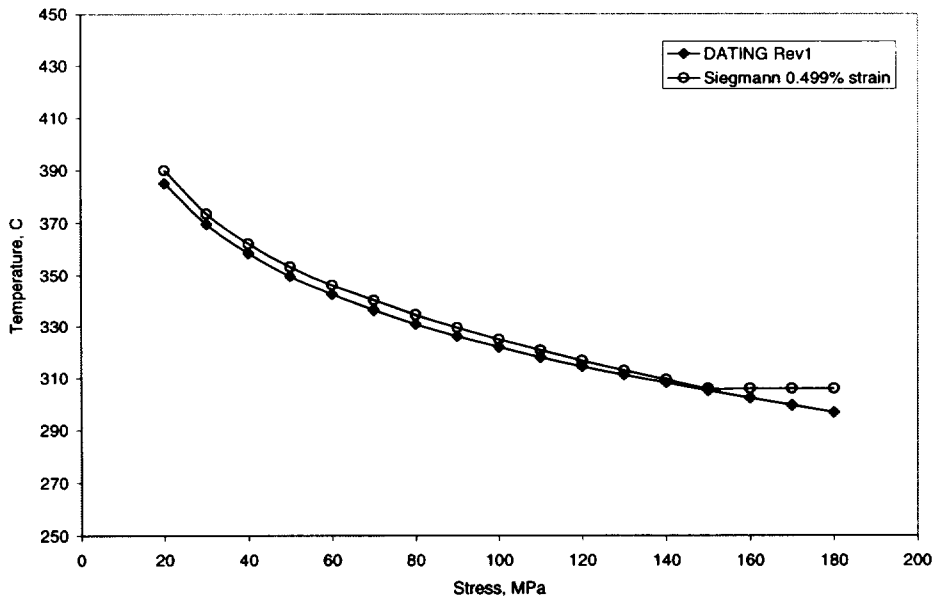


**Figure 5.10** Comparison of Calculated Temperature Limits from CSFM Rev. 1 (Conservative Monkman-Grant) and Siegmann 2000 Model Using Best Estimate Creep and Conservative Failure Strain (0.499% at 2% Probability) for Low Burnup Fuel (30 GWd/MTU and 10 Year Cooled).

#### **5.4. Comparison of CSFM Rev. 1 Temperature Limits using Monkman-Grant Correlation Versus Use of a Strain Limit for Rupture.**

The DATING code was altered to calculate time-to-rupture based on a uniform strain limit and the calculation of primary and steady-state strain using CSFM Rev. 1A creep models. The uniform rupture strain limits were assumed to be 2% strain for temperatures above 350 °C and 1% strain below 350 °C. These strain limits were selected to bound the data in Figure 4.13. A comparison of initial temperature limits calculated with the bounding uniform strain limit and the conservative Monkman-Grant coefficient (Equation 4.13) with both rupture limits using the CSFM Rev. 1A creep model (equation 4.20) is shown in Figure 5.11. These calculated initial temperature limits are for high burnup fuel with 10 years cooling prior to dry storage. The comparison shows that the strain limit approach calculates a slightly higher (~5°C) temperature limit. The calculation of similar temperature limits is not surprising because both the Monkman-Grant rupture model and the strain limit approach are based on a bounding fit to the same rupture data. The primary difference is that Monkman-Grant is only based on steady-state creep rate while the strain limit approach includes primary creep strains in addition to steady-state creep strains.

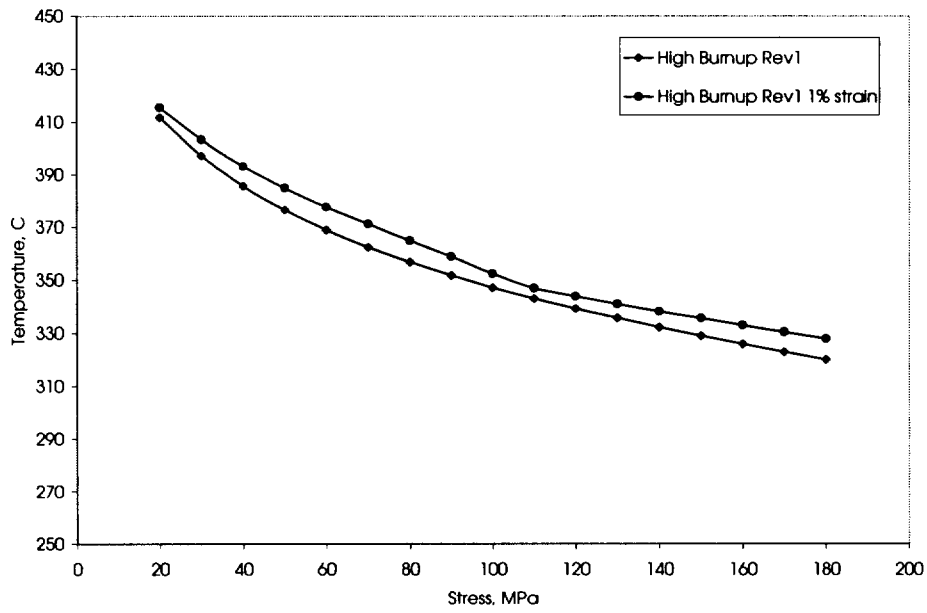


**Figure 5.11 Comparison of CSFM Rev. 1 Calculated Temperature Limits Versus Stress Using a Monkman-Grant Correlation and a Strain Limit Criterion for High Burnup Fuel with 10-Year Cooling.**

## **6. FINDINGS, CONCLUSIONS AND RECOMMENDATIONS**

The CSFM methodology has been revised (Rev.1) based on new creep and creep rupture data from unirradiated and irradiated specimens of Zircaloy cladding from SNF. The creep and creep rupture database collected for this effort is nearly all new and different from the database collected for CSFM Rev. 0. CSFM Rev. 1 retains the same six creep mechanisms for steady-state creep, and only the grain boundary sliding (GBS) and low temperature climb (LTC) mechanisms are significant within the range for dry cask storage which is the same as for CSFM Rev. 0. However, the creep models have been modified from Rev. 0 to include the addition of a primary creep model, changes to the unirradiated creep coefficients for GBS, LTC and Coble creep mechanisms, and incorporation of a creep reduction factor due to irradiation damage for some creep mechanisms. The CSFM Rev. 1 uses only one creep rupture model (Monkman-Grant) within the temperature and stress range for dry cask storage while the Rev. 0 methodology assumed that two rupture models, diffusion controlled cavitation growth (DCCG) and Monkman-Grant, were active within this range. The Rev. 1 Monkman-Grant coefficient has been modified from that used in the Rev. 0 rupture correlations.

From the review of the data and use of the revised CSFM methodology proposed in this report, the following findings, conclusions and recommendations are made:

### **6.1. Findings**

- The CSFM methodology Rev. 1 results in similar predicted temperature limits (within 5°C) to the Rev. 0 methodology for low and high burnup fuel with 5 years cooling time. However, for 10 year cooled low and high burnup fuel, the CSFM Rev. 1 methodology predicts lower temperature limits than the Rev. 0 methodology by 10°C to 20°C for stresses between 110 to 140 MPa. The DATING code is used to predict the temperature limits for both CSFM Rev. 0 and CSFM Rev. 1 methodology. (Section 5.1)

- Thermal annealing tests for SNF cladding indicate that cask drying at temperatures below 400°C should have little impact on creep and temperature limits for times less than a month. Exposure of the SNF cladding to pre-storage temperatures above 400°C may anneal the irradiated microstructure and increase the creep rate, thereby reducing the calculated cask storage temperature limit. Thermal annealing at temperatures above 400°C may also result in hydride reorientation that could reduce ductility and reduce storage temperature limits. (Section 4.3.4)
  
- Experimental creep data from some new tests of unirradiated Zircaloy show that grain boundary sliding by grain boundary diffusion occurs at a rate faster than that assumed in CSFM Rev. 0. Consequently, higher creep rates are predicted for unirradiated cladding with CSFM Rev. 1 for a given temperature and stress than that predicted by Rev.0. (Section 4.1.2)
  
- The transition from grain boundary sliding to climb/glide mechanisms is initiated at higher stress than that assumed in CSFM Rev. 0.
  
- Comparison of CSFM Rev. 1 DATING results (using the conservative Monkman-Grant coefficient) to other recent methodologies that predict dry cask storage temperature limits demonstrate the following:
  - The Spilker et al. (1997) methodology predicts lower temperatures (15 to 20°C) for high burnup fuel and predicts similar or slightly higher temperatures to the conservative Rev. 1 for low burnup fuel for dry cask storage conditions.
  - The Siegmann (2000) methodology offers a probability function for failure. As expected the best-estimate (assumes 50% of SNF rods will fail) Siegmann model predicts significantly higher temperature limits (~30°C) for the high burnup fuel and low burnup fuel (~40°C) between stresses of 110 to 150 MPa. The conservative Siegmann model (assumes 2% probability for failure or 98% of SNF rods will not fail) predicts lower temperature limits (~10°C) for high burnup fuel than the conservative

CSFM Rev. 1 and nearly the same temperature limits ( $< 3^{\circ}\text{C}$  difference) for low burnup fuel between stresses of 110 to 150 MPa. (Section 5.1)

- Use of the mean Monkman-Grant coefficient from Rev. 1 in the DATING code results in 11 to 12  $^{\circ}\text{C}$  higher temperature limits than the conservative Monkman-Grant coefficient. The use of the mean Monkman-Grant coefficient in DATING still bounds all of the creep rupture data when the conservative Rev. 1 steady-state creep models are used in DATING.

## **6.2. Conclusions**

- Two steady-state creep models were developed (1A and 1B) and concluded that 1B was slightly better. The two models predict nearly the same temperature limits within the range of conditions for dry cask storage. (Section 4.4)
- Comparison of new creep data for irradiated cladding to data from unirradiated cladding suggests that the steady-state creep rate for some creep mechanisms is significantly decreased as a result of irradiation. The degree of reduction in creep appears to be dependent on fabrication parameters of the Zircaloy. Neutron irradiation damage appears to retard the creep by GBS by impeding dislocation motion within the grains. This same damage also retards creep by LTC and glide climb. The Coble creep mechanism does not appear to be impacted by irradiation damage and this is consistent with the theory for Coble creep. Because only a few creep tests have been done on irradiated cladding in the Coble creep range and the microstructural characterization is limited, this conclusion in regards to Coble creep is considered preliminary. (Sections 3.2 and 4.3.1)
- Examination of the unirradiated creep data shows a large variability (factor of 10 to 1000) in the data at a given temperature and stress. This variability appears to decrease for the irradiated creep data but the variability is still relatively large (factor of 5 to 20). The variability in the creep data appears to be due to fabrication parameters. (Sections 3 and 4)

- Analyses of the creep rupture data for both unirradiated and irradiated cladding suggest that there is no difference in rupture life between unirradiated and irradiated cladding. Some of the rupture data suggest that there may be a dependence between rupture strain or time-to-rupture and hydride content but this can not be quantified because of the lack of rupture data from high burnup rods with high hydrogen levels. Hydride blisters formed due to oxide spallation have been shown to significantly reduce the ductility of high burnup cladding during tensile and burst tests. Consequently, there is considerable uncertainty regarding the impact of the hydride blisters and embrittlement on creep-to-rupture times. (Sections 4.2, 4.3.2 and 4.3.3)
- Analyses of the creep rupture data for both unirradiated and irradiated cladding indicate that rupture life is consistent with the Monkman-Grant correlation. This conclusion is considered preliminary because there is only one unirradiated and no irradiated rupture data within the design-basis stress range for dry storage. (Section 4.2)
- The creep rupture data also suggest that the Monkman-Grant coefficient (strain-to-failure) decreases with decreasing temperature. The decrease in the coefficient with temperature may be due to different failure mechanisms such as triple point and transgranular cracking that may become more active at the lower temperatures and a decrease in strain-to-failure. (Section 4.2.2)
- The proposed Monkman-Grant correlation is only valid for high burnup fuel with hydrogen levels less than 660 ppm and no oxide spallation. (Section 4.3.3)

As noted, the Monkman-Grant correlation for Rev. 1 shows that the creep strain-to-failure is not a single value. Rather, it is dependent on the initial storage temperature of the cladding, e.g., the strain-to-failure varies from 3.6% (best estimate value at 400°C) to below 1% depending on temperature and the desired level of conservatism. In comparison, ISG-11 (NRC 2000) prescribes a 1% creep strain limit and a criteria using

cladding oxide thickness as the basis for determining fuel failure. The ISG-11 1% strain limit is based on a limited set of tensile and burst to rupture data and the current understanding of the properties of high burnup fuel at the time ISG-11 was issued.

The ISG-11 (NRC-2000) 1% uniform strain criterion may be overly conservative for temperatures above 350 °C but may be a reasonable conservative value for temperatures below 350 °C. The Monkman-Grant correlation was preferred for CSFM Rev. 1 rather than the simple strain limits of 2% and 1%, because it fits the rupture data well and can be related to theoretical rupture models.

It should be noted that both the conservative and best-estimate Monkman-Grant coefficients in this report predict conservative time-to-rupture values when the conservative CSFM Rev. 1 creep models are used; however, this may not be true if a less conservative creep model is used. This will also be the case if the conservative 2% (> 350 °C) and 1% (< 350 °C) strain limits are used with a less conservative creep model.

### **6.3. Recommendations**

- Creep data are needed from high burnup SNF rods with high corrosion within the temperature and stress range for dry cask storage of 310°C to 380°C and 110 to 150 MPa, respectively. These data are needed because very little creep data exist in this temperature and stress range and no data exist in this range for high burnup fuel with high cladding oxidation and oxide spallation.
- Creep rupture data from high burnup fuel rods with high corrosion (including rods with oxide spallation) are needed within the temperature and stress range for dry cask storage of 310°C to 380°C and 110 to 150 MPa, respectively. It may not be possible to obtain rupture data within a reasonable amount of time at the stresses typical for dry cask storage; therefore, it is recommended that stress levels be increased to the necessary level for rupture rather than increasing temperature level. This is because rupture data evaluated in this report suggests that rupture strains (and time-to-rupture) increase with increasing temperature. Also, tensile and burst tests (at high stresses

and strain rates) suggest that failure strains may be significantly reduced when high oxidation and spallation is present in high burnup fuel rods. Therefore, creep rupture data are needed from these high burnup fuel rods to verify that reduced creep rupture strains do not result in failure. These creep rupture data are also needed to confirm that DCCG is not an active rupture mechanism at dry cask storage conditions.

- Creep rupture data are needed from high burnup rods after some time in interim dry cask (post) storage to confirm there is sufficient deformation life required for permanent storage following dry cask storage.
- Fracture toughness data are also needed from high burnup rods with high oxidation and spallation near room temperature. These data are needed from both pre- and post-storage high burnup rods to confirm that the rods can be retrieved after interim dry cask storage for placement in a permanent storage facility. These data are also needed to determine the high burnup fuel response to cask accidents that involve impact loads on the fuel while in the cask.

It is noted that the information in this draft report is preliminary and should not be used for licensing decisions until it has been peer reviewed by a panel of experts on creep behavior of zirconium alloys and high burnup fuel behavior.

## 7. REFERENCES

- Baty, D. L., W. A. Pavinich, M. R. Dietrich, G. S. Clevinger, and T. P. Papazoglou. 1984. "Deformation Characteristics of Cold-Worked and Recrystallized Zircaloy-4 Cladding," Zirconium in the Nuclear Industry: Sixth International Symposium, ASTM STP 824, 306-339, American Society for Testing and Materials, Philadelphia, Pennsylvania.
- Bauer, A. A. and L. M. Lowry. 1978. "Tensile Properties and Annealing Characteristics of HB Robinson Spent Fuel Cladding," Nuclear Technology, 41:359-372, American Nuclear Society, LaGrange Park, Illinois.
- Bell, L. G. 1963. "The Effect of Hydrogen on the Creep Properties of Zircaloy-2," AECL-1826, Chalk River, Ontario.
- Billiaux, M. R., F. Sontheimer, V. I. Arimescu, and H. Landskron. 2000. "Fuel and Cladding Properties at High Burnup," 2000 International Topical Meeting on Light Water Reactor Fuel Performance Inn at Prospector Square, Park City, Utah, April 10-13, 2000.
- Blackburn, L. D., D. G. Farwick, S. R. Field, L. A. James, and R. A. Moen. 1978. "Maximum Allowable Temperature for Storage of Spent Nuclear Reactor Fuel," HEDL-TME 78-37, Hanford Engineering Development Laboratory.
- Bouffioux, P. and L. Legras. 2000. "Effect of Hydriding on the Residual Cold Work and Creep of Zircaloy 4 Cladding Tubes," Light Water Reactor Fuel Performance International Topical Meeting, 951-958 Vol. II American Nuclear Society, LaGrange Park, Illinois.
- Bouffioux, P. and N. Rupa. 2000. "Impact of Hydrogen Pick up on Plasticity and Creep of Unirradiated Zircaloy-4 Cladding Tubes," ASTM STP 1354, pp. 399-422, Twelfth International Symposium on Zirconium in the Nuclear Industry, American Society for Testing and Materials, West Conshohocken, Pennsylvania.
- Bredel T., C. Cappelaere, R. Limon, G. Pinte, and P. Bouffioux. 2000. "Long Term Creep Behavior of Spent Fuel Cladding for Storage and Disposal," Mat. Res. Soc. Symp. Proc. 608:11-29, Materials Research Society.
- Brun, G., J. Pelchat, J. C. Floze, and M. Galimberti. 1987. "Cumulative Fatigue and Creep-Fatigue Damage at 350 C on Recrystallized Zircaloy-4," ASTM STP 939, 597-616, Zirconium in the Nuclear Industry: Seventh International Symposium, American Society for Testing and Materials, Philadelphia, Pennsylvania.
- Burton B. and G. L. Reynolds. 1995. "In Defense of Diffusional Creep," Materials Science and Engineering, A191: 135-141.

Cappelaere C. and P. Bouffieux. 2000 "Long Term Storage of Spent Fuel Subassemblies, CEA EDF R&D Program", Presentation at Creep Test Review Meeting October 4, 2000, at Pacific Northwest National Laboratory, Richland, Washington.

Chin, B. A. and E. R. Gilbert. 1989. "Prediction of Maximum Allowable Temperatures for Dry Storage of Zircaloy Clad Spent Fuel in Inert Atmosphere", Nucl. Tech. 85:575, American Nuclear Society, LaGrange Park, Illinois.

Chin, B. A, M. A. Khan, and J. Tarn. 1986. "Deformation and Fracture Map Methodology for Predicting Cladding Behavior During Dry Storage, " PNL-5998, Pacific Northwest Laboratory, Richland Washington.

Chung, H. M., F. L. Yaggee, and T. F. Kassner. 1987. "Fracture Behavior and Microstructural Characteristics of Irradiated Zircaloy Cladding," ASTM STP 939, 775-801, Zirconium in the Nuclear Industry: Seventh International Symposium, American Society for Testing and Materials, Philadelphia, Pennsylvania.

Cunningham, M. E., E. P. Simonen, R. T. Allemann, I. S. Levy, R. F. Hazelton. 1987. "Control of degradation of spent LWR fuel during dry storage in an inert atmosphere," PNL-6364, Pacific Northwest Laboratory, Richland, Washington.

Einzig, R. E. and R. Kohli. 1984. "Low-Temperature Rupture Behavior of Zircaloy-Clad Pressurized Water Reactor Spent Fuel Rods under Dry Storage Conditions," Nucl. Tech., 67:107-122, American Nuclear Society, LaGrange Park, Illinois.

Fiala, J., J. Cadek. 1985. "Creep in Zirconium at Low Stresses and Temperatures From 748 to 973 K", Materials Science and Engineering , v 75, p 117-126.

Frenkel, J. M. and Weisz M. 1973. "Influence of Various Metallurgical Parameters and Neutron Flux on Creep of Zircaloy 4 Cladding Tubes," International Conference on Nuclear Fuel Performance, London, Great Britain.

Fuketa, T., F. Nagase, K. Ishijima, T. Fujishiro. 1996. "NSRR/RIA experiments with high-burnup PWR fuels" Nuclear Safety, Vol. 37, No. 4, p 328-342.

Garde, A. M. 1986. "The Hot Cell Examination of Oconee 1 Fuel Rods After 5 Cycles of Irradiation, " DOE/ET/34212-50.

Garde, A. M., G. P. Smith, and R. C. Pirek. 1996. "Effects of Hydride Precipitate Location and Neutron Fluence on the Ductility of Irradiated Zircaloy-4," ASTM STP 1295, Zirconium in the Nuclear Industry: Eleventh International Symposium, 407-430, E.R. Bradley and G.P. Sabol, Eds, American Society for Testing and Materials.

Gilbert, E. R., W. J. Bailey, A. B. Johnson, Jr., and M. A. McKinnon. 1990a. "Advances in Technology for Storing Light Water Reactor Spent Fuel." Nuclear Technology 89:141-161.

Goll, W., H. Spilker, and E. H. Toscano. 2001. "Short-Time Creep and Rupture Tests on High Burnup Fuel Rod Cladding," *J. Nucl. Mater.*, 289:3:247-253, Elsevier Science, Amsterdam, The Netherlands.

Hayes, T. A., R. S. Rosen, and M. E. Kassner. 1999a. "Critical Analysis of Dry Storage Temperature Limits for Zircaloy-Clad Spent Nuclear Fuel Based on Diffusion Controlled Cavity Growth," UCRL-ID-131098, Lawrence Livermore National Laboratory, Livermore, California.

Hayes, T. A., R. S. Rosen, M. E. Kassner, and K. S. Vecchio. 1999b. "Analysis Of Dry Storage Temperature Limits For Zircaloy-Clad Spent Nuclear Fuel," Symposium on Scientific Basis for Nuclear Waste Management XXIII- Cladding and Spent Fuel, Materials Research Society Fall Meeting, Boston, Massachusetts.

Herman, A. 1999. "Fuel Cladding Integrity at High Burnups (Part I)," Draft Final Report, EPRI-TR-108753-P1, Electric Power Research Institute, Palo Alto, California.

Hindle, E. D. and G. F. Slattery. 1971. "Stress Orientation of Hydride Platlets In Zirconium Alloys Tubing and Its Effect on Mechanical Properties, " Proceedings of the International Conference on Corrosion, British Nuclear Energy Society.

Hindmarsh, A. C. 1974. GEAR: Ordinary Differential Equation System Solver. Lawrence Livermore Laboratory Report UCID-30001, Rev. 3, Livermore, California.

Jones, R. B. 1966. "Diffusion-Creep in Zirconium Alloys," *J. Nucl. Mater.*, 19:204-207, Elsevier Science, Amsterdam, The Netherlands.

Kaspar, G, M. Peehs, R. Bokelmann, D. Jorde, H. Schonfeld, W. Haas, A. Bleier, and F. Rutsch. 1985a. Release of Fission Products and Post-Pile Creep Behavior of Irradiated Fuel Rods Stored Under Dry Conditions, BMFT KWA 2100 B0, Kraftwerk Union, Erlangen, Federal Republic of Germany.

Kaspar, G., M. Peehs, E. Steinberg, and H. Schonfeld. 1985b. "Experimental Investigation of Post-Pile Creep of Zircaloy Cladding Tubes," Trans 8th International Conference on Structural Mech. In Reactor Technology.

Lagneborg, R. 1978. "Creep Deformation Mechanisms," Creep of Engineering Materials and Structures, 7-34, G Bernasconi and G Paitti, eds., Applied Science Publishers Ltd., London.

Langdon, T. G. 1994. "A Unified Approach to Grain Boundary Sliding in Creep and Superplasticity," *Acta Metall. Mater.*, 42:7:2437-2443, Elsevier Science Ltd, Great Britain.

Langdon, T. G. 2000a. "Identifying Creep Mechanisms at Low Stresses," *Materials Science and Engineering*, A283:266-273, Elsevier Science Ltd, Great Britain.

Langdon, T. G. 2000b. Low Stress Creep in CW Alloys, Email response from Professor Terence G. Langdon on December 7, 2000 to an Email request from E. R. Gilbert on December 6, 2000.

Levy, I. S., B. A. Chin, E. P. Simonen, C. E. Beyer, and E. R. Gilbert. 1987. Recommended temperature limits for dry storage of spent light water reactor zircaloy-clad fuel rods in inert gas. Pacific Northwest Laboratory. Report PNL-6189 Richland Washington.

Limback, M. and T. Andersson. 1996. "A Model for Analysis of the Effect of Final Annealing on the In- and Out-of-Reactor Creep Behavior of Zircaloy Cladding," ASTM STP 1295, 449-468, Eleventh International Symposium on Zirconium in the Nuclear Industry, American Society for Testing and Materials, West Conshohocken, Pennsylvania.

Limon, R, C. Cappelaere, T. Bredel, and P. Bouffioux. 2000. "A Formulation of the Spent Fuel Cladding Creep Behavior for Long Term Storage 2000 International Topical Meeting on Light Water Reactor Fuel Performance Inn at Prospector Square, Park City, Utah, April 10-13, 2000.

Louthan, M. R. and R. P. Marshall. 1963. "Control of hydride Orientation in Zircaloy," J. Nucl. Mater., 9: 170-184. Elsevier Science, Amsterdam, The Netherlands.

Luthy, H, R. A. White, and O. D. Sherby. 1979. "Grain Boundary Sliding and Deformation Mechanism Maps," Materials Science and Engineering, 39:211-216, Elsevier Sequoia, The Netherlands.

Maki, H. and T. Hara. 1975. "Out-of-Reactor Study on External-Pressure Creep of Zircaloy-2 Fuel Cladding Tubes," J. Nucl. Mater., 12:43-52. Elsevier Science, Amsterdam, The Netherlands.

Matsuo, Y. 1987. "Thermal Creep of Zircaloy-4 Cladding under Internal Pressure," J. Nucl. Sci. and Tech., 24:2:111-119.

Mayuzumi, M. and K. Murai. 1993. "Post Irradiation Creep and Rupture of Irradiated PWR Fuel Cladding," Proceedings of Nuclear Waste Management and Environmental Remediation, 607-612, Prague Czech Republic.

Monkman, T. C. and N. H. Grant. 1956. "An Empirical Relationship Between Rupture Life and Minimum Creep Rate in Creep-Rupture Tests," Proceedings American Society for Testing and Materials, 56:593-605, Philadelphia, Pennsylvania.

Murty, K. L. 1999. "Creep Studies for Life Prediction and New Generation Zircaloy - Application to Nuclear Technology," J. of Metals, AIME.

- Nix, W. D. 1983. "Introduction to the Viewpoint Set on Creep Cavitation," *Scripta Metallurgica*, 17:1-4, Pergamon Press Ltd., USA.
- NRC. 1997. "Standard Review Plan for Dry Cask Storage Systems - Final Report," United States Nuclear Regulatory Commission Regulation, NUREG-1536, January 1997.
- NRC. 2000 Interim Staff Guidance No. 11, Revision 1, "Transportation and Storage of High Burnup Fuel," United States Nuclear Regulatory Commission Regulation.
- Pankaskie, P. J. 1962. "Creep Properties of Zircaloy-2 for Design Application," HW-75267, General Electric Company, Richland, Washington.
- Peehs, M. and J. Fleisch. 1986. "LWR Spent Fuel Storage Behavior," *J. Nucl. Mater.*, 137:190-202, Elsevier Science Publishers, North Holland, Amsterdam, The Netherlands.
- Pescatore, C. and M. Cowgill. 1994. Temperature Limit Determination for the Inert Dry Storage of Spent Nuclear Fuel, EPRI-TR-103949, Electric Power Research Institute, Palo Alto, California.
- Pickman, D. O. 1972. "Properties of Zircaloy Cladding," *Nucl. Eng. Des.*, 21: 212 – 234.
- Prasad, N., G. Malakondaiah, K. Muraleedharan, and P. Rama Rao. 1988. "Creep of Zircaloy-2 at Low Stresses," *J. Nucl. Mater.*, 158:30-41, North-Holland Publishing Co, Amsterdam, The Netherlands.
- Raj, R. and M.F. Ashby. 1975. "Intergranular Fracture at Elevated Temperature," *Acta Metallurgica.*, 23:1.
- Ruano, O. A., A. K. Miller, and O. D. Sherby. 1981. "The Influence of Pipe Diffusion on the Creep of Fine-Grained Materials," *Materials Science and Engineering*, 51:9-16, Elsevier Sequoia, The Netherlands.
- Saegusa, T., M. Mayuzumi, C. Ito, and K. Shirai. 1996. "Experimental Studies on Safety of Dry Cask Storage Technology of Spent Fuel," *J Nucl. Sci. and Tech.*, 33:3:250-258.
- Schäffler, I., P. Geyer, P. Bouffioux, P. Delobelle. 2000. "Thermomechanical behavior and modeling between 350 C and 400 C of Zircaloy-4 cladding tubes from an unirradiated state to high fluence (0 to  $85 \times 10^{24} \text{ nm}^{-2}$ ,  $E > 1 \text{ MeV}$ )" *Journal of Engineering Materials and Technology*, v. 122(2) p. 168-176.
- Schwartz, M. W. and M. C. Witte. 1987. "Spent Fuel Cladding Integrity During Dry Storage," UCID-21181, Lawrence Livermore National Laboratory.
- Shober, F. R., J. A. Van Echo, and L. L. Marsh. 1957. Battelle (USA) Report BMI-1168.

Siegmann, E. 2000. "Cladding Degradation - Summary and Abstraction, " ANL-WIS-MD-000007 Rev 00 ICN 01, U.S. Department of Energy, Washington, DC.

Simonen, E. P. and E. R. Gilbert. 1988. "DATING - A Computer Code for Determining Allowable Temperatures for Dry Storage of Spent Fuel in Inert and Nitrogen Gases, " PNL-6639, Pacific Northwest Laboratory, Richland, Washington.

Spilker, H., M. Peehs, H. P. Dyck, G. Kaspar, and K. Nissen. 1997. "Spent LWR Fuel Dry Storage in Large Transport and Storage Casks after Extended Burnup," J. Nucl. Mater., 250:63-74, Elsevier Science, Amsterdam, The Netherlands.

Tarn, J, N. H. Madsen, and B. A. Chin. 1986. "Deformation and Fracture Map Methodology for Predicting Cladding Behavior During Dry Storage, " PNL-5998, Pacific Northwest Laboratory.

Vierge, K. and C. Herzig. 1990. "Grain Boundary Diffusion in  $\alpha$ -Zirconium Part I: Self-Diffusion," J. Nucl. Mater., 173:117-129, North-Holland Publishing Co, Amsterdam, The Netherlands.

United States Federal Register, 10 CFR Part 72, U.S. Printing Office, Washington, D.C.

United States Federal Register, 10 CFR Part 71, U.S. Printing Office, Washington, D.C.

Wadsworth, J, O. A. Ruano, and O. D. Sherby. 1998. "Deformation by Grain Boundary Sliding and Slip Creep Versus Diffusional Creep," UCRL-JC-132348, The Minerals, Metals and Minerals 1999 Annual Meeting.

Yvon, P, A. Soniak, D. Gilbon, J. Royer, V. Basini, J. P. Mardon, and P. Bouffioux. 1999. "Deformation Behavior of Zirconium Alloys under and after Irradiation," High Burn-up Fuel Performance, Safety and Reliability and Degradation of In-Core Materials and Water Chemistry Effects, HPR-351, Vol. II, OECD Halden Reactor Project, Loen, Norway.

## APPENDIX A - SUPPLEMENT

### Description of the Computer Code DATING Rev. 1

A more complete description of the DATING code and required input to run the code is provided by Simonen and Gilbert (1988).

#### Computational method

The cumulative-damage fraction is calculated from life fraction (Equation 4.21) that integrates from the specified initial fuel age to the specified end-of-life age for a given temperature and stress history using the creep rate and rupture-time equations. The time step for the integration is controlled by the GEAR subroutine package (Hindmarsh 1974), and is adjusted to provide a solution with a minimum number of time steps while maintaining control of the numerical error. The allowable temperature/stress limit for storage corresponds to a damage fraction of unity for a specified initial temperature and stress.

#### Cumulative Damage Fraction

For a given initial stress and temperature, DATING calculates the cumulative-damage fraction using Equation 4.21 and the time-to-rupture for each time step. The time-to-rupture is calculated using either Equation 4.12 or 4.13 (conservative or mean Monkman-Grant coefficient) and steady-state creep rate. The steady-state creep rate is calculated using the temperature and stress for the time step and Equation 4.20. The temperature and stress at each time step are calculated analytically from the equations or input for the decay of temperature and stress. The initial time step is  $10^{-6}$  s. If that is too large for control of error, then GEAR automatically reduces the initial time step until it is small enough to pass the error-control test. The time step is adjusted by GEAR to be as large as possible while maintaining appropriate control of the error.

The steady-state creep rate mechanisms depend on temperature and stress as calculated with Equations 4.6, 4.7, 4.9 and 4.20. The creep rate is calculated for each of the three mechanisms and the sum of the creep rates (Equation 4.20) is used as the appropriate rate for the calculated cumulative-damage fraction. The temperature at each time is compared to the temperature limit for athermal creep. If the cladding temperature is below the athermal limit, then the creep rate is calculated based on the temperature at the athermal limit, not the actual cladding temperature which is below the limit. It should be noted that the athermal creep rate is relatively low and contributes little to the damage fraction.

Similarly, the Monkman-Grant time-to-rupture depends on temperature and stress, i.e. steady-state creep rate. The Monkman-Grant relationship is used for all temperatures and stresses. This is different from Dating Rev. 0 for which competing rupture mechanisms were calculated and the minimum of those was used as the assumed rupture time.

The radiation-damage annealing rate is assumed to be independent of stress but dependent on temperature as indicated in Equation 4.18. The accumulated annealing fraction is calculated and used to reduce the assumed creep reduction factor due to irradiation and increase the creep rate as defined in Equation 4.20.

### **Determination of Temperature Limit**

The allowable temperature limit is determined by estimating the maximum temperature for which the cumulative fraction does not exceed unity at the specified end-of-life, nominally 40 years. For a given stress, there is an initial temperature corresponding to a cumulative fraction of unity as seen in Figure 3 of Simonen and Gilbert (1988).

DATING uses a numerical search procedure to determine this temperature from a temperature and stress that is changing (decaying) in dry cask storage. To establish an initial estimate of allowable temperature, the cumulative fraction is initially calculated at 340°C and 340.5°C. Based on the cumulative fraction at those two temperatures, a linear relationship is established between reciprocal temperature and cumulative-damage fraction (see Figure 3 of Simonen and Gilbert 1988). A new estimate of temperature

corresponding to a cumulative fraction of unity is calculated. The correct cumulative fraction is then calculated for that revised temperature. If the correct cumulative fraction is greater than unity, an updated linear relationship is established based on the revised temperature and the revised temperature less 0.5°C. If the correct cumulative fraction is less than unity, then the relationship is based on the revised temperature and the revised temperature plus 0.5°C. With each iteration an improved estimate of the temperature corresponding to a cumulative fraction of unity is obtained. When the newer estimate of temperature is less than 0.025°C different from the previous estimate and a cumulative fraction near unity is achieved, the search is concluded, and the temperature is output as the temperature limit for the assumed stress.

### **Description of Code**

The DATING code computes cumulative creep behavior of Zircaloy cladding for time-dependent temperature and stress histories. Creep strain, radiation-damage annealing, and cumulative life-fraction are integrated for user-specified temperature and stress histories. The temperature must be below the alpha/beta transition temperature, 800°C, for Zircaloy. The stress must be below the yield stress. Note that Figures 4.39 and Figures 4.40 indicate that the Nabarro- Herring creep mechanism dominates only for temperatures above 900°C and therefore is not allowed in DATING calculations.

Although the principal purpose of the code is to provide estimates of allowable temperature limits, the code also provides estimates of creep strain, annealing fraction and life fraction as a function of storage time. Equations for the temperature of spent fuel in inert and nitrogen gas storage are included explicitly in the code for fuel with a burnup of ~30 GWd/MTU; however, an option is included for a user-specified cooling history in tabular form for higher burnup fuel. Also, an option is contained in the DATING code for creating tables of the temperature and stress dependencies of creep-strain rate and creep-time-to-rupture for Zircaloy at constant temperature and constant stress or constant ratio of stress/modulus.

The DATING Rev. 1 code consists of three components: a) the main DATING Rev. 1 program, b) the DIFFUN subroutine, and c) the GEAR package. The DATING Rev. 1 program establishes input parameters, initial conditions, GEAR options, and output of data. The DIFFUN Rev. 1 subroutine contains the rate equations which are simultaneously integrated using the GEAR package. The GEAR package is a set of subroutines for the numerical solution of the rate equations specified in DIFFUN Rev. 1. The rate equations include the creep rate, the rate of radiation damage annealing, and the rate of accumulating creep damage.

Lastly, the user must supply a data input file, HIST, for the case of the user-specified temperature history or temperature and stress history. The table HIST can be used with two options. The first option, described as TABLE FORM, uses the time and temperature table to calculate a rate of cooling as a function of time. This table is used for determining the temperature stress limit because it applies to any initial temperature. The second option, described as TABLE VALUES, uses the time, temperature and stress table to calculate the strain as a function of time. This table can only be used for the run option, 3, to calculate cumulative damage fraction because the cooling history is exactly as defined in the table including the initial temperature. It is important to note that the time value used in the table is the fuel age in years and is not the storage time.

### **Main Program**

The MAIN program, DATING Rev. 1, contains the input options, calls subroutines DIFFUNrev1 and DRIVE (in GEAR), and outputs results of calculations. The input data are entered from the keyboard and the output data are written to the file DATING Rev. 1.OUT on the default drive. The user-specified temperature or temperature and stress history is read from the DATING Rev. 1 program. Error messages result if the assumed stress is above the yield stress or if the temperature is above the  $\alpha$  to  $\beta$  transition temperature of  $\sim 800$  °C.

## **DIFFUN Subroutine**

The DIFFUN Rev. 1 subroutine contains the rate equations used for the integration of creep strain, radiation-damage fraction annealed and accumulated creep-damage fraction. The parameters in the DIFFUN Rev. 1 subroutine call include the number of rate equations NEQ, the time TT, the array Y and the array YDOT. The arrays Y and YDOT are the integrated values and the rates of change of the values being integrated. The DIFFUN Rev. 1 subroutine is called from GEAR to perform the integration. Also, the subroutine is called from the DATING Rev. 1 program when the verification option is selected.

## **GEAR Package**

Details of the GEAR method options are discussed by Hindmarsh (1974). The GEAR package can be obtained from the National Energy Software Center at Oak Ridge National Laboratory. The DRIVE statement in the DATING Rev. 1 program calls on the GEAR package. The DATING Rev. 1 program also provides input options to run GEAR. These options include the initial time step, H0, the error-control parameter, EPS, and the method flag, MF. The initial time step is set at  $10^{-6}$  s in DATING Rev. 1. If a smaller time step is required, then GEAR will reduce the time step by an order of magnitude repeatedly until the time step satisfies the error-control criteria.

The EPS parameter is set at  $10^{-8}$  in the DATING Rev. 1 program, and has been found to be appropriate for the present applications. Larger values for EPS could result in unstable solutions; whereas, smaller values results in more integration steps without significant improvement in accuracy.

The method flag is set at 22 which causes the solution to be obtained using the backward-differentiation-formula method and the cord method with the Jacobian generated internally for the corrector iteration method.

## **HIST File**

The user-specified temperature or temperature and stress history is contained in the file HIST. The first line in the file states the number (integer) of values of time that are in the list. A maximum of 50 values are allowed in the file. Each subsequent line contains the time, temperature and stress written with a decimal point. Numbers must be included in the stress column even when only the temperature history is used for the history option, "TABLE FORM."

## **RUN Options**

The input options are in two categories: 1) selection of output parameters and 2) selection of assumed values for temperature, stress or temperature-stress history. The first user option is to select whether 1) the allowable temperature limit for dry storage is desired, or 2) the creep rate and rupture magnitudes are to be verified, or 3) the cumulative fraction as a function of time is desired. These options appear on the screen as follows:

1. TEMPERATURE STRESS LIMIT
2. VERIFY CREEP RATE, RUPTURE TIME
3. CUMULATIVE DAMAGE FRACTION VS TIME

Each of these options lead to subsequent options for desired temperatures, stresses, or temperature/stress transients. Note that the above options must be entered as integers.

## References

Hindmarsh, A. C. 1974. GEAR: Ordinary Differential Equation System Solver.  
Lawrence Livermore Laboratory Report UCID-30001, Rev. 3, Livermore, California.

Simonen, E. P. and E. R. Gilbert. 1988. "DATING - A Computer Code for Determining Allowable Temperatures for Dry Storage of Spent Fuel in Inert and Nitrogen Gases," PNL-6639, Pacific Northwest Laboratory, Richland, Washington.